

UNIVERSITY OF ARARAQUARA

**GRADUATE PROGRAM IN BIOTECHNOLOGY IN REGENERATIVE MEDICINE
AND MEDICINAL CHEMISTRY**

BRUNA CAROLINA DORM

**SYNTHESIS OF AMINO ACID-BASED MONOMERS AS BUILDING BLOCKS FOR
THE PRODUCTION OF FURAN POLYMERS BY DIELS-ALDER REACTIONS**

**Araraquara, SP
2024**

BRUNA CAROLINA DORM

**SYNTHESIS OF AMINO ACID-BASED MONOMERS AS BUILDING BLOCKS FOR
THE PRODUCTION OF FURAN POLYMERS BY DIELS-ALDER REACTIONS**

Thesis presented to the Graduate Program in Biotechnology in Regenerative Medicine and Medicinal Chemistry at the University of Araraquara - UNIARA - as part of the requirements for the degree of Doctor of Biotechnology, Concentration Area: Biotechnology in Regenerative Medicine and Medicinal Chemistry.

Advisor: Dr. Eliane Trovatti

Araraquara, SP
2024

FICHA CATALOGRÁFICA

D756s Dorm, Bruna Carolina

Synthesis of amino acid-based monomers as building blocks for the production of furan polymers by Diels -Alder reactions/Bruna Carolina Dorm. – Araraquara: Universidade de Araraquara, 2024.
150f.

Tese (Doutorado) - Programa de Pós-Graduação em Biotecnologia em Medicina Regenerativa e Química medicinal – UNIARA

Orientador: Profa. Dra. Eliane Trovatti

1. Polímeros. 2. Reações de Diels Alder. 3. Biomateriais.
4. Aminoácidos. 5. Click chemistry. I. Título.


CDU 577.4

BRUNA CAROLINA DORM

Tese apresentada a Universidade de Araraquara - UNIARA,
como parte dos requisitos para obtenção do título de Doutora
em Biotecnologia em Medicina Regenerativa e Química
Medicinal.


Araraquara, 06 de agosto de 2024.

BANCA EXAMINADORA

Documento assinado digitalmente
 **ELIANE TROVATTI**
Data: 19/08/2024 15:01:24-0300
Verifique em <https://validar.iti.gov.br>

Prof^a Dr^a ELIANE TROVATTI (Orientadora)

Universidade de Araraquara – UNIARA

Documento assinado digitalmente
 **LUCAS HENRIQUE STAFFA**
Data: 07/08/2024 10:33:29-0300
Verifique em <https://validar.iti.gov.br>

Prof. Dr. LUCAS HENRIQUE STAFFA

Departamento de Engenharia de Materiais – UFSCar – São Carlos – SP




Prof. Dr. EZEQUIEL ROSSI

Instituto Tecnológico de Buenos Aires - Argentina



Prof^a Dr^a MARIA INÉS ERREA

Instituto Tecnológico de Buenos Aires - Argentina

Documento assinado digitalmente
 **MARCELO APARECIDO CHINELATTO**
Data: 07/08/2024 11:15:56-0300
Verifique em <https://validar.iti.gov.br>

Prof. Dr. MARCELO APARECIDO CHINELATTO

Escola de Engenharia de São Carlos - USP – São Carlos – SP

AGRADECIMENTOS

Não se chega à lugar nenhum sozinho. Por isso quero agradecer a todos que, de alguma forma, contribuíram para que eu chegasse até aqui.

Ao meu esposo, **Leandro**, que desde o início dessa jornada acadêmica tem me acompanhado e sido crucial para que eu acreditasse em mim e enfrentasse todos os desafios. Muito obrigada por toda a ajuda em todos os âmbitos que eu precisei.

Aos meus pais, **Ana** e **Joel** pela educação, carinho e por permitirem que eu pudesse continuar estudando e minha irmã, **Ana Beatriz**, por sempre acreditarem em mim e vibrarem a cada conquista minha.

À minha orientadora, Dr^a **Eliane Trovatti**, pela oportunidade de ingressar no doutorado, pela orientação, pela confiança e por todos os ensinamentos, apoio e conversas que tivemos. Muito obrigada por me ajudar a evoluir academicamente, profissionalmente e pessoalmente.

Às minhas supervisoras durante a visita técnica no Institute of Technical Sciences, em Belgrado, Sérvia, Dr^a **Lidija Mancic**, Dr^a **Marina Vukovic** e Dr^a **Ivana Dinic**. Muito obrigada por todo aprendizado que eu tive com vocês, por me receberem tão bem e me ajudarem a conduzir nosso trabalho de forma tão brilhante e satisfatória. *Hvala!*

Aos meus supervisores de Estágio de Pesquisa no Instituto Tecnológico de Buenos Aires, na Argentina, Dr^a **María Inés Errea** e Dr. **Ezequiel Rossi**. Agradeço a oportunidade de trabalhar com vocês e por todo o aprendizado. Muito obrigada também por participarem da minha banca de qualificação e por todas as sugestões e correções que fizeram e que foram de grande valia. *Muchas gracias!*

Aos membros da banca avaliadora, por disponibilizar seu precioso tempo para avaliar e contribuir muito para a melhoria desse trabalho.

Aos meus orientadores de IC, Dr^a **Lucimara Forato** e Dr. **Luís Alberto Colnago**, por darem a oportunidade de ingressar na pesquisa e me acompanharem, de certa forma, até hoje na vida acadêmica.

Aos meus colegas de laboratório, principalmente: **Carol, Neto, Rauany, Tatiane Araújo, Roberta, Aline, Anielly** e aos demais **colegas do Laboratório de Biomateriais e Biotecnologia**. Muito obrigada por toda a ajuda técnica e principalmente por tornarem o ambiente de trabalho muito mais leve e divertido. Obrigada pelas sessões de terapia grátis!

Aos amigos de longa data, que me acompanham nessa jornada e de certa forma, sempre estão presentes na minha vida: **Bruno, Tamar, Gabriel, Gabriela Pereira, Gabriela Nogueira, Laryssa, Marcela, Mirella, Monique Amorim**. Aos meus *pets* **Frajola** e **Thor** pelo amor puro

e incondicional e à minha psicóloga **Rafaela**, essencial no meu amadurecimento pessoal e profissional. Ao meu afilhado **Pedro** e todos meus familiares que me apoiaram sempre.

À **Universidade de Araraquara**, por permitir que eu fizesse o doutorado de forma gratuita e pela estrutura oferecida para que eu pudesse desenvolver meu trabalho. Aos seus funcionários por toda disponibilidade e ajuda ao decorrer desses anos. Agradeço principalmente às secretárias **Sandra e Rosana** por sempre estarem dispostas a ajudar e por serem tão amáveis.

À **FAPESP**, pelas bolsas concedidas, de doutorado direto e BEPE (processos 2020/ 09059- 1 e 2022/09328- 8), sem as quais eu não teria condições de me dedicar integralmente aos trabalhos desenvolvidos durante esses anos.

A **todos que acreditam na Ciência e na Educação**, como forma de libertação e crescimento do país. Principalmente aos que lutam para que isso torne-se uma realidade.

Muito obrigada!

*“Sem a curiosidade que me move, que me inquieta,
que me insere na busca, não aprendo nem ensino.”*

Paulo Freire

RESUMO

O aumento da incidência de doenças e lesões relacionadas à idade é refletido pelo aumento da expectativa de vida da população mundial e a mudança no estilo de vida dos indivíduos. Dessa forma, faz-se necessária a ampliação da gama de biomateriais disponíveis para aplicação médica. Portanto, nesse trabalho de doutorado propôs-se o desenvolvimento de novos biomateriais poliméricos baseados em aminoácidos e moléculas de origem natural e renovável, em busca de propriedades potenciais para a área, assim como a modificação de hidroxiapatita a partir da inserção de aminoácidos em sua estrutura, para melhoria das propriedades de adesão celular desse biomaterial. Esse trabalho está dividido em capítulos, contendo a síntese e/ou modificação química de um biomaterial com aplicação médica. No capítulo I, poli (ácido aspártico) (PASP) foi sintetizado a partir de ácido aspártico, sendo posteriormente modificado com furano (PASP_{fur}). Uma reação de Diels Alder entre o polímero furânico e antibiótico maleinizado foi conduzida para síntese de um novo pró-fármaco. No capítulo II, uma nova bismaleimida foi sintetizada a partir de lisina, sendo posteriormente conduzida a reticulação entre essa e o PASP_{fur}, obtendo-se assim um novo polímero. No capítulo III é apresentada a síntese de um novo polímero a partir de cisteína e aduto furano anidrido maleico. Nos capítulos IV e V, poli (ácido lático), quitosana e amido foram modificados a partir da inserção de aminoácidos para induzir e/ou melhorar as propriedades antimicrobianas desses polímeros. Por fim, no capítulo VI, foi conduzida a modificação química da hidroxiapatita com o aminoácido alanina para aumento da adesão celular na superfície desse biomaterial. Todos os biomateriais foram caracterizados quanto às suas propriedades físico químicas e estruturais. Além disso, foram realizadas caracterizações biológicas, incluindo viabilidade celular e ensaios microbiológicos que mostraram a potencial aplicação desses biomateriais, principalmente na área médica.

Palavras chave: Polímeros, reações de Diels Alder, biomateriais, aminoácidos, Click Chemistry.

ABSTRACT

The increase in life expectancy and changes in lifestyles have led to a rise in the incidence of age-related diseases and injuries. Thus, it is essential to expand the range of biomaterials available for medical applications. In this work, is proposed the development of new polymeric biomaterials based on amino acids and molecules of natural and renewable origin, aiming to discover properties beneficial for medical applications. Additionally, sought to modify hydroxyapatite by incorporating amino acids into its structure to enhance the cell adhesion properties of this biomaterial. This work is divided into chapters, each detailing the synthesis and/or chemical modification of a biomaterial intended for medical use. In Chapter I, poly(aspartic acid) (PASP) was synthesized from aspartic acid and modified with furan (PASP_{fur}). A Diels-Alder reaction between the furan polymer and a maleated antibiotic was performed to synthesized a new prodrug. Chapter II details the synthesis of a new bismaleimide from lysine, which was then cross-linked with PASP_{fur} to create a new polymer. Chapter III describes the synthesis of a novel polymer from cysteine and furan maleic anhydride adduct. In Chapters IV and V, poly(lactic acid), chitosan, and starch were modified by incorporating amino acids to induce or enhance the antimicrobial properties of these polymers. Finally, Chapter VI focuses on the chemical modification of hydroxyapatite with the amino acid alanine to improve cell adhesion on the biomaterial's surface. All biomaterials were characterized regarding their physical, chemical, and structural properties. Additionally, biological characterizations, including cell viability and microbiological tests, were conducted, demonstrating the potential medical applications of these novel developed biomaterials.

Keywords: Polymers, Diels Alder reactions, biomaterials, amino acids, Click Chemistry.

SUMMARY

GENERAL INTRODUCTION	12
GENERAL OBJECTIVE	16
SPECIFIC OBJECTIVES	16
<i>CHAPTER I: SYNTHESIS OF THE ANTIMICROBIAL PRODRUG POLY(ASPARTIC ACID)- SULFAMETHOXAZOLE VIA A DIELS ALDER REACTION.....</i>	17
1 INTRODUCTION	17
2 MATERIALS AND METHODS	24
3 RESULTS AND DISCUSSION.....	30
4 CONCLUSIONS	39
<i>CHAPTER II: SYNTHESIS OF A NEW BISMALEIMIDE FROM L-LYSINE AND ITS CROSSLINKING WITH A FURAN POLYMER</i>	40
1 INTRODUCTION.....	40
2 MATERIALS AND METHODS	44
3 RESULTS AND DISCUSSION.....	48
4 CONCLUSIONS	53
<i>CHAPTER III: SYNTHESIS OF A CYSTEINE DIELS-ALDER BASED POLYMER BY SIMULTANEOUS DOUBLE CLICK CHEMISTRY AND ITS CYTO- GENOTOXICITY EVALUATION</i>	54
1 INTRODUCTION.....	54
2 MATERIALS AND METHODS	56
3 RESULTS AND DISCUSSION.....	61
4 CONCLUSIONS	70
<i>CHAPTER IV: LYSINE GRAFTED POLY(LACTIC ACID): AN INTRINSICALLY ANTIMICROBIAL POLYMER</i>	71
1 INTRODUCTION.....	71
2 MATERIALS AND METHODS	74
3 RESULTS AND DISCUSSION.....	79
4 CONCLUSION	89
<i>CHAPTER V: CHEMICAL MODIFICATION OF STARCH AND CYSTEINE FOR THE PREPARATION OF POLYSACCHARIDE CONJUGATES FOR BIOMEDICAL APPLICATIONS</i>	90
1 INTRODUCTION.....	90
2 MATERIALS AND METHODS	93
3 RESULTS AND DISCUSSION.....	100
4 CONCLUSIONS	113

CHAPTER VI: SYNTHESIS AND BIOLOGICAL PROPERTIES OF ALANINE GRAFTED HYDROXYAPATITE NANOPARTICLES	114
1 INTRODUCTION	114
2 MATERIALS AND METHODS	116
3 RESULTS AND DISCUSSION.....	119
4 CONCLUSIONS	129
REFERENCES	130

GENERAL INTRODUCTION

Lifestyle and the increasing average age of the global population have contributed to the rise in health problems, including tissue injuries. In many surgical cases involving small tissue loss, the injured tissue becomes the target of surgical approaches using grafts. These grafts can be autologous (taken from the patient's body), allogeneic (taken from an individual of the same species), or xenogeneic (taken from another species)(SHIBUYA; JUPITER, 2015). However, limiting factors in the use of these types of grafts include deficiencies at the donor site in the case of autologous grafts and immune response associated with rejection in the case of allogeneic and xenogeneic grafts (FERRAZ, 2023).

An alternative to reduce the problems related to the use of the mentioned types of grafts is the use of biomaterials for tissue repair. Biomaterials can be used for permanent or temporary substitution of tissues or organs and among them, biodegradable polymers such as poly (lactic acid) and poly-(caprolactone) stand out (PIRES; BIERHALZ; MORAES, 2015). One strategy to improve the quality of treatments for injured tissues and the quality of life of patients would be the regenerative medicine. Regenerative medicine involves the combination of cells and bioactive molecules with a biological support (biomaterial) for tissue regeneration. The support allows the growth of cells within it, which give rise to new tissue (BHAT; KUMAR, 2012).

In addition to the application of regenerative medicine mentioned above, biomaterials have broad applicability in the development of medical devices, such as implant materials (heart valves and bone substitutes), and devices used in hospital settings or procedures, such as nasal cannulas and catheters (ZANDER; BECKER, 2018). A challenge arising from the use of biomaterials and hospital-acquired infections is the increasing number of infections due to the use of polymer-based materials. This is attributed to the chemical properties of some of these polymeric devices, such as some polyurethane surfaces, which, despite having various applications in the medical field, have shown limitations. When their surface is hydrophobic, and in contact with bodily fluids, proteins can adhere to their surface, accumulating on the device's wall, leading to microbial adhesion and biofilm formation (JAIN et al., 2014).

Despite the advances in biomaterials over the past decades, there is still a limitation in terms of commercially available materials. Common problems with materials available for clinical use

are low degradation rates (e.g., PCL and derivatives), release of the synthesis byproducts such as catalysts and monomers, and generation of degradation byproducts that may be toxic to the body (HEIN; LIU; WANG, 2008).

The increase in the infection rates is not only attributed to the materials used in medical treatments but also to the growing increase in microbial resistance observed in recent times. This issue is primarily associated with the inadequate and indiscriminate use of antimicrobials in treatments. Therefore, it is crucial to not only to develop biomaterials with antimicrobial properties but also to enhance the efficacy of antimicrobial drugs to achieve effective treatments (MORRISON; ZEMBOWER, 2020; WEINER-LASTINGER et al., 2020).

Considering the specific properties required for medical use, this study focuses mainly on the design, preparation, and characterization of polymer-based and a ceramic- based biomaterials for medical applications. Several studies were carried out aiming the development of new biomaterials for healthcare applications and each work is presented as a chapter, as described in the next topics:

- **Chapter I. Synthesis of the antimicrobial prodrug poly(aspartic acid-sulfamethoxazole via a Diels Alder reaction):** Describes the synthesis of poly(aspartic acid) (PASP) from aspartic acid followed by its chemical modification by furan insertion. This derivate, PASP_{fur} was reacted via Diels Alder Reaction with a maleated sulfamethoxazole (SMX_{MA}), generating the $\text{PASP}_{\text{fur}}\text{-SMX}_{\text{MA}}$ adduct, that was analysed by physical chemical and biological characterizations, showing promising application as an antibiotic prodrug.
- **Chapter II. Synthesis of a new bismaleimide from L-lysine and its cross linking with a furan polymer:** Describes the synthesis of a new water soluble bismaleimide from L-lysine and its use to crosslink PASP_{fur} (Chapter I) by a Diels Alder reaction. The polymer was characterized by FTIR, ^1H NMR and rheology.
- **Chapter III. Synthesis of a cysteine Diels-Alder based polymer by simultaneous double click chemistry and its cyto-genotoxicity evaluation:** Describes the synthesis of the new polymer from cysteine, by click reaction with furan maleic anhydride adduct, a Diels Alder adduct. The mixture of the cysteine with the adduct in solution, gives rise to the

double simultaneous thiol-ene/amine maleimide click reactions. Preliminary safety and biocompatibility tests of this new polymer and its starting reagents were carried out. This material is interesting for application in several fields, since it has the advantage of using natural and renewable raw materials, in addition to its handling safety.

- ***Chapter IV: Lysine grafted poly(lactic acid): an intrinsically antimicrobial polymer:*** In this work, in order to infer antimicrobial activity to poly(lactic acid), it was modified by maleation, followed by L-lysine grafting to its structure. The chemical modifications were confirmed by FTIR and ¹H NMR analysis. The antimicrobial activity was tested using *Escherichia coli* and *Staphylococcus aureus* and the results showed that the modified PLA (PLA-g-Lys) was capable of inhibiting about 99 % of the *S. aureus* and about 80% of the *E. coli* growth by contact. Cytotoxicity was also tested using the L929 mouse cells and the results indicated no cytotoxic effect. These results indicated the sample antimicrobial potential, without affecting the normal eukaryotic cells. In addition, the processability of PLA-g-Lys was improved without compromising its mechanical properties, as shown by thermal analysis and tensile tests. Thus, this novel PLA derivative can be seen as a promising material for future applications in the manufacturing of biomedical devices.

- ***Chapter V: Chemical modification of starch and cysteine for the preparation of polysaccharide conjugates for biomedical applications:*** In this work, starch was successfully transformed into its methacrylated derivative, and then submitted to a Thiol-Michael addition between the double bond of the methacrylic moiety and the thiol group of cysteine. The product of the Thiol-Michael reaction was then subjected to an exhaustive methylation reaction. Besides, an exhaustive methylation of chitosan allowed it to synthesize its quaternary ammonium salt. Furthermore, chitosan was also modified with L-Cysteine, using NHS-EDC as activating of the amino acids' carboxyl group and the product was also submitted to an exhaustive methylation reaction, affording its ammonium quaternary salt. These derivatives were evaluated by FTIR, ¹H and ¹³C NMR, conductometric titration, zeta potential, Ellman's assay and as antimicrobial agents against *Escherichia coli* and *Staphylococcus aureus*, showing a greater methylation for the methylated chitosan and methylated chitosan- Cys and a greater antibacterial activity of these samples. This work was conducted at the Instituto

Tecnologico de Buenos Aires (ITBA) during a research internship in Buenos Aires, Argentina.

- **Chapter VI: Synthesis and biological properties of alanine grafted hydroxyapatite nanoparticles:** Effect of amino acid grafting on Hydroxyapatite (HAp) nanoparticles was investigated in biocompatibility. To this, two L-alanine sources (L-alanine acid and L-alanine methyl ester hydrochloride) and three grafting methods (simple mixing, thermal induction and *in situ* grafting) were used for HAp surface functionalization. The efficiency of grafting was determined by X-ray powder diffraction (XRPD), UV-VIS spectroscopy, Fourier-transform infrared spectroscopy (FTIR), thermal analyses (TG/DTA, DSC), and field emission scanning electron microscopy (FESEM). Protein adsorption, cell adhesion and viability studies were carried out to evaluate biological properties of the materials. The alanine grafted HAp prepared *in situ* and by simple mixture showed the most promising properties for cell adhesion, indicating their potential use as a graft.

This work was the result of scientific visit to the Institute of Technical Sciences of the Serbian Academy of Sciences and Arts (ITS-SASA) in Belgrade, Serbia.

GENERAL OBJECTIVE

The general objective of this work was to develop new biomaterials for medical applications, including tissue repair and medical devices, using mainly from Click Chemistry reactions for their preparation.

SPECIFIC OBJECTIVES

- Synthesis of poly(aspartic acid) from aspartic acid, and its physical-chemical characterization;
- Chemical modification of poly(aspartic acid), inserting a furan group into its structure, and the physical and chemical characterization of the product;
- Synthesis and characterization of a new bismaleimide from the amino acid lysine;
- Crosslinking the modified PASP and bismaleimide, by Diels Alder reaction, and its rheological characterization;
- Chemical modification of the antibiotic sulfamethoxazole by maleation and the physicochemical characterization of the product;
- Diels Alder reaction between modified PASP and modified sulfamethoxazole, for preparation of a new prodrug and the physicochemical and biological characterization of the product;
- Synthesis of a new polymer from the amino acid cysteine and furan adduct maleic anhydride and its physicochemical and biological characterization;
- Chemical modification of chitosan and starch by reaction with the amino acid cysteine and posterior methylation to synthesize polysaccharide conjugates with antimicrobial properties. Physical-chemical and biological characterization of the materials;
- Chemical modification of hydroxyapatite inserting alanine into its structure and physicochemical and biological characterization of the materials.

CHAPTER I

SYNTHESIS OF THE ANTIMICROBIAL PRODRUG POLY(ASPARTIC ACID)-SULFAMETHOXAZOLE VIA A DIELS ALDER REACTION

1 INTRODUCTION

1.1 Antimicrobial resistance

Antimicrobial resistance (AMR) is a global multifaceted challenge and occurs when microorganisms such as bacteria, viruses and fungi do not respond to treatment with antimicrobials (ABUSHAHEEN et al., 2020). In this way, these medications become ineffective, making it difficult to treat infections and increasing the risk of disease spread, patient disability and even death (MORRISON; ZEMBOWER, 2020).

Clinically, it is responsible for high rates of unsuccessful treatments, leading to prolonged hospitalizations and an increase in the number of deaths, also causing losses in the veterinary and agricultural sectors, as plants and animals are also affected by microbial infections caused by resistant pathogens (ANJUM et al., 2021). It is estimated that bacterial AMR was directly responsible for 1.27 million global deaths in 2019 and contributed to 4.95 million deaths. Furthermore, resistance rates among bacterial pathogens reported in 76 countries were 42% for third-generation cephalosporin-resistant *Escherichia coli* and 35% for methicillin-resistant *Staphylococcus aureus*. In 2020, according to this report, in urinary tract infections caused by *E. coli*, 1 in 5 cases showed reduced susceptibility to standard antibiotics such as ampicillin, co-trimoxazole and fluoroquinolones (MURRAY et al., 2022).

Economically, it generates high costs and long- time treatment, overloading health systems (PULINGAM et al., 2022). According to the World Bank, additional health care costs will amount to \$1 billion by 2050 (MURRAY et al., 2022). Furthermore, AMR can compromise medical procedures, such surgeries and therapies, causing the nosocomial infections.

The AMR's is a global problem that impacts all countries and does not depend on the development levels of each country (MAJUMDER et al., 2020). But its consequences are greater in poor countries, due to less access to basic sanitation and more effective and modern treatments against infections caused by resistant pathogens.

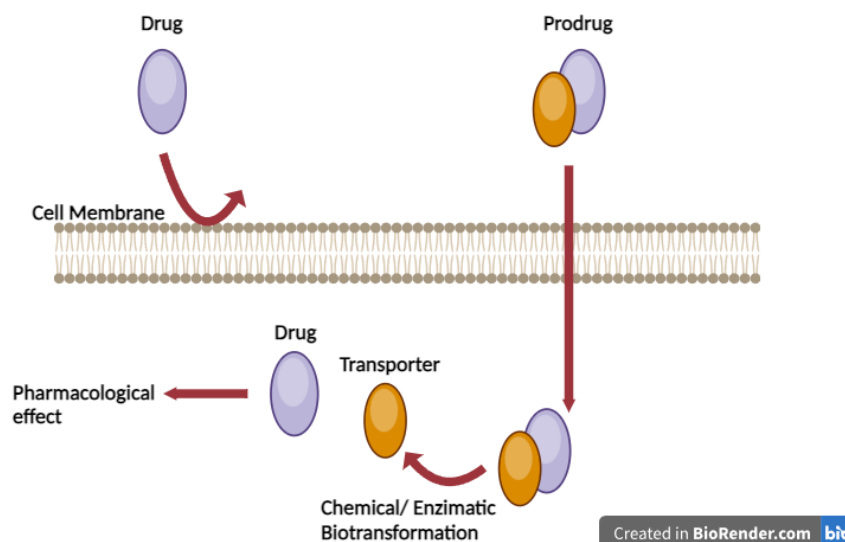
AMR occurs naturally over time by genetic changes in pathogens. However, its emergence and spread are accelerated by human activity, mainly by the improper and excessive use of antimicrobials to treat, prevent or control infections in humans, animals and plants

(MURUGAIYAN et al., 2022). Priorities for combating AMR include preventing infections, which can result in inappropriate use of antimicrobials; ensure universal access to quality diagnosis and adequate treatment of infections; and strategic information and innovation, for example, surveillance of AMR and antimicrobial use, and research and development of new vaccines, diagnostics and medicines. In this sense, the search for new antimicrobial drugs and/or improvement of existing drugs is extremely important, aiming to develop therapeutic alternatives against resistant pathogens (JIN et al., 2022).

1.2 Prodrugs

The entry of new drugs onto the market requires time and investment. Drug solubility is a crucial factor that can influence its effectiveness and success in treatment. In antibiotics, the solubility can influence in various factors like bioavailability, once solubility is important for the drug to be absorbed into the bloodstream and higher solubility ensures that drug reaches therapeutic levels, enhancing its ability to combat infections; tissue penetration and uniform distribution, due the fact of soluble antibiotics can better penetrate tissues and reach the site of infection; efficacy and potency, once solubility impacts the concentration and lead to a faster onset of action. Furthermore, higher solubility can impact at drug absorption rate and excretion, maintaining consistent levels of the antibiotic in the bloodstream and helping the prevention of the development of antibiotic resistance. Therefore, one way to solve the solubility problems of existing drugs is the development of prodrugs (DHARUN et al, 2021; GUPTA et. al, 2009). A classic strategy for optimizing drug action is latentiation, which consists of transforming the drug into an inactive form, or prodrug, which when released *in vivo* undergoes chemical or enzymatic reactions, becoming active at the site of action or near that location. The transformation of a drug into a prodrug has several uses, including: increased site specificity, decreased toxicity of certain medications and increased bioavailability and solubility of the drug, which occurs when water-soluble groups are linked to the drug molecules (CHUNG et al., 2005; SHAH et al., 2020). A general scheme of prodrug conception is shown in Figure 1.

Figure 1. General scheme of a prodrug. Adapted from Chung et. al, 2005 (CHUNG et al., 2005)



Conventional prodrug activation strategies often rely on intrinsic changes at the site of action, such as overexpressed enzymes, an acidic pH microenvironment, and an increase in reactive oxygen species (ROS). These changes are highly specific for prodrug activation and can result in a generalized action of the drug, leading to an increase in adverse reactions (WANG et al., 2020).

Therefore, the search for new prodrugs based on milder and more specific reactions has grown. In this context, the strategy of using Click reactions has been highlighted.

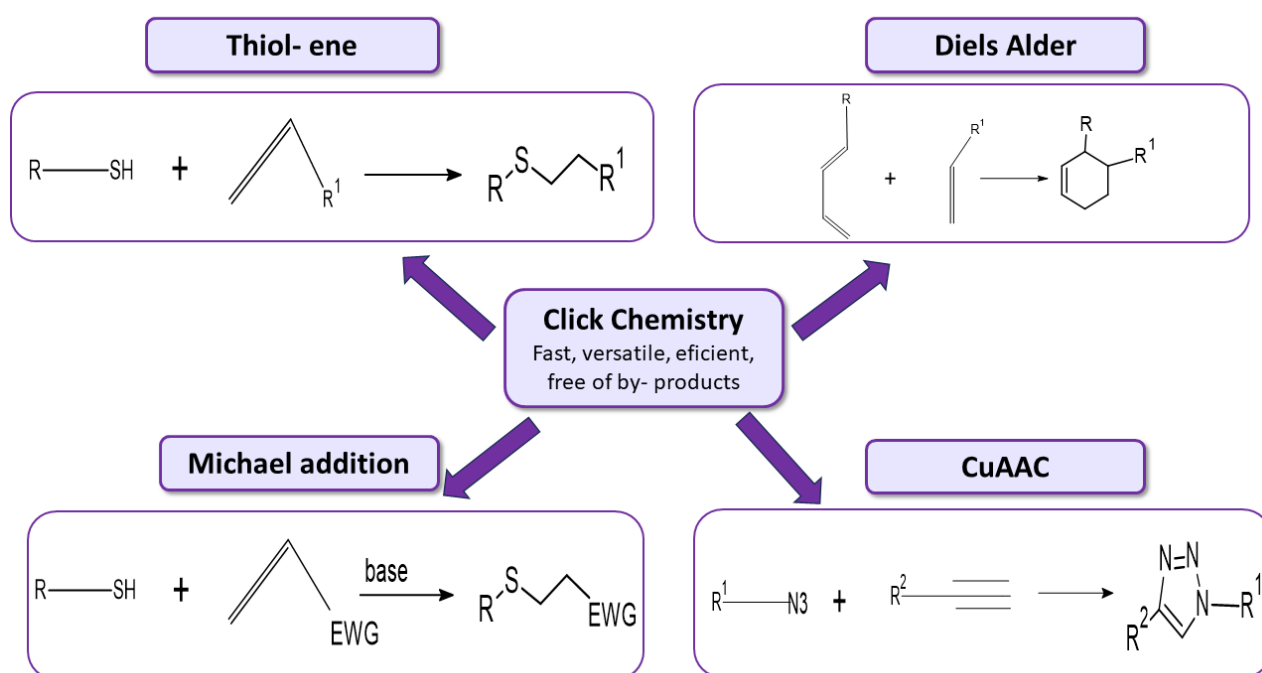
1.3 Click Chemistry

Click chemistry reactions are based on pairs of functional groups that react quickly and selectively, for this reason the name 'click'. Moreover, these reactions have high yields, do not require catalysts or initiators, have easily isolable products, are virtually free of by-products and generally are stable in physiological conditions (HEIN; LIU; WANG, 2008).

Due to these characteristics, Click Chemistry reactions have been extensively studied for their application in the medical field, as residues or catalysts from conventional reactions often have side effects. Therefore, Click Chemistry reactions have a lower chance of affecting the biocompatibility of the resulting product. Medical applications of these reactions include the development of new drugs, bioactive molecules, and polymers (BATTIGELLI; ALMEIDA; SHUKLA, 2022).

Several reactions can be classified as Click Chemistry, with the most common ones being copper(I)-catalyzed azide-alkyne cycloaddition (CuAAC), copper-free strain-promoted azide-alkyne cycloaddition (SPAAC), thiol-ene, Thiol- Michael addition, and the Diels-Alder (DA) reaction (OZTURK; AMNA, 2021). Some examples of these reactions are presented in Figure 2.

Figure 2. Some examples of Click Chemistry reactions. Adapted from Geng et al, 2021 (GENG et al., 2021)



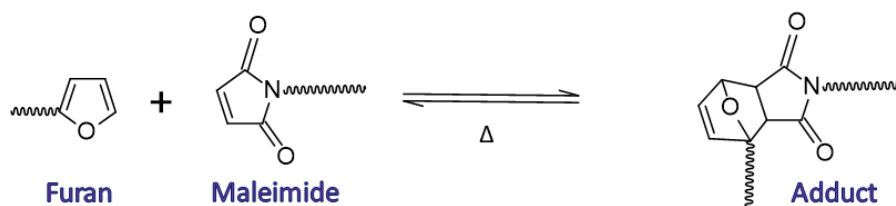
The Diels Alder reaction was introduced in 1928 by German chemists Otto Diels and Kurt Alder, who were awarded the Nobel Prize in 1960 for the discovery of the reaction (GREGORITZA; BRANDL, 2015). Diels-Alder reactions are widely used in the synthesis of organic compounds and, like all Click reactions, they are simple, efficient, clean (no generation of reaction by-products), and they are thermoreversible, can be conducted at room temperature, and can occur in water.

The DA reaction is also known as [4+2] cycloaddition because it combines a four-electron π system (the diene) with a two-electron π system (an alkene, the dienophile). This cycloaddition between the diene and the dienophile occurs by a concerted mechanism, meaning that the breaking and formation of chemical bonds happen in one step (SMITH et al., 2018). The product of this reaction is a stable cyclohexene, named adduct. Like other Click reactions, the DA reaction is used in various fields and applications, such as pharmaceutical product modification,

development of polymers and biopolymers, preparation of hydrogels for drug delivery, and tissue engineering (ANTUNES et al., 2022; CADAMURO; RUSSO; NICOTRA, 2021).

One of the most commonly used diene-dienophile pairs in DA reactions is the furan-maleimide pair (Figure 3). In this pair, there is an interesting characteristic regarding the reversibility of the DA reaction: Between 30 and 60 °C, the reaction is shifted toward the coupling of furan with maleimide, i.e., the formation of the adduct (GANDINI; BELGACEM, 2008a). However, at temperatures close to 100 °C, the reaction becomes shifted toward the recovery of the reactants (GANDINI, 2013). For use in the synthesis of biomaterials for use inside the body, the first step is the most used, once the retro-DA is not performed at low body temperature.

Figure 3. General scheme of a Diels-Alder reaction involving furan-maleimide.



1.4 Poly(aspartic acid)

Poly(aspartic acid) (PASP) is a polymer synthesized from aspartic acid, an amino acid found in many proteins very often present in animal and plant tissues. There are three different methods for PASP synthesis: i) thermal polymerization under microwave irradiation; ii) polycondensation of *N*-carboxyanhydride (NCA) or activated esters; and iii) bulk thermal polymerization of aspartic acid using acid catalysis, with the intermediate product poly(succinimide) (PSI) (KUMAR, 2012). The latter is the simplest and most commonly used methodology for PASP synthesis. In this method, aspartic acid and phosphoric acid are heated to 200 °C, eliminating water and forming poly(succinimide). PSI reacts with sodium hydroxide in an aqueous medium, causing partial cleavage of its ring and generating PASP. Advantages of this methodology include lower condensation temperature and reaction time, as well as high yield, favoring its industrial-scale application (MATSUBARA; NAKATO; TOMIDA, 1997; NAKATO; KUSUNO; KAKUCHI, 2000).

PASP has been studied due to its many interesting characteristics, such as biodegradability and water solubility, making it an excellent alternative to replace polycarboxylates and polyacrylates, which have low degradation rates, in applications such as detergent composition, dispersants, and water treatment, reducing the environmental impact caused by conventional polymers (KUMAR, 2012). Another promising application is in the development of energy storage batteries which is capable of storing and releasing electrical energy with high efficiency (ZHOU et al., 2022). In addition to these applications, PASP has great potential for biomedical use, such as scaffolds, controlled drug release agents, and orthopedic implants (ADELNIA et al., 2021).

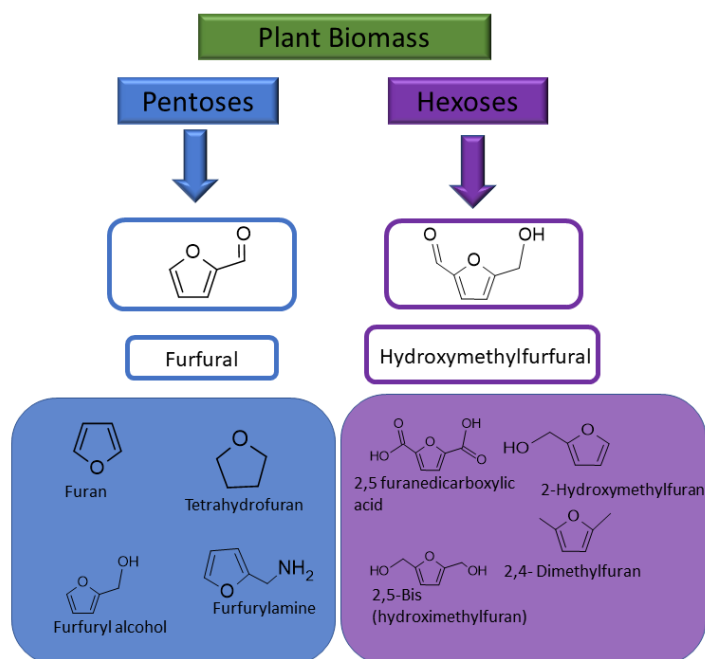
1.5 Furanic Compounds

Furanic compounds are organic molecules with a furan ring (a heterocyclic compound containing four carbons and one oxygen) in their structure. They are furfural and hydroxymethylfurfural derivatives, from acid hydrolysis of cellulose and hemicellulose, polysaccharides that make up plant biomass, such as sugarcane bagasse, rice husks, oats, and wood (GANDINI; BELGACEM, 2008a).

There is a wide range of furan derivatives, making this molecule extremely versatile. Some examples of these derivatives are tetrahydrofuran (THF) and furfuryl alcohol, being this last one the most abundant in the industry due to its application in resin production. Other derivatives of furfural and hydroxymethylfurfural are shown in Figure 4. These derivatives are widely used in the industry as solvents, varnishes, resins and intermediates in the synthesis of pharmaceutical and agrochemical products. Moreover, there is a growing interest in studying their application as biofuels and biodegradable plastics, precisely because they are derived from industrial by-products, making them renewable and sustainable (YONG et al., 2022).

Due to their chemical structure, furan compounds can act as dienes in Diels-Alder reactions, making them an interesting material for such purposes, especially since they are highly diverse and have a natural and renewable origin.

Figure 4. Furanic compounds Adapted from Fernandes,2021



Considering the prodrugs obtained from click chemistry reactions, studies involving a novel dual-responsive prodrug nanogel was synthesized using a Diels-Alder reaction, incorporating doxorubicin, and demonstrated selective toxicity towards cancer cells while remaining stable under physiological conditions was found (CAO et al., 2021). Additionally, another study involving a dual-responsive core cross-linked micelle system for prednisolone 21-acetate (PA) was efficiently prepared using alkyne-azide click chemistry, offering high drug loading efficiency, structural stability under physiological conditions, and controlled release in response to pH and reduction conditions (CAO et al., 2016). Regarding the Diels Alder reaction, several studies involving the furan-maleimide pair were found for the production of mainly antitumor agents, for example Pt(IV) complexes, considered antitumor prodrugs, were successfully functionalized with maleimide-containing ligands for drug targeting, and demonstrated the ability to undergo click reactions with furan and silica nanoparticles, highlighting their potential for targeted drug delivery (GABANO et al., 2019).

Regarding studies involving the synthesis of antimicrobial prodrugs through click chemistry reactions, few studies have been found in the literature, such as biodegradable microsphere carrier with bone-targeting properties was developed for local antibiotic delivery, demonstrating sustained antibiotic release and enhanced affinity to bone minerals, potentially improving treatment of persistent bone infections (ROTMAN et al., 2020). Thus, the study of

the use of the furan-maleimide pair for the synthesis of new antimicrobial prodrugs via Diels Alder reaction is an open area to be explored.

Considering the topics covered above, the objective of this chapter was to synthesize a new prodrug by modifying sulfamethoxazole with poly(aspartic acid). Sulfamethoxazole is a widely used antibiotic, poorly soluble in physiological environments. The focus was on increasing the drug's solubility aiming to enhance its bioavailability and antimicrobial activity. To achieve this aim, PAsp was synthesized from aspartic acid using an acid catalysis strategy, followed by esterification to incorporate furan groups into its structure, generating PAsp_{fur}. Meanwhile, sulfamethoxazole was modified by maleation, enabling it to react with PAsp_{fur} via Diels-Alder reaction. The reaction products were characterized by physical, chemical, and biological analyses, revealing its potential as a prodrug.

2 MATERIALS AND METHODS

2.1 Materials

L- aspartic acid 99%, Phosphoric acid 98%, deionized water, methanol 100%. L-lysine (monohydrochloride), ethanol, hydrochloric acid (HCl), and sodium hydroxide (NaOH) were purchased from Synth (São Paulo, Brazil). Dimethyl sulfoxide (DMSO) and glycerol, both purchased from Exodo Científica (São Paulo, Brazil). Furfuryl alcohol, deuterium oxide (D₂O), and deuterated DMSO were acquired from Sigma-Aldrich (Saint Louis, USA). Furan-maleic anhydride adduct (previously synthesized according to a methodology already used by the group)(GANDINI; COELHO; SILVESTRE, 2008a). Nutrient broth (beef extract 1.0; yeast extract 2.0; peptone 5.0; sodium chloride 5.0 g. L⁻¹, Kasvi, (São Paulo, Brasil), Agar (Dinâmica, São Paulo, Brasil), Tryptone Soya Broth (Himedia, Nashik, India) and distilled water. *Escherichia coli* (ATCC 43895), *Staphylococcus aureus* (ATCC 25923) and methicillin-resistant *Staphylococcus aureus* (ATCC 33591).

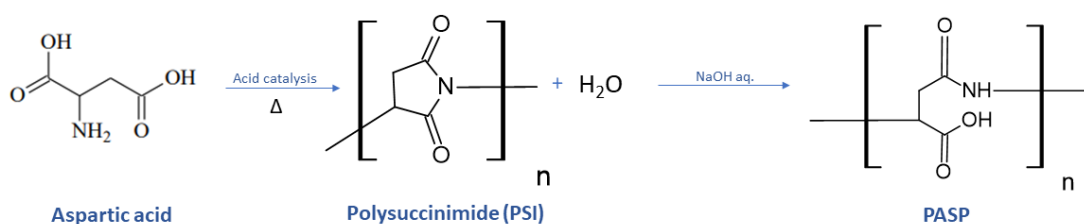
2.2 Methods

2.2.1 Synthesis of PASP from Aspartic Acid

Aspartic acid (100 g) and phosphoric acid (5.32 mL) were mixed. The resulting mixture was transferred to a Petri dish and subjected to a vacuum oven at 200 °C for 6 hours. Every two hours, the mixture was homogenized by manual stirring. Following this period of time, the sample rest to cool and was then washed with distilled water until reaching a neutral pH. It was then rinsed with methanol. The product, polysuccinimide (PSI) was dried in a vacuum oven at 85° C for approximately 5 hours.

In the second step, sodium hydroxide (32 g) was dissolved in deionized water (460 mL). This solution was then placed in a beaker, which was submerged in an ice bath with continuous stirring. During stirring, PSI was gradually introduced. After this procedure, the solution continued stirring without the ice bath for one hour. The solution was precipitated in 10 times its volume of methanol, cooled to -10 °C. The resulting precipitate was vacuum-filtered using a Büchner funnel. The product, poly(aspartic acid) (PASP), was dried in a vacuum oven at 40°C on Teflon® plates for 7 days. The reaction scheme is show in Figure 5.

Figure 5. Synthesis of PASP from aspartic acid.



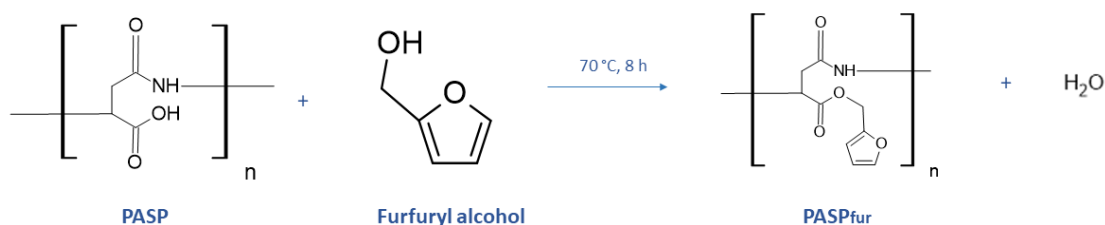
2.2.2 Modification of PASP by esterification

The methodology for PASP modification was adapted from Antunes et al (ANTUNES et al., 2022). In a round-bottom flask, PASP (1 g) was wet using distilled water (50 μ L). Then, furfuryl alcohol (200 μ L) and 0.1 M HCl (60 μ L) were added to the mixture. The reaction proceeded

for eight hours at 70 °C under magnetic stirring at 200 rpm. After this period of time, 0.1 M NaOH solution (250 μ L) was added to stop the reaction.

The reaction product was washed with ethanol six times, resulting in a viscous material that stayed at room temperature for solvent evaporation, generating the PASP_{fur} product. The reaction scheme is shown in Figure 6:

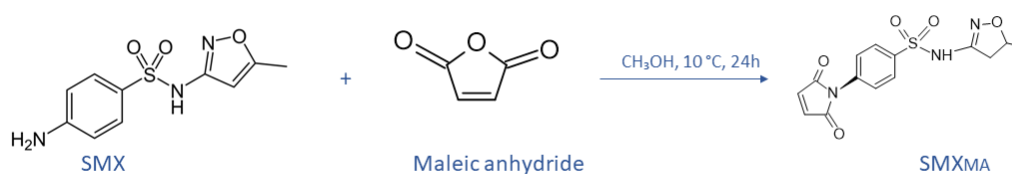
Figure 6. Esterification reaction of PASP for furan group insertion.



2.2.3 Chemical modification of sulfamethoxazole (SMX)

Maleic anhydride (0.98g) was dissolved in methanol (5 mL). SMX (2.53 g) was dissolved in 5 mL of methanol and then dropped into the maleic anhydride solution at room temperature and continuous stirring. The reaction was carried out at 10 °C for 24 hours. Following the reaction, the solution remained at room temperature for 48 hours to facilitate the evaporation of the solvent. Crystallization was observed during this process, forming the SMX_{MA} product. The reaction scheme is shown in figure 7.

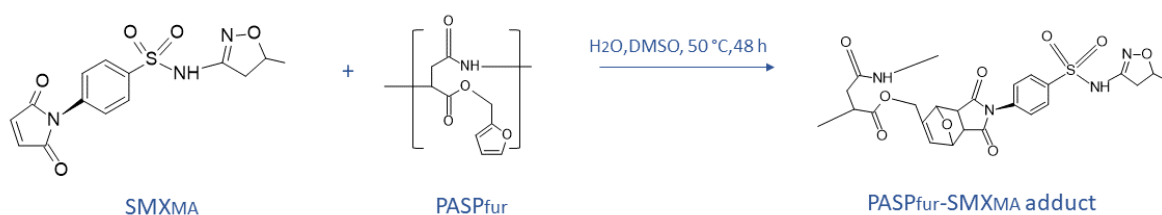
Figure 7. Chemical modification of SMX by maleation.



2.2.4 PASP_{fur}-SMX_{MA} adduct synthesis

PASP_{fur} (0.514 g) was solubilized in distilled water (3 mL). SMX_{MA} (0.32 g) was added to the solution. The reaction was carried out for 30 minutes at 50°C. DMSO (2 mL) was added. The reaction continued for 48 hours. The product was dried in an oven at 50 °C for 48 hours, washed with methanol three times in a centrifuge at 3000 rpm for 2 minutes, and dried at room temperature, generating the product, PASP_{fur}-SMX_{MA} adduct. The reaction scheme is represented in Figure 8.

Figure 8. PASP_{fur}-SMX_{MA} adduct synthesis by Diels Alder reaction.



2.2.5 Characterization

2.2.5.1 Gel permeation chromatography

Chromatogram analysis was used to determine the molar mass and corresponding distribution of PSI. Data were obtained on a Shimadzu model LC-10 AD HPLC chromatograph with refractive index detector. For analysis, a combination of four columns was used, two Styragel HR 4 and two Styragel HR 5, filled with rigid particles of the poly(styrene-co-divinylbenzene) copolymer. Calibration was performed using polystyrene standards, Scientific Polymer Products, with molar masses between 2,500 and 600,000 g mol⁻¹. Tetrahydrofuran (THF) was used as eluent and to prepare the standards and samples, a mass of 5 mg dissolved in 2 mL of tetrahydrofuran was used. Measurements were carried out at 23 °C with a flow of 0.7 mL×min⁻¹.

2.2.5.2 Fourier Transform Infrared Spectroscopy (FTIR)

Aspartic acid, PSI, PASP, PASP_{fur} , SMX, SMX_{MA} and $\text{PASP}_{\text{fur}}\text{-SMX}_{\text{MA}}$ adduct samples were analyzed using a Perkin-Elmer Spectrum 100 FT-IR Spectrometer equipped with an attenuated total reflectance (ATR) device of diamond coated with zinc selenide crystal. The spectra were in the range of 650 to 4000 cm^{-1} , with 4 cm^{-1} resolution and 16 scans, the spectral outputs were recorded in transmittance.

2.2.5.3 ^1H Nuclear Magnetic Resonance (^1H NMR)

^1H NMR spectra were acquired using a Bruker Avance II HD equipment, at 600 MHz. The samples were dissolved in deuterated solvent at 1 % wt. (w/v). The parameters used 11 s 90° pulse width; recycle delay 500 ms; acquisition time: 3.9s; 16 scans, spectral width 6.4 and lb.: 1. The PASP, PASP_{fur} and $\text{PASP}_{\text{fur}}\text{-SMX}_{\text{MA}}$ adduct were dissolved in D_2O at 1% concentration (m/v) while the SMX and SMX_{MA} was dissolved in $\text{DMSO-}d_6$, in the same concentration.

2.2.5.4 Conductometric Titration

The number of carboxylic groups in PASP samples before and after chemical modification by esterification was determined by conventional conductometric titration using NaOH (0.1 M) as the titrant. For this, PASP (100 mg) and PASP_{fur} (100 mg) were dissolved in distilled water (3 mL). The pH of this solution was adjusted to 2.5 with 0.1 M HCl. The titration was performed by pipetting NaOH solution ($50\text{ }\mu\text{L}$) at 20-second intervals under magnetic stirring at 200 rpm and room temperature. Equation 1 was used for the quantification of carboxylic groups in the samples:

$$X = [C \cdot (v_2 - v_1)] / w \quad (1)$$

Where: C is the titrant concentration, W is the sample mass and V_1 e V_2 are the volumes of titrant solution (in liters) used to neutralize and determine the carboxyl groups in the sample.

2.2.5.5 Melting Point Determination

SMX (5 mg), PASP_{fur} (5 mg), and $\text{PASP}_{\text{fur}}\text{-SMX}_{\text{MA}}$ adduct (5 mg) were weighted in an analytical balance and dried in an oven for 24 hours at 50 °C. Then, each sample was insert into the capillary tube and the melting point apparatus (Mod. 431D-Fisatom) was calibrated to 80 V power. The capillary tube loaded with the sample was inserted into the melting point apparatus and the samples were observed with a magnifying lens until the melting point was reached. Then, the temperature was recorded. This analysis was made in triplicate.

2.2.5.6 Minimum inhibitory concentration (MIC)

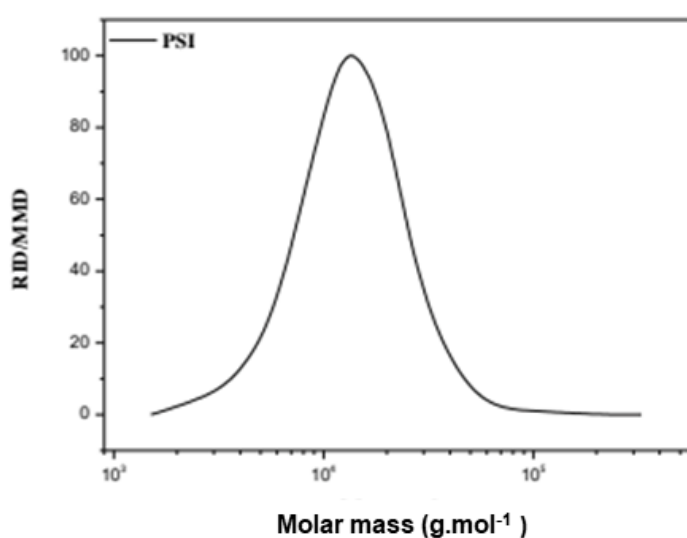
The antibacterial activity of PASP_{fur} and $\text{PASP}_{\text{fur}}\text{-SMX}_{\text{MA}}$ adduct samples was measured by minimum inhibitory concentration (MIC) against *E. coli*, *S. aureus* and methicillin- resistant *S. aureus* (MRSA). PASP_{fur} and $\text{PASP}_{\text{fur}}\text{-SMX}_{\text{MA}}$ adduct were tested at concentrations between 1.25- 20 mg/ mL against *E. coli* and *S. aureus* and 2.5- 40 mg/ mL against MRSA; serial dilutions of each sample were prepared in liquid culture medium. To prepare inoculum, bacteria were inoculated in nutrient agar and grown for 18 hours at 37 °C. Microorganisms were then suspended into 0.85 % sterile sodium chloride solution to reach the turbidity equivalent to McFarland standard 0.5 ($\sim 1.5 \times 10^8$ CFU. mL⁻¹). Further dilutions were performed with sterile 0.85 % sodium chloride solution to reach a bacterial concentration of 1×10^6 CFU. mL⁻¹. A control containing only culture medium, a negative control containing culture medium and bacterial inoculum, as well as a positive control containing SMX (20 mg/mL to *S. aureus* and *E. coli* and 40mg/mL to MRSA assay), culture medium and bacterial inoculum were included. The tubes were incubated at 37 °C for 18 hours, after which the results were optically read at 600 nm. The MIC was considered the lowest concentration of antimicrobial that inhibits visible bacterial growth.

3 RESULTS AND DISCUSSION

3.1 Gel Permeation Chromatography

The molar mass distribution is shown in figure 9. The weight-average molar mass of poly(succinimide) was $1.627 \times 10^4 \text{ g.mol}^{-1}$.

Figure 9. Molar mass distribution of PSI

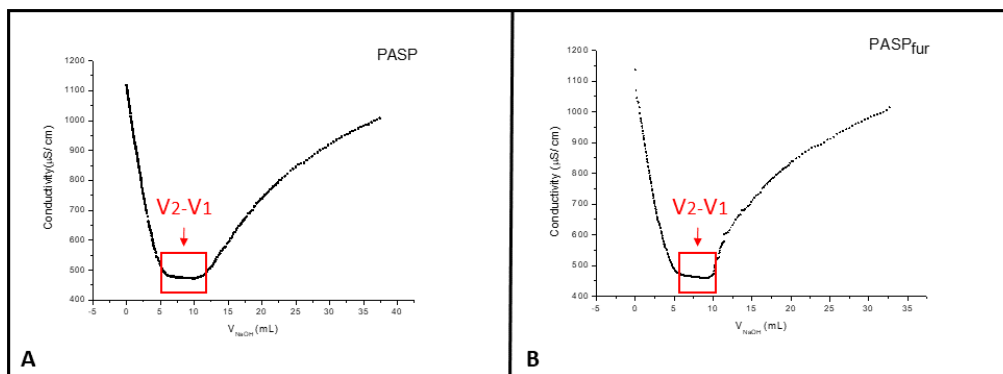


This value aligns with the founded in the literature under similar reaction conditions (KIM et al., 2011)), indicating that the intermediate reaction product was successfully synthesized.

3.2 Conductometric Titration

The graphs from the conductometric titration of PASP and PASP_{fur} samples, respectively, are represented in figure 10. It shows that the volume of titrant used in the titration of the PASP_{fur} sample is smaller than the volume used in the titration of the PASP sample, indicating the substitution of carboxylic groups by furan groups (ANTUNES et al., 2022).

Figure 10: Conductometric titration of PASP (A) and PASP_{fur} (B).

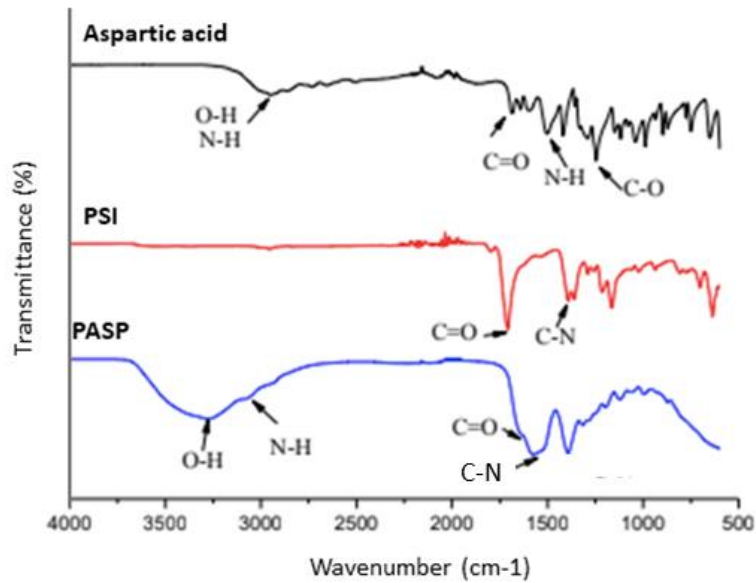


After the titration, the volume of titrant used was determined based on the volume used in the region where the recorded conductivity is stable (highlighted in the graphs in image 10). This volume was used to determine the degree of substitution of carboxylic groups in the samples using Equation 1. Thus, the degree of substitution of carboxylic groups in PASP_{fur} was determined to be 1.07 mmol/ g. Then, 20 % of the carboxylic groups in poly(aspartic acid) were esterified.

3.3 FTIR

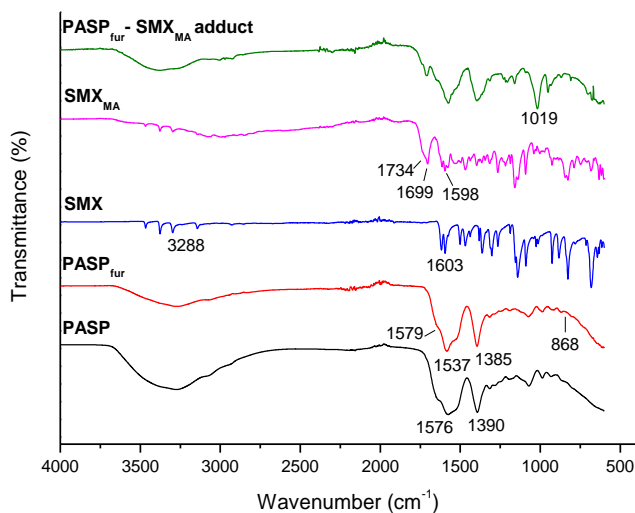
The poly(succinimide) product showed a low content of the O-H group, after drying, and was used in the next stage of the synthesis of poly(aspartic acid). The product of the polymerization of aspartic acid into poly(aspartic acid) with an intermediate product of poly(succinimide) is a combination of the functional groups of the reactants, presenting groups with N-H, C-N and C=O bonds (KIM et al., 2011). The spectra for aspartic acid, poly(succinimide) and poly(aspartic acid) are represented in Figure 11.

Figure 11. FTIR spectra of Aspartic acid, PSI and PASP



The FTIR spectra of PASP, SMX and its derivatives are shown in Figure 12. In PASP spectrum, the bands in 1576 and 1600 cm^{-1} are due to the C-N and C=O, respectively (KIM et al., 2011; YOSHIKAWA et al., 2024). In the PASP_{fur} spectrum, these bands are preserved, but new bands appear in 1579 and 868 cm^{-1} and are related to the furan bands (D'AMICO et al., 2021), inserted in the PASP structure after the esterification. The SMX spectrum shows characteristic bands in 3288 and 1603 cm^{-1} related to NH₂ groups and C=N ring, respectively (PERVAIZ et al., 2020). These bands turn weaker in SMX_{MA} spectrum and bands in 1734 and 1699 cm^{-1} appear, related to maleimide groups inserted in SMX structure after reaction with maleic anhydride. Finally, in PASP_{fur}-SMX_{MA} adduct spectrum a new band in 1019 cm^{-1} , related to C-O-C in adduct structure, indicating the Diels Alder reaction between PASP furan and SMX maleimide.

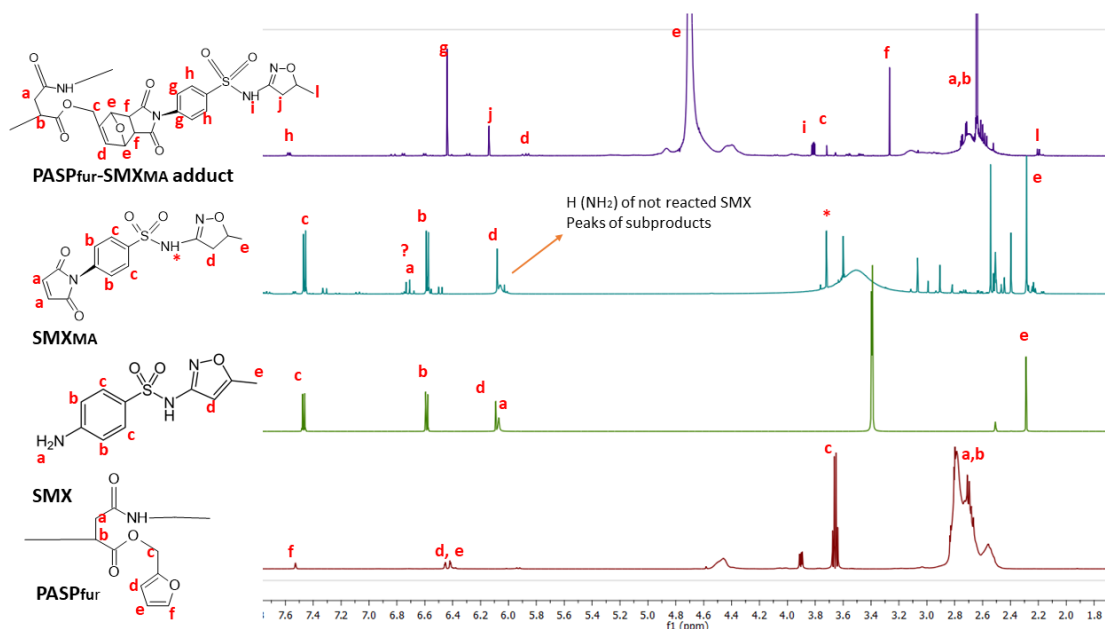
Figure 12. FTIR spectra of PASP, PASP_{fur}, SMX, SMX_{MA}, and PASP_{fur}-SMX_{MA} adduct.



3.4 ¹H NMR

¹H NMR spectra of PASP_{fur}, SMX, SMX_{MA} and PASP_{fur}-SMX_{MA} adduct are shown in Figure 13. PASP_{fur} spectrum shows peaks at 2.6 and 2.8 ppm, correspondent to CH₃ and CH protons of polymer backbone (ADELNIA et al., 2021), peaks at 6,4, 6,3 and 7,5 ppm correspond to furan protons inserted into PASP structure after esterification (TROVATTI et al., 2015a). SMX spectra shows typical peaks like **b** and **c**, correspondent to the benzene ring of SMX and **d**, correspondent to the methylene protons (BORMIO NUNES et al., 2015). In **a**, it is shown the peak from NH₂ protons. In the SMX_{MA} spectrum, the SMX peaks are preserved, except the peak of NH₂ protons, with the appearance of a new peak in 6,9 ppm, correspondent to the maleimide protons (TROVATTI et al., 2015b). Actually, the peak in **a**, is preserved in SMX_{MA} spectrum, corresponding to the untreated SMX. Another small double peak is observed in this spectrum, which can correspond to subproducts generated in the maleation reaction. In the adduct spectrum, peaks correspondent to PASP_{fur} and SMX_{MA} appears, in addition to new peaks in **c**, **e** and **f**, corresponding the furan maleimide adduct formed after Diels Alder reaction (GIL ALVARADEJO et al., 2018), indicating that the reaction occurred.

Figure 13. ^1H NMR spectra of PASP_{fur} , SMX , SMX_{MA} and $\text{PASP}_{\text{fur}}\text{-SMX}_{\text{MA}}$ adduct



3.5 Melting Point Determination

The temperatures recorded for each sample analyzed were as follows: 169 °C for SMX, while $\text{PASP}_{\text{fur}}\text{-SMX}_{\text{MA}}$ adduct began to melt at 220 °C, not completing its melting until 300 °C, the detection limit of the equipment. The PASP_{fur} sample did not begin to melt until the 300 °C analyzed.

Melting point determination is a complementary analysis in chemistry used to assess the purity, identity, and thermal properties of organic compounds. The melting point of 169 °C for SMX is in concordance with the literature values typically reported for this compound (ALTAMIMI; NEAU, 2018). Sulfamethoxazole, a sulfonamide antibiotic, is known for its relatively low melting point. The consistency between the experimental result and literature values indicates the high purity and integrity of the sulfamethoxazole sample analyzed.

PASP, a polymer, tends to exhibit higher melting points compared to small organic molecules like sulfamethoxazole (PEREIRA et al., 2020). The melting point exceeding 300 °C for PASP suggests its high thermal stability. The modification of PASP with SMX introduces chemical alterations that may impact its thermal properties, including its melting point. The intermediary melting point for the PASP_{fur} suggests the partial influence of the chemical modification on the thermal behavior of the polymer. This result implies that while the incorporation of sulfamethoxazole affects the thermal properties of PASP, it does not entirely alter its thermal stability. The intermediary melting point of PASP_{fur} suggests a balance between the thermal properties of PASP and the influence of sulfamethoxazole modification and indicates that the reaction between these two compounds occurred.

3.6 Minimum Inhibitory Concentration (MIC)

Strains of *E. coli*, *S. aureus*, and MRSA were subjected to microbial growth inhibition tests using PASP_{fur} and PASP_{fur}-SMX_{MA} samples, along with a positive control, SMX, to determine the MIC of these samples. The results of *E. coli* growth inhibition are shown in Figure 14 and, as well as the table (Table 1) with optical density values at 600 nm for each sample concentration.

Figure 14. Optical density of the *E. coli* suspension (A) showing its growth inhibition, measured at 600 nm and the visual aspect of the measured samples (B).

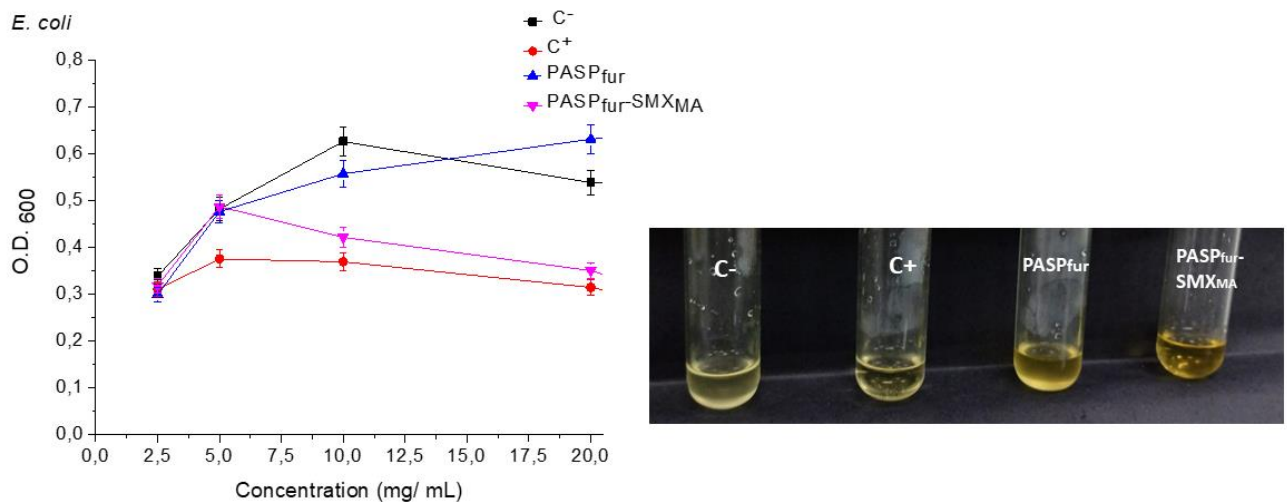


Table 1. *E. coli* growth inhibition assay with optical density values.

Concentration (mg/ mL)	O.D. ₆₀₀ - <i>E. coli</i>			
	C ⁻	C ⁺	PASP _{fur}	PASP _{fur} -SMX _{MA}
20	0.502	0.103	0.728	0.018
10	0.539	0.315	0.632	0.351
5	0.627	0.37	0.558	0.422
2,5	0.483	0.376	0.477	0.488
1,25	0.339	0.311	0.3	0.319

It can be observed that at 20 mg/ mL PASP_{fur}-SMX_{MA} completely inhibits bacterial growth, more than SMX (positive control) at the same concentration. At 10 mg/mL and 5 mg/mL, both PASP_{fur}-SMX_{MA} and SMX demonstrate higher inhibition compared to the control and PASP_{fur}.

The results of *S. aureus* growth inhibition are presented in Figure 15 and in Table 2.

Figure 15. Optical density (A) of the *S. aureus* suspension showing its growth inhibition, measured at 600 nm and the visual aspect of the measured samples (B).

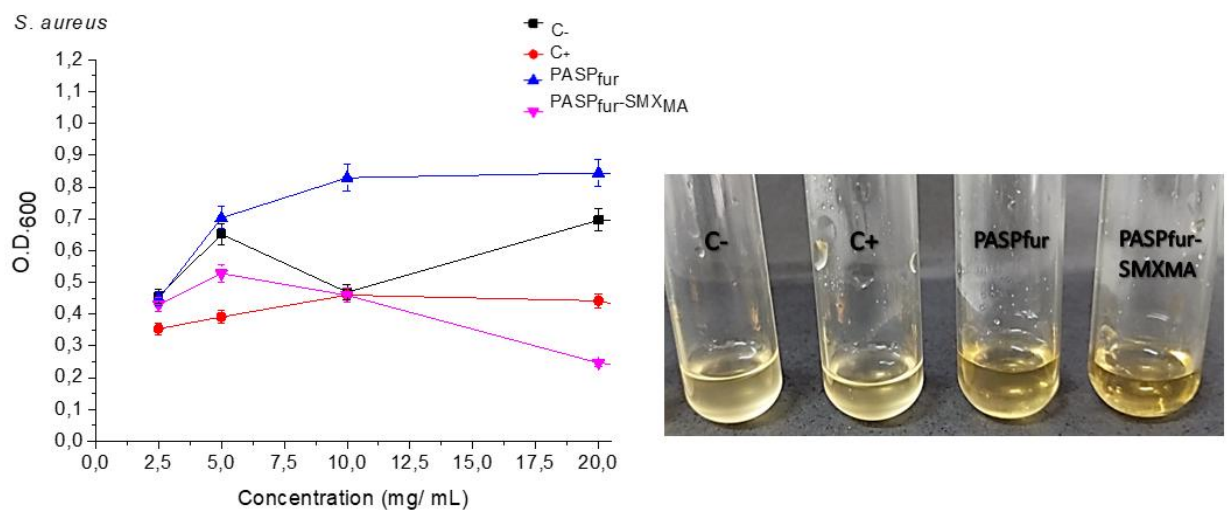


Table 2. *S. aureus* growth inhibition assay with optical density values.

Concentration (mg/ mL)	O.D. ₆₀₀ - <i>S. aureus</i>			
	C ⁻	C ⁺	PASP _{fur}	PASP _{fur} -SMX _{MA}
20	0.655	0.065	0.695	0.103
10	0.696	0.442	0.844	0.246
5	0.469	0.46	0.829	0.459
2.5	0.651	0.391	0.703	0.528
1.25	0.455	0.354	0.448	0.43

It can be observed that at 20 mg/mL, inhibition is nearly total for both PASP_{fur}-SMX_{MA} and SMX. However, at 10 mg/mL, PASP_{fur}-SMX_{MA} shows notably greater inhibition than SMX. At lower concentrations, the values remain similar.

The results of methicillin-resistant *S. aureus* growth inhibition are presented in Figure 16 and Table 3.

Figure 16. Optical density (A) of the MRSA suspension showing its growth inhibition, measured at 600 nm and the visual aspect of the measured samples (B).

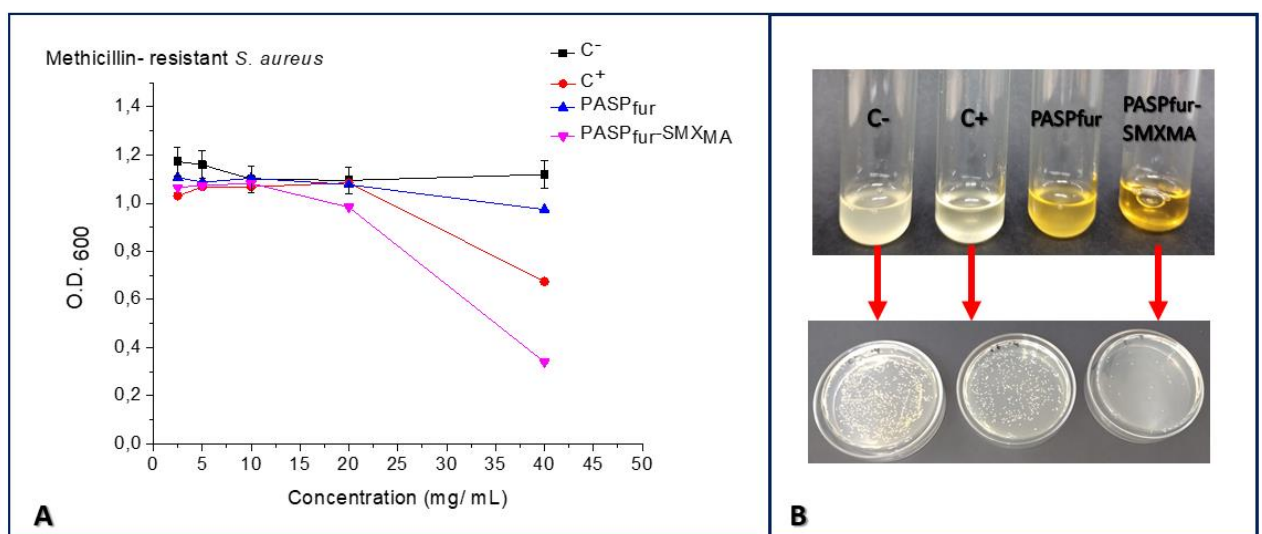


Table 3. MRSA growth inhibition assay with optical density values.

Concentration (mg/ mL)	O.D. ₆₀₀ – Methicillin- resistant <i>S. aureus</i>			
	C ⁻	C ⁺	PASP _{fur}	PASP _{fur} -SMX _{MA}
40	1,119	0,675	0,974	0,340
20	1,095	1,085	1,077	0,983
10	1,100	1,068	1,104	1,082
5	1,159	1,068	1,087	1,079
2,5	1,173	1,030	1,107	1,066

Up to 10 g/mL, the inhibition shown by all samples tested against MRSA remained very close. At 20 mg/ mL there is a notable increase in inhibition shown by PASP_{fur}-SMX_{MA}. Finally, at 40 mg/ mL the PASP-SMX sample exhibits almost complete inhibition of bacterial growth compared to other samples, including SMX_{MA}.

The results of this assay can be attributed to the increased solubility of PASP_{fur}-SMX_{MA} compared to SMX_{MA}. Solubility is a crucial factor for an antibiotic, as it enhances its bioavailability, meaning the amount of medication that reaches the sites of infection. Higher solubility in water facilitates the antibiotic's absorption by bacterial cells, thereby increasing its therapeutic potential (MA et al., 2007). This effect is particularly evident in the test against MRSA, a resistant microorganism, which showed significantly greater inhibition when exposed to doses of 40 and 20 mg/mL of PASP_{fur}-SMX_{MA} compared to SMX.

SMX is a poorly water- soluble antibiotic (0.5 g/ L) (RUDY; SENKOWSKI, 1973), while PASP is well soluble in water (PIATKOWSKI et al, 2015.) The PASP_{fur}-SMX_{MA} adduct was soluble in water up to the tested concentration of 80 mg/ mL, showing a higher solubility than SMX and due to the incorporation of this antibiotic into PASP.

The solubility of an antibiotic affects not only its bioavailability and cellular penetration but also other critical aspects of therapeutic efficacy, such as distribution in body fluids, ensuring the antibiotic reaches the target infection site, and the stability of the drug, allowing for various therapeutic forms of administration (GAO et al., 2020). These characteristics directly influence the dosage required, which in turn impacts the development of microbial resistance (YANG et al., 2020)

4 CONCLUSIONS

Poly(aspartic acid) was synthesized from aspartic acid via an acid catalysis reaction. This polymer was modified by esterification, generating a furanic polymer (PASP_{fur}). In parallel, sulfamethoxazole (SMX) was modified by maleation, producing a derivative containing an exposed maleimide group. These chemical modifications enabled a Diels Alder reaction between the furanic polymer and maleated sulfamethoxazole, resulting in PASP_{fur}-SMX_{MA} adduct. FTIR and ¹H NMR analyses confirmed the success of the modifications. Additionally, GPC analyses were performed on the PSI sample, and melting point measurements were taken for the SMX, PASP_{fur} and PASP_{fur}-SMX_{MA} samples, confirming the success of the reactions. PASP_{fur}-SMX_{MA} was subjected to antimicrobial activity assays against both gram-negative and gram-positive bacteria including a resistant strain. The results demonstrated superior growth inhibition compared to SMX against all bacteria tested. This improvement is attributed to the increased solubility provided by the binding of the antibiotic to PASP_{fur}, which enhanced its bioavailability. This makes PASP_{fur}-SMX_{MA} a promising prodrug for treating infections, offering an advantage over antibiotics with low solubility that require high doses to achieve therapeutic effects, thereby contributing to the issue of increased microbial resistance

CHAPTER II

SYNTHESIS OF A NEW BISMALEIMIDE FROM L-LYSINE AND ITS CROSSLINKING WITH A FURAN POLYMER¹

1 INTRODUCTION

1.1 Polymer crosslinking

The crosslinking of polymer chains is a chemical modification process that connects polymer chains to form hybrid polymer network (GONSALVES et al., 2011). An objective of crosslinking is to modify specific properties of polymers, such as chemical and thermal stability, structural rigidity, permeability, color, and biodegradability, once it introduces chemical groups that may be susceptible to biodegradation (TILLET; BOUTEVIN; AMEDURI, 2011).

Covalent crosslinking occurs by various reaction mechanisms, depending on the type of crosslinking agent employed. These reactions often irreversible connect reactive sites of different polymer chains by primary chemical bonds or distinct regions of the same chain by intramolecular bonds (ZHANG et al., 2019).

Conversely, physical (ionic) crosslinking is characterized by a simple reaction mechanism and a single-step experimental procedure but demonstrates lower stability due to high sensitivity to pH changes and the ionic strength of the medium, making the crosslinking process reversible (LILING et al., 2016).

An alternative to conventional covalent crosslink is the Diels-Alder (DA) reaction, that involves a cycloaddition of a diene to a dienophile, sharing inter- and intramolecular electrons to form the base structure (MOROZOVA, 2023). This involves the formation of covalent bonds. The procedure has certain advantages over conventional covalent crosslinking, such as not

¹ Note: The work presented in this Chapter is currently in the writing phase for the purpose of obtaining a patent.

generating by-products in the reaction, allowing experiments to be carried out at room temperature, reversibility, and other characteristics (KIRCHHOF et al., 2015).

More details of the Diels Alder reactions were discussed in 1.4 subsection of **Chapter 1**.

1.2 Hydrogels: types and applications

Hydrogels are three-dimensional networks of polymers interconnected by covalent bonds or physical interactions. They are highly hydrophilic and capable of absorbing large amounts of water or other fluids. Typically, these structures maintain dimensional stability even after water absorption, behaving like solutions where soluble molecules can diffuse. The swelling of a hydrogel is directly influenced by the degree of crosslinking or intertwining of its chains (BASHIR et al., 2020; ULLAH et al., 2015).

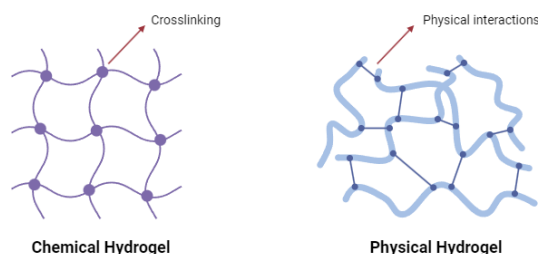
Hydrogels can be synthesized by physical or chemical crosslinking (Figure 17). Physical crosslinking generally involves Van der Waals forces or hydrogen bonds and forms temporary structures that can be dissolved by stimuli such as temperature and pH changes (AHMAD et al., 2022). Chemical hydrogels, on the other hand, form permanent structures that cannot be undone.

Based on their origin, hydrogels can be derived from natural sources (such as chitosan, alginate, and collagen), synthetic polymers (such as polyethylene glycol and polyacrylic acid), or composites that combine the properties of multiple polymeric networks (KAITH et al., 2021). To obtain a suitable hydrogel, it is essential to consider water absorption properties, biocompatibility, and mechanical properties, depending on the intended application. Applications range from absorbent products, tissue engineering, and drug delivery systems to sensors and smart devices (CHAI; JIAO; YU, 2017). Hydrogels are often applied in injectable forms, and this requires the formation of the hydrogel to occur in situ, that is, in the patient's body. Therefore, it is necessary for the material to flow in the syringe and lose its fluidity at the site of action, forming the hydrogel.(ALDANA et al., 2021).

In this context, the Diels-Alder (DA) reaction is an excellent method for synthesizing hydrogels, as it promotes clean, by-product-free, and rapid crosslinking. Regarding the synthesis of hydrogels from Diels Alder reactions, there are studies involving a polymeric diene first

synthesized by the functionalization of poly(2-aminoethyl methacrylate) hydrochloride with furfural. Suited bisdienophiles are prepared by modification of Jeffamine® ED of different molecular weights with maleic anhydride (GARCÍA-ASTRAIN et al., 2015). In another study, cellulose fibres derived from hardwood were submitted to shearing and surface TEMPO-oxidation before being modified with furfurylamine. The ensuing pendant furan moieties were reacted with a water-soluble bismaleimide via Diels-Alder coupling at 65 °C to produce a hydrogel, whose deconstruction was induced by the corresponding retro-Diels-Alder reaction carried out at 95 °C (KRAMER et al., 2019a). Finally, poly (styrene-co-furfuryl methacrylate) networks were prepared by the Diels–Alder (D–A) reaction in solution at 25 °C between the linear copolymer and bismaleimide (BM), and swelling properties were studied by gravimetric and dimensional measurements (GOITI; HUGLIN; REGO, 2004).

Figure 17. General scheme of chemical and physical hydrogels. Adapted from Bortolin et al, 2013



Created in BioRender.com bio

1.3 Bismaleimide

Bismaleimides are molecules terminated by two maleimide functional group, derived from natural or synthetic sources. They are commonly used in the industry as crosslinking agents in thermosetting polymers, elastomers and as bonding agents in coatings such as paints and varnishes (IREDALE; WARD; HAMERTON, 2017).

Some important properties of bismaleimides include high thermal resistance, chemical stability, and low viscosity, which make them suitable, for example, for use in injection molding processes (XIONG et al., 2022). Examples of commercially available bismaleimides are *N, N'*-(4-methyl-1,3-phenylene) bismaleimide, BMOE (bis-maleimidoethane), and BM(PEG)2 (1,8-bismaleimide-diethylene glycol), one of the few water-soluble bismaleimides commercially available. Due to the importance of this material, several patents have been generated involving bismaleimides. Some patents include TWI406859, a bismaleimide synthesized from a diamine and maleic anhydride; BR 1120180100692A2, which involves the development of a new thermoreversible adhesive from an acrylate and bismaleimide and finally, CN102531994B, which describes the synthesis of bismaleimide involving microwave radiation. Patents regarding the method used to synthesize a new bismaleimide are also found, such as CN108129659B, which describes a new method for the synthesis of bismaleimide from different diamines.

Due to the properties mentioned above, bismaleimides have also been studied for use in medicine as crosslinking agents for injectable materials such as hydrogels (OCANDO et al., 2021). Considering this application, it is very important to use a bismaleimide that has a natural and renewable origin, such as amino acids, for example, lysine.

The content of pages 42 to 53 is hidden because this data is in the process of being applied for patent.



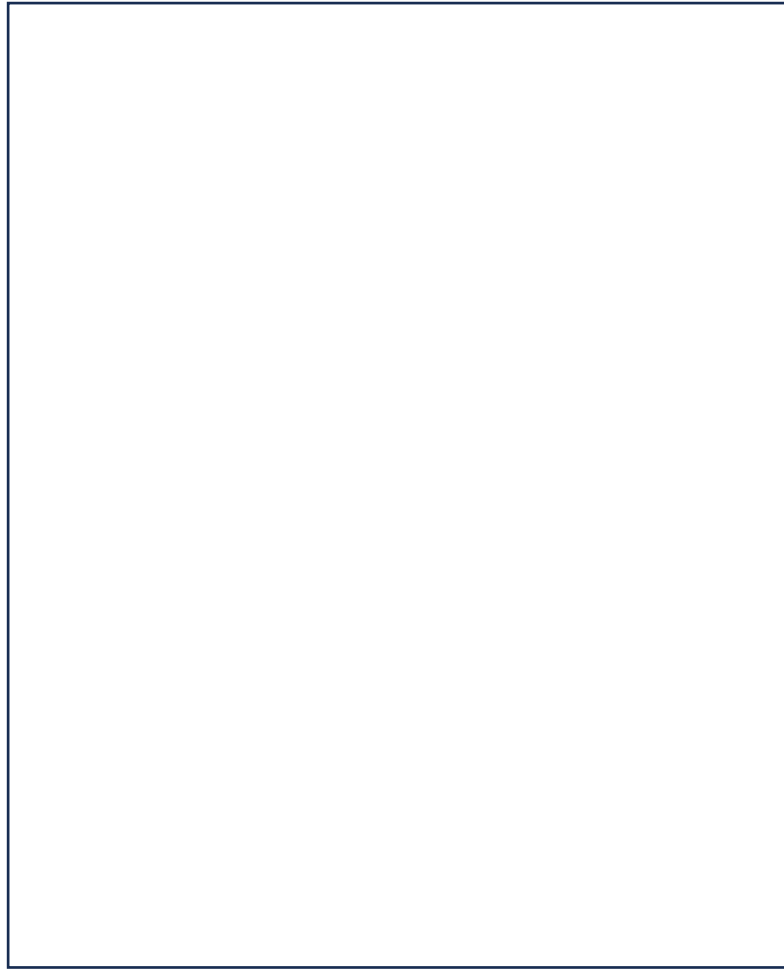












CHAPTER III

SYNTHESIS OF A CYSTEINE DIELS-ALDER BASED POLYMER BY SIMULTANEOUS DOUBLE CLICK CHEMISTRY AND ITS CYTO-GENOTOXICITY EVALUATION²

1 INTRODUCTION

Polymeric hydrogels can be derived from natural or synthetic sources and it is essential that these materials have good water absorption properties, biocompatibility, and mechanical properties, depending on the intended application, that can range from tissue engineering, drug delivery systems and absorbent materials as was discussed at Chapter 2, section 1.2. In this context, click chemistry reactions are good methods to create new hydrogels, as click chemistry are cleaner, faster and generally by-product free when compared with another conventional methods. The concepts of Click Chemistry and one of most important of these class of reactions, Diels Alder reaction, are more detailed at **Chapter 1, sections 1.3 and 1.4**.

1.1 Thiol- ene reaction

Thiol-ene and thiol-yne systems are based on reactions between the reactive carbon-carbon double bonds and thiols and occur via Michael-addition or radical step-growth polymerization generating carbon-sulfur bonds. These reactions are widely used in polymer chemistry, sensors, synthesis of drug molecules, and other areas (KADE; BURKE; HAWKER, 2010).

The growing demand for new materials, including polymers with improved properties such thermal stability, mechanical strength, flexibility, low shrinkage and biocompatibility for application in fields such as 3D printing technologies, packaging and biomedicine, and especially those based on renewable resources, encourage the search for new advantageous

² This chapter was published as an article in the journal *Macromolecular Research*, on November 14, 2023 and can be consulted at: <https://doi.org/10.1007/s13233-023-00216-8>

processes for polymer development. Even, the click chemistry reactions have been extensively used to generate new polymers for several applications (RYU; OH; KIM, 2016; WEI et al., 2021), including the biological field, few biocompatibility studies have been displayed for these emerging materials. The production process scales up of any chemical substance requires safe conditions for handling the raw materials and the products.

1.2 Cysteine

The amino acids represent an available natural and renewable source of monomers, used for solid phase peptide synthesis, but few of them have been exploited for the synthesis of polymer, monomers, or other molecules (THOMPSON; SCHOLZ, 2021). A natural source of thiol-based molecules that can match the requirements for the thiol-ene reactions are the amino acids with pending thiol side chains.

Cysteine bears a thiol group capable of participating in click chemistry reactions and an amine functional group, also very reactive. The high reactivity of this amine group with the anhydride function can be used as a strategy to transform rapidly and efficiently the monofunctional amino acid in the polymer by click chemistry reactions.

Even the use of click chemistry is growing and can lead to large scale production in which people handle the reagents and products few information can be found with respect to the safety of the chemical products used in their production chain. With this in mind, we have planned a polymer based on the furan/maleimide pair to study the safety of the reagents and resulting products. In order to preserve the predominance of furan/maleimide within the structure, a minimalist polymer was designed using cysteine as the second building block for synthesis.

As described at introduction in the previous chapter (Chapter 2), polymers obtained from click chemistry reactions are widely studied, however, here the proposal is the synthesis of polymers using these reactions, but using monomers not yet described in the literature and strategically selected based on desired properties in terms of low (or absence) of cytotoxicity to human cells and possibility of degradation under physiological conditions.

The idea is to modify the chemical structure of cysteine, inserting into its amine group the furan maleic anhydride adduct, generating a dynamic structure capable of performing two simultaneous reactions. For such, the furan maleic anhydride adduct was synthesized by the classical Diels-Alder reaction (GANDINI; BELGACEM, 2008b) and mixed with the cysteine in solution. The efficiency of the new heterobifunctional click chemistry system was tested in

a condensation reaction, in which the furan maleic anhydride adduct reacts with the amine from cysteine and the thiol reacts with the double bond of the DA adduct, simultaneously.

2 MATERIALS AND METHODS

2.1 Materials

L-Cysteine was supplied by Ajinomoto (98 % wt., Brazil), maleic anhydride (98 % wt.) was purchased from Exodo (Brazil), methanol, dimethyl sulfoxide (DMSO) and glycerol were purchased from Synth (Brazil), microsomal fraction (S9 fraction) was purchased from Moltax Molecular Toxicology Inc., Boone, USA, and fetal bovine serum (FBS) was purchased from Nutricell. Furan, deuterated dimethyl sulfoxide (DMSO_d_6) was purchased from Sigma Aldrich. Dulbecco's Modified Eagle Medium (DMEM), nicotinamide adenine dinucleotide phosphate sodium salt (NADP), D-glucose-6-phosphate disodium salt, magnesium chloride (MgCl_2), potassium chloride (KCl), L-histidine monohydrate, D-biotin, 4-nitro-o-phenylenediamine (NPD), mitomycin C (MMC), sodium azide (SA), 2-anthracene (2-AA), 2-aminofluorene (2-AF), and resazurin sodium salt were purchased from Sigma-Aldrich® MERCK (St. Louis, MO, USA). Oxoid Nutrient Broth No. 2 and Bacto Agar, used as bacterial media, were purchased from Oxoid and BD Bacto, respectively. D-Glucose, magnesium sulfate, citric acid monohydrate, anhydrous dibasic potassium phosphate, sodium ammonium phosphate, monobasic sodium phosphate, dibasic sodium phosphate and sodium chloride were purchased from Merck (Whitehouse Station, NJ, USA). The strains TA98, TA100, TA102 and TA97a of *Salmonella* Typhimurium, used in the genotoxicity assay (Ames test) were provided by Dr. B.N. Ames (Berkeley, CA, USA).

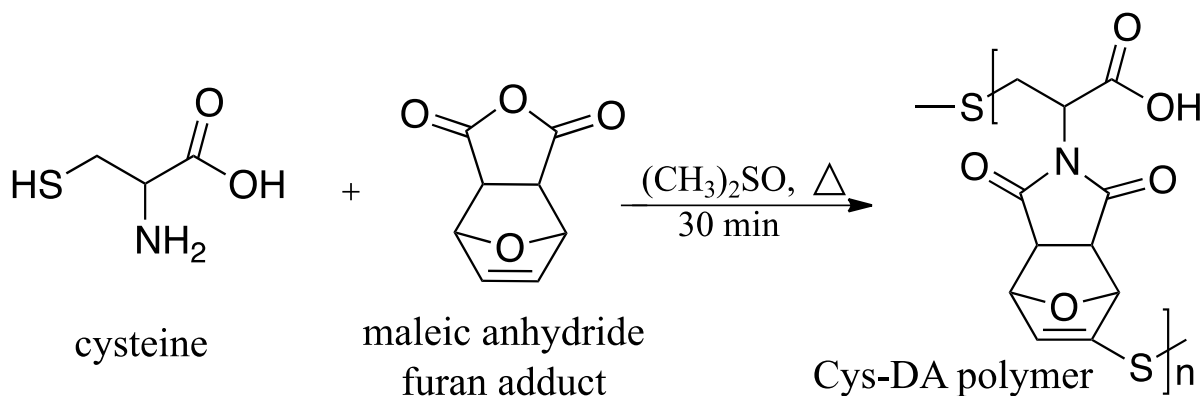
2.2 Methods

2.2.1 Chemical modification of cysteine and polymer synthesis

Maleic anhydride furan adduct (1.67 g, 0.01 mol) was dissolved in methanol (20 mL). Cysteine (1.21 g, 0.01 mol) was weight, added into the solution and magnetically stirred at 50 °C for five hours, followed by solvent evaporation at room temperature. Then, DMSO (7 mL) was added to the resulting material and the solution was stirred for 30 minutes at 50 °C. The product was washed three times with methanol and three times with water followed by centrifugation (2500 rpm for 2 min) to separate the solvents in each washing cycle. Finally, the product was dried in

an oven at 50 °C for 24 hours. The proposed chemical reactions are shown in the scheme of Figure 25.

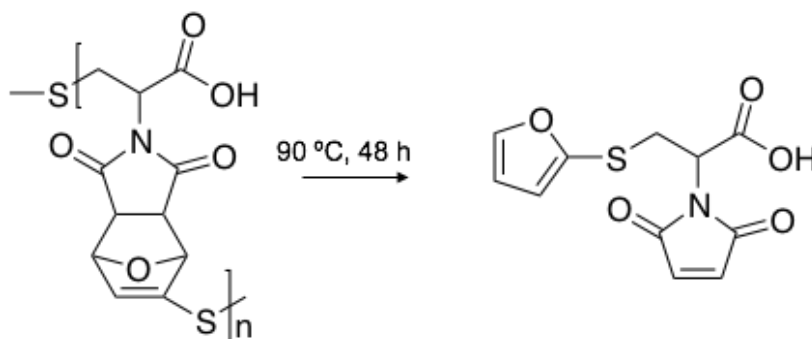
Figure 25. Reaction of cysteine with furan-maleic anhydride adduct forming the Cys-Adu polymer



2.2.2 rDA reaction of Cysteine-Adduct polymer

The rDA reaction of the polymer from the reaction described at 2.2.1 was performed by dissolving the polymer in DMSO and heating the mixture at 90 °C for 48 h in an oil bath. The scheme of the chemical reaction is shown in Figure 26.

Figure 26. Retro Diels-Alder reaction from the Cys-Adu polymer and its possible product



2.3 Structural and physical-chemical characterization

2.3.1 Fourier Transform Infrared Spectroscopy (FTIR)

The dried samples were analyzed using a Perkin-Elmer Spectrum 100 FT-IR Spectrometer equipped with an attenuated total reflectance (ATR) device of diamond coated with zinc selenide crystal. The spectra were in the range of 600 to 4000 cm^{-1} , with 4 cm^{-1} resolution and 16 scans, the spectral outputs were recorded in transmittance.

2.3.2 ^1H and ^{13}C NMR Spectra

^1H and ^{13}C NMR spectra were acquired at 14.1 T, 600.23 MHz for ^1H and 150.93 MHz for ^{13}C observation, using a Bruker Avance II HD equipment. The samples were dissolved in deuterated solvent (DMSO_{d6}) at 1 % wt. (w/v). For ^1H spectra observation: it 90° pulse of 11.02 μs ; recycle delay 500 ms; acquisition time 3.9s; 128 scans, spectral width 14 ppm and lb 1. The data from ^1H NMR were used to calculate the Mn of the polymer, following the classical methodology described by Izunobi and Higginbotham, 2011 (IZUNOBI; HIGGINBOTHAM, 2011). For ^{13}C NMR Spectra observation: a 90° pulse of 11.25 μs ; recycle delay 2 ms; acquisition time 0.9s; 1024 scans, spectral width 240 ppm and lb 1.

2.3.3 Rheology

The rheological properties were analyzed using an Anton Paar MCR92 rheometer, fitted with a 25 mm parallel plate geometry to evaluate the viscoelastic properties of the samples. The samples (50 mg) were dissolved in DMSO (0.5 mL) and were loaded onto the rheometer and the upper plate was lowered to a gap size of 0.20 mm. The test was performed at 37 °C and 0.01 rad s^{-1} for 240 seconds.

2.3.4 Thermal analysis

The thermal decomposition behavior was estimated using thermogravimetric analysis (TGA55, TA Instruments) at heating rate of 10 °C/ min from 25 to 600 °C. The thermal properties were investigated by Differential Scanning Calorimetry (DSC) using a DSC250, TA Instruments. The sample was conditioned at 40 °C for 24 h before testing. Dried samples (6 mg) were inserted into the hermetically sealed aluminum pan and the tests were carried out under nitrogen flow (50 mL/ min), at heating rate of 10 °C/ min from 25 °C to 200 °C (isothermal for 10 min),

and cooling to $-65\text{ }^{\circ}\text{C}$ at a rate of $20\text{ }^{\circ}\text{C}/\text{min}$, followed by the second heating until $200\text{ }^{\circ}\text{C}$ at a rate of $10\text{ }^{\circ}\text{C}/\text{min}$.

2.3.5 Biological characterization

2.3.5.1 Cytotoxicity

Cytotoxicity tests were carried out following the standard resazurin reduction method (PAGE; PAGE; NOEL, 1993). The human keratinocyte HaCat cell line was seed in DMEM culture medium supplemented with 10 % vol of FBS and maintained in a humidified atmosphere of 5 % CO_2 and 95 % air, at $37\text{ }^{\circ}\text{C}$, in culture flask (Corning). For the test, the cells were seeded into the wells of a 96-well microplate (1.0×10^4 cells/well) and incubated for 24 hours for adhesion. L-cysteine, maleic anhydride furan adduct and Cys-DA polymer were diluted in culture medium (concentrations ranging from 1000 to $31.2\text{ }\mu\text{g mL}^{-1}$, in serial dilution) and this culture medium was used to replace the original DMEM medium in the wells with the adhered cells, and then, incubated at the described growth conditions for further 24 h. The negative control was the culture medium, and the positive control was the mixture of DMSO and DMEM (50 % vol). After this period, the culture medium was replaced by $50\text{ }\mu\text{L}$ of 0.01 % wt. resazurin aqueous solution. The plates were incubated for 4 hours at the growth conditions. The fluorescence was measured in a CaryEclipse spectrofluorometer (Agilent Technologies - Santa Clara, USA), at $\lambda_{\text{ex}}= 530\text{ nm}$ and $\lambda_{\text{em}}= 590\text{ nm}$. The viability was calculated in proportion percentage relative to the negative growth, which was taken as 100 % of cell viability. The results represent the mean \pm standard deviation of triplicates of three independent experiments. Data were checked for normality using the K-S test (Kolmogorov-Smirnov test) and submitted to analysis of variance (ANOVA) followed by Dunnett's comparison post-test, with the negative control as a reference. Statistical analysis and graphing were performed using the GraphPad Prism 7.0 program (Intuitive Software for Science, San Diego, CA, USA), as well as the calculation of the IC_{50} , which represents the concentration required to reduce the viability of cells to 50%.

2.3.5.2 Genotoxicity - Reverse gene mutation assay with *Salmonella* Typhimurium (Ames test)

Ames test was performed according to the pre-incubation method (MARON; AMES, 1983). *S. typhimurium* strains TA98, TA100, TA102 and were grown in 30 mL of Nutrient Broth at 37°C, for 12-16 hours, in an orbital shaker (160 rpm), in order to reach 1-2 x10⁹ bacteria/mL.

Cysteine, the adduct and the polymer, solubilized and diluted in 0.2 M phosphate buffer solution, pH 7.4, were tested at the maximum concentration (5 mg/plate) recommended for routine testing (Test No. 492: Reconstructed human Cornea-like Epithelium (RhCE) test method for identifying chemicals not requiring classification and labelling for eye irritation or serious eye damage, 2019). Each sample (concentration ranging from 0.62 to 5 mg/plate) was mixed individually with 0.5 mL of phosphate buffer (in assays without metabolic activation) or S9 mix (in assays with metabolic activation) and 0.1 mL of bacterial suspension, in a test tube, and incubated for 30 min at 37 °C. After this time, 2 mL of top agar (supplemented with L-histidine and D-biotin) was added to the mixture. The tubes were gently homogenized and poured into Petri dishes containing minimal agar. After the solidification of the top agar, the plates were incubated for 48 h at 37 °C, and the revertant colonies were counted manually. The assay was performed in triplicate. The mutagens (positive control) NPD (10 µg/plate, for TA98 and TA97a), SA (1.25 µg/plate, for TA100) and MMC (0.5 µg/plate, for TA102) were used in the experiments without metabolization. In the experiments with metabolic activation, 2-AA (1.25 µg/plate) was used for the strains TA98, TA97a, TA100, and 2-AF (10 µg/plate) for TA102. The negative control (with no treatment) is equivalent to the spontaneous reversion rate of the bacteria.

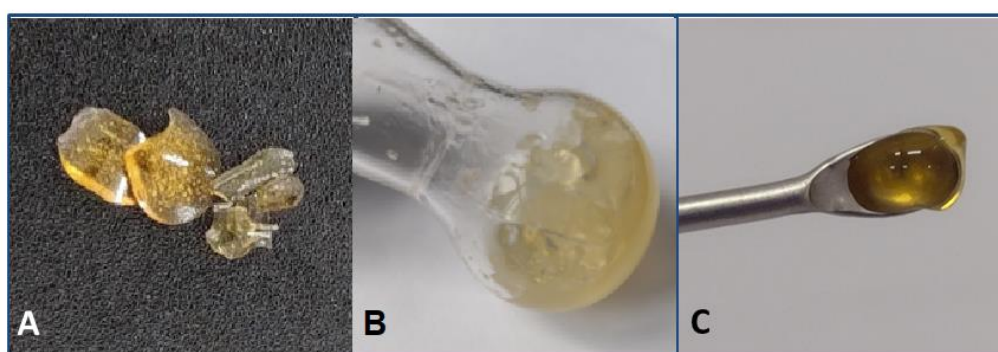
The solution for metabolic activation (S9 mix) is composed (in % vol) of 4% S9 fraction, 1% KCl, 1% MgSO₄, 0.5% glucose-6-phosphate, 4% β-nicotinamide adenine dinucleotide phosphate, 50% phosphate buffer and 39.5% sterile distilled water (MARON; AMES, 1983)

The results were analyzed using Salanal statistical data software (U.S. Environmental Protection Agency, Monitoring Systems Laboratory, Las Vegas, NV, version 1.0, Research Triangle Institute, RTP, North Carolina, USA), using the model described by Bernstein et al (BERNSTEIN et al., 1982) Data (revertants/plate) were evaluated by analysis of variance (ANOVA), followed by linear regression. The mutagenicity index (MI) was calculated for each concentration tested, which is the mean number of revertants/plate with the test sample (induced revertants) divided by the mean number of revertants/plate with the control (solvent) negative. The test solution was considered mutagenic when a dose-response relationship was detected and a twofold increase in the number of mutants ($MI \geq 2$) was observed for at least one concentration (MORTELMANS; ZEIGER, 2000)

3 RESULTS AND DISCUSSION

The dissolved cysteine and the DA adduct generated a transparent material with a vitreous film appearance when dried. After addition of DMSO, the material swelled in less than 30 min. The polymer is high soluble in water and insoluble in organic solvents such as methanol, ethanol, and diethyl ether. In DMSO, the polymer exhibits a swelling behavior (about 50 mg in 500 μ L), forming an organo-gel. The image of the polymer can be seen in Figure 27.

Figure 27. Image of the dried polymer (A), the polymer swelled in DMSO (B) and dissolved in water (C).



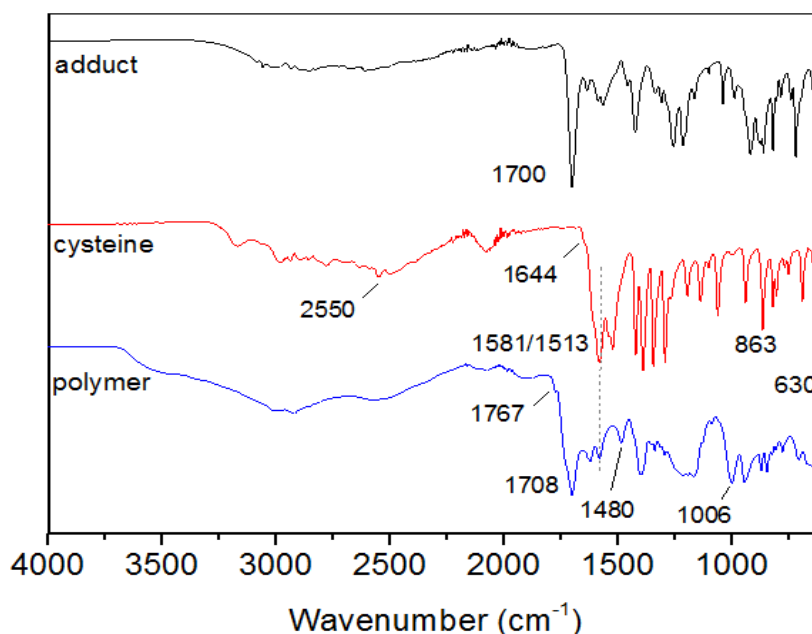
3.1 FTIR

Figure 28 shows the spectra of the furan-maleic anhydride adduct, cysteine and Cys-Adu polymer. The spectrum of the furan-maleic anhydride adduct shows a strong band at 1700 cm^{-1} attributed to the C=O stretching of the maleimide, at 719 cm^{-1} the typical band of the C=C bond vibration of the adduct and at 920 cm^{-1} the band related to the adduct ring breathing.

The cysteine spectrum absorption peaks at 3167 and 2937 cm^{-1} correspond to its primary amine vibrations, the peak at 1644 cm^{-1} corresponding to the -C=O vibrations, the bands at 1582 and 1313 cm^{-1} corresponding to N-H deformation vibrations, at 1056 cm^{-1} , corresponding to C-O stretching vibration, at 2550 cm^{-1} the typical band of the S-H bond (THOMPSON; SCHOLZ, 2021), and at 630 and 863 cm^{-1} , the C-SH stretching vibration.

The spectrum of the Cys-Adu polymer displayed bands at 1622 and 1702 cm^{-1} , corresponding to the C=O group of the cysteine and maleimide (from the adduct), respectively. The appearance of the new band at 1480 cm^{-1} indicated the formation of the C-N bond, and the appearance of the new band at 1006 corresponding to the C-S stretching vibration, indicate the formation of the C-S-C bond. In addition, the band at 2550 cm^{-1} corresponding to the S-H of cysteine disappeared in the polymer spectrum, as well the NH_2 band at 3178 cm^{-1} . These results are in agreement with the proposed polymer structure, strongly suggesting its formation.

Figure 28. FTIR spectra of the adduct furan maleic anhydride, cysteine, and the polymer



3.2 ^1H NMR

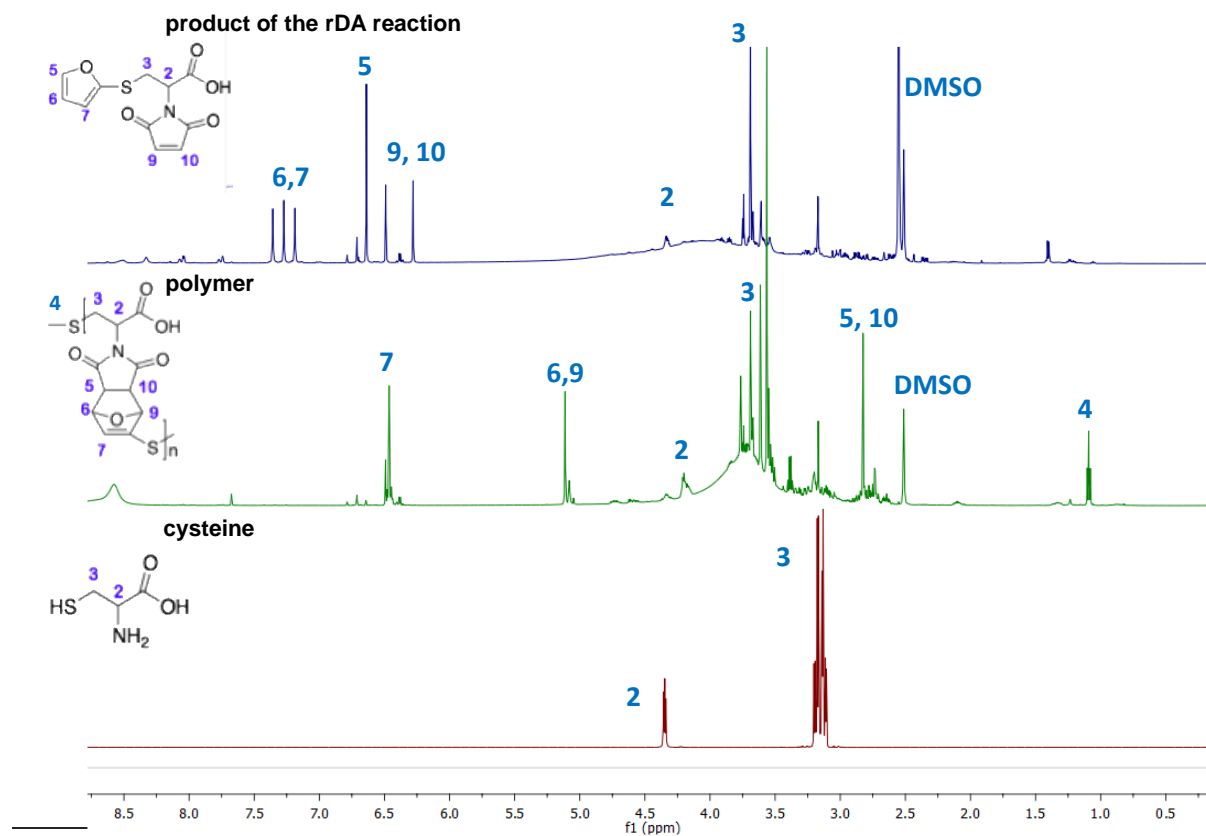
The cysteine-DA adduct polymerization was also followed by ^1H NMR spectroscopy in solution. The polymerization was carried out in the reaction flask and a small fraction collected for ^1H NMR analysis. First, the DA reaction was performed by heating the system at 50 °C and thereafter, the polymer underwent the retro-DA reaction (90 °C for 48 h). The spectra of the cysteine and Cys-Adu polymer acquired before and after the retro Diels Alder reaction are shown in Figure 29. The cysteine spectrum shows high intensity peaks at 3.1 and 4.3 ppm, corresponding to its CH_2 (3) and CH (2) protons.

The polymer spectrum showed the typical peaks of the monosubstituted furan ring coupled to the maleimide, in which the heteroatom is the sulfur from the cysteine. The peaks at 5.11 (6 and 9), 6.26 (7) and 3.56 ppm (5 and 10) correspond to the protons from the adduct ring (VAUTHIER et al., 2019). The peak at 1.09 ppm (4) correspond to the terminal SH hydrogen. These results confirm the structure of the cysteine-adduct polymer, indicating its formation. These results, namely the integration peaks, were used to estimate the M_n of the polymer, which was about 3.380.

The retro Diels-Alder spectrum indicated the success of the reaction. It was carried out with the aim of show the formation of the polymer and not the thermos-reversibility or recycling capability of the reaction, once, for use within the body, it is not adequate. The most important evidence of the retro Diels-Alder reaction can be seen at 6.28 ppm, corresponding to the peaks of the maleimide protons (9 and 10), as well the disappearance of the adduct peaks at 5.11 ppm

and the decrease of the peak intensity at 3.56 ppm. The protons of the free furan heterocycle can be seen at 6.64 ppm (5), and at 7.19 and 7.36 ppm (6 and 7), respectively. These results confirm the occurrence of the cysteine-adduct polymer thermal reversibility. The peak at 6.49 and 3.56 ppm indicated the fraction of the polymer that did not display rDA products at the moment of ^1H NMR analysis, which contributes with about 50 % of the detected composition. This fraction is probably the result of the DA repolymerization. Given that no side product is eliminated during the rDA reaction, the rDA product normally undergo the DA reaction when the temperature is lowered, including at room temperature, to form the polymer again. The reversibility of the reaction favors the DA reaction products.

Figure 29. ^1H NMR spectra of the cysteine (in deuterium oxide) and cys-DA based polymer (in DMSO_{d6}) before and after the deprotection of the maleimide moieties by the retro-DA reaction

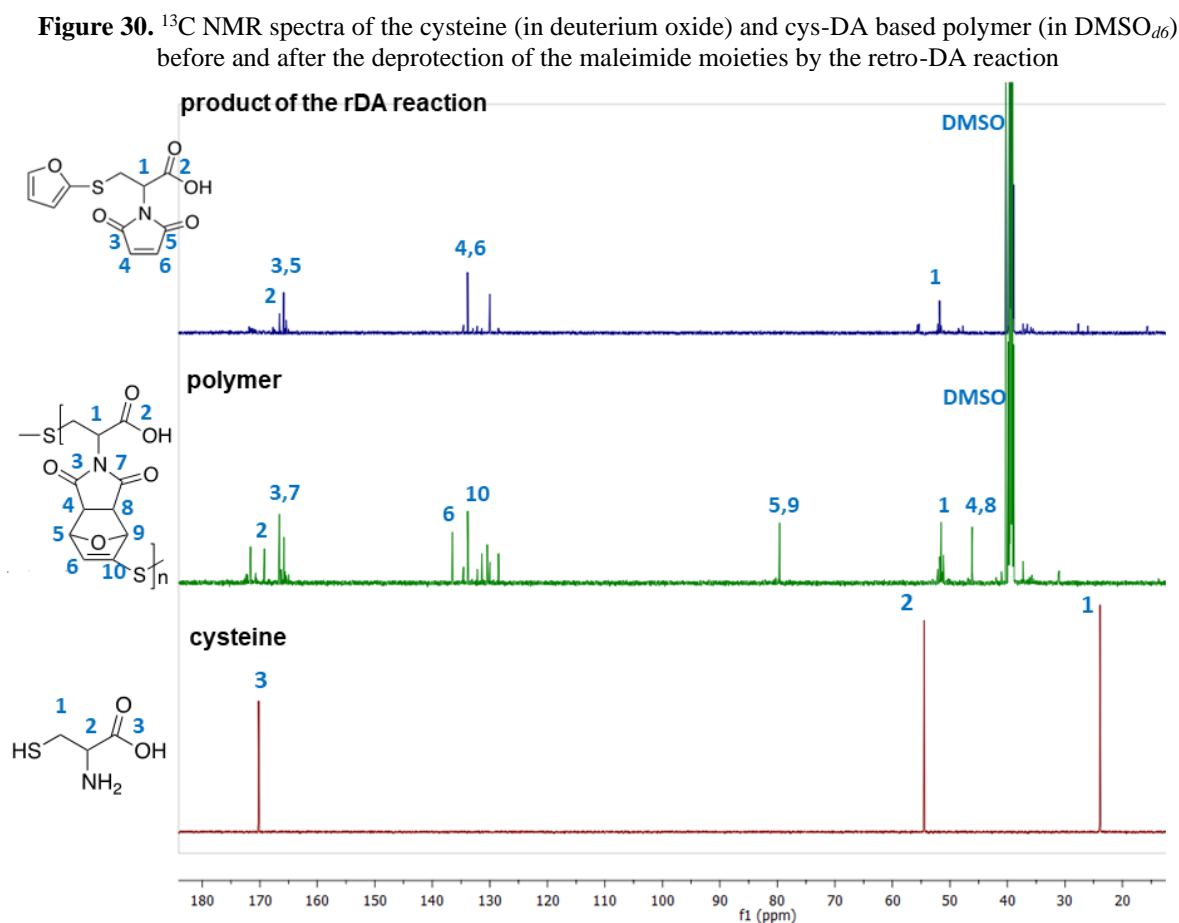


3.3 ^{13}C NMR

The ^{13}C NMR spectra of the cysteine and Cys-Adu polymer acquired before and after the retro Diels Alder reaction are shown in Figure 30. The cysteine spectrum shows high intensity peaks at 24.21, 54.87 and 170.18 ppm, corresponding to C-SH (1), C-N (2) and C=OOH (3), respectively.

The polymer spectra showed peaks of the furan ring coupled to the maleimide. The peaks at 79.95 (1 and 4), 45.81 (2 and 3) 136.60 and 133.66 ppm (5 and 6) correspond to the protons from the adduct ring, and the peak at 166.54 (7 and 8) correspond to the maleimide carbons (C=O) (RZAYEV et al., 2016; VISWANATHAN; JETHMALANI, 1993). The peak at 51.94 (9), correspond to C-N bond. These results confirm the formation of the cysteine-adduct polymer.

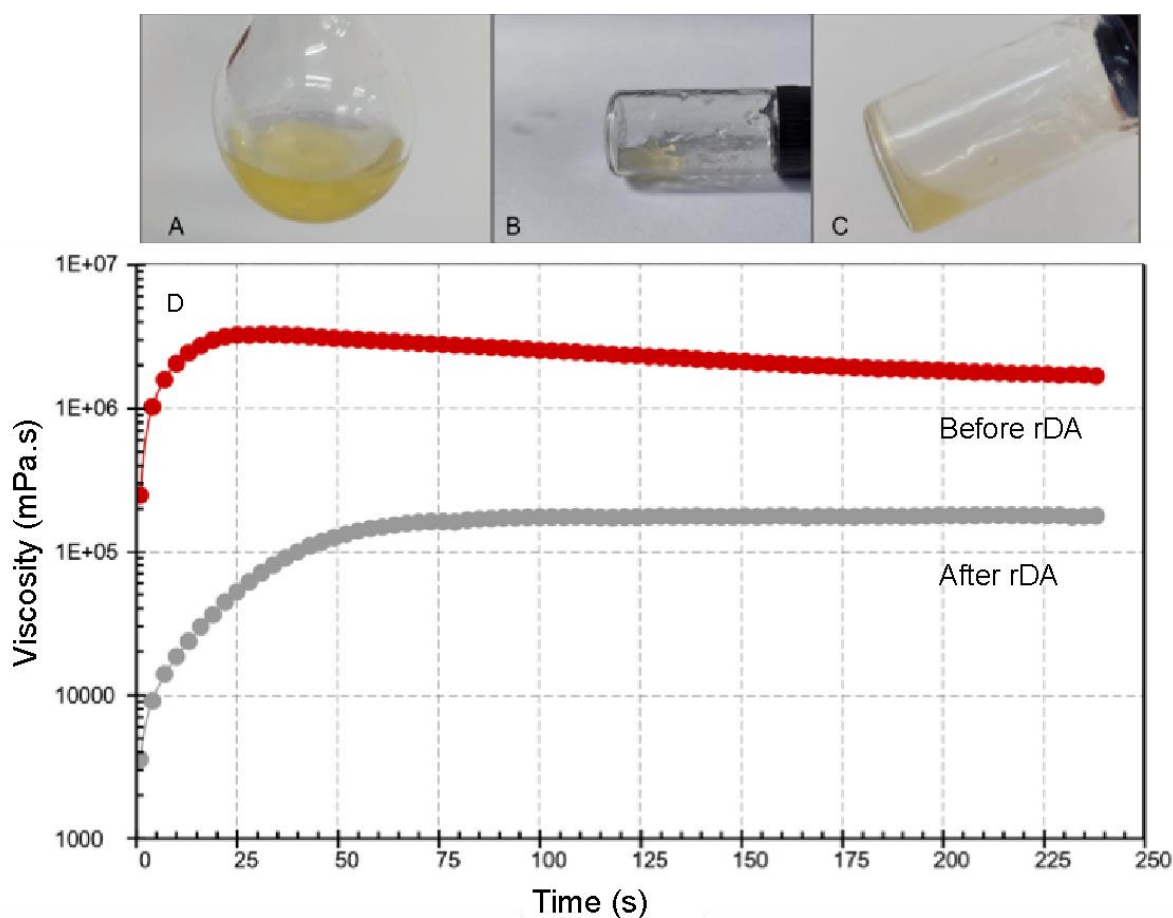
Evidence of the retro Diels-Alder reaction can be seen at 133.67 (1 and 2) and 165.85 ppm (3,4), corresponding to the peaks of the maleimide carbons, as well the disappearance of the adduct peaks at 79.95 and 45.81 ppm. These results confirm the occurrence of the cysteine-adduct polymer thermal reversibility.



3.4 Rheology

Figure 31 shows the visual aspect of the polymer before (A) and after (B) the rDA reaction. The synthesis generated a material that displayed a gel consistency, which did not flow. The rheological behavior of the polymer was followed in a condition of low oscillation to avoid the influence of the shear on the viscosity response of the material. The temperature was kept at 37 °C and the viscosity measured for 360 seconds, as shown in Figure 31 D. The viscosity of the polymer was constant, and relatively high, about $2 \cdot 10^6$ mPa.s. The results of the sample viscosity after the rDA reaction evidenced the dramatic decrease of its viscosity, viz. to about $2 \cdot 10^5$ mPa.s, and flow, confirming that the polymer can be de-polymerized by rDA upon heating. These results are in agreement with the ^1H NMR results.

Figure 31. Images of the products of each reaction step. A) Initial solution, B) polymer, C) polymer after the rDA reaction and D) rheology curves

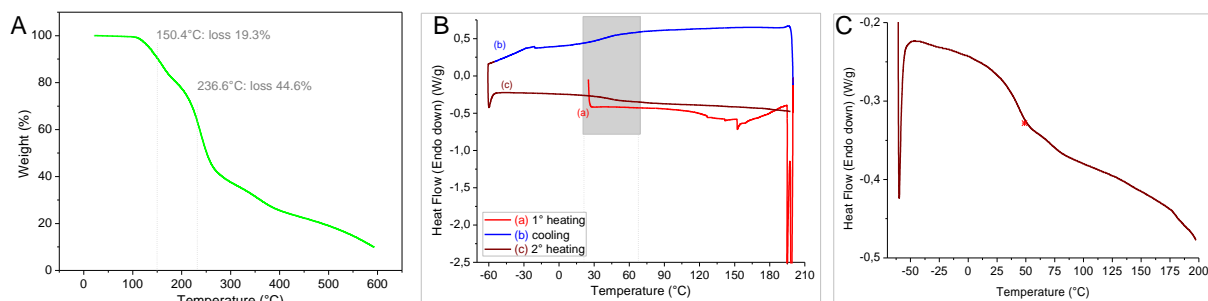


3.5 Thermal properties of Cys-DA polymer

The results of the thermogravimetric analysis (TGA) of the Cys-DA polymer is shown in Figure 32 A, in which the weight loss (T_{onset}) is about at 182 °C. At around 150.4 °C the weight loss was about 19.3 %wt, which can be attributed to the loss of the furan ring by as the result of the rDA reaction (DISPINAR; SANYAL; SANYAL, 2007). The second temperature decomposition, at 236.6 °C, with weight loss around 44.6 %wt, can be attributed to the depolymerization of the end groups. The solid residual was 10 %wt at 600 °C.

The DSC curves of the polymer are shown in Figure 32 B and C. The thermograms indicated the endothermic transition peak around 50 °C, associated with occurrence of the rDA reaction that deconstructed the furan/maleimide adduct during the cooling process. This result is in agreement with the rheological studies. No T_g was detected, and a significant decomposition (T_d) was found at 195 °C, in agreement with TGA results.

Figure 32. Thermogravimetric analysis of Cys-DA polymer (A); DSC heating and cooling curves for Cys-DA polymer. The endothermic step around 50 °C indicates the Diels Alder reaction (B); DSC second heating curve for Cys-DA polymer shows the temperature transition around 50°C attributed to Diels Alder reaction (C).

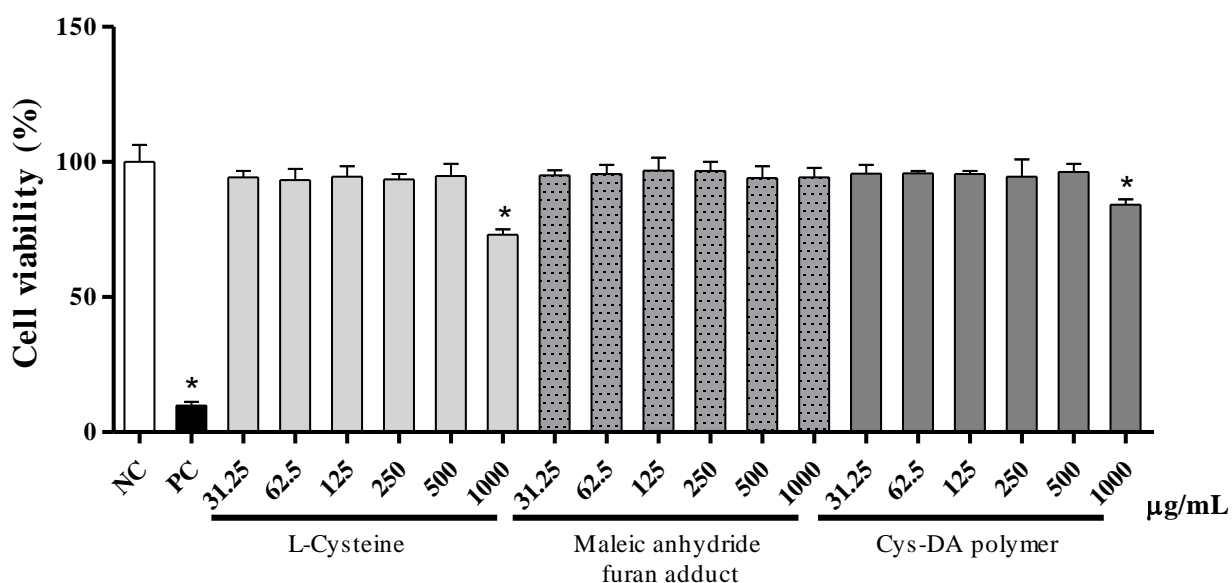


3.6 Cytotoxicity test

The results from Resazurin redox test are shown in Figure 33. All the samples, cysteine, the adduct and the cysteine-derived polymer, showed the cell viability higher than 70 %, indicating, according to ISO10993-5 standard (STANDARD, I. “BIOLOGICAL EVALUATION OF MEDICAL DEVICES—PART 5: TESTS FOR IN VITRO CYTOTOXICITY.” GENEVE, SWITZERLAND: INTERNATIONAL ORGANIZATION FOR STANDARDIZATION (2009)., [s. d.]), that all of them, in all the tested concentrations did not show any cytotoxic effect to the human HaCat cells. Most of the concentrations led to cell viability close to 100 %, with no significant decrease among the samples. The most concentrated ($1000 \mu\text{g mL}^{-1}$) samples of cysteine and polymer showed significant difference when compared to the others, however, it was also higher than 70%,

indicating no cytotoxic effect to HaCat human cells. The estimated IC_{50} values were 1.24 ± 0.12 $mg\ mL^{-1}$ for L-cysteine, 2.91 ± 0.1 $mg\ mL^{-1}$ for adduct and 1.37 ± 0.07 $mg\ mL^{-1}$ for polymer.

Figure 33. Viability of HaCat cells treated for 24 hours with different concentrations of L-cysteine, maleic anhydride furan adduct and cys-DA polymer. NC: negative control (DMEM with 10% fetal bovine serum); PC: positive control (50% DMSO, 12.1 ± 1.4 % cell viability). The results represent the average of three independent assays. *Statistically different from NC ($p < 0.05$, ANOVA, followed by Dunnett's test)



3.7 Reverse gene mutation assay with *Salmonella typhimurium* (Ames test)

The results of Ames test are shown in Table 4. Ames test evaluate the genetic damage of chemicals at the single base level in DNA in tester strains of bacteria. The chemical's genotoxicity is measured by its capability of inducing reverse mutations in these specific bacterial strains. The results showed that the crude cysteine, the adduct and the polymer did not induce direct gene mutations in any bacterial strain. The test with metabolic activation (using the S9 mix activation system) of cysteine and the polymer induced mutagenic response. Cysteine elicited a positive mutagenic response in *S. typhimurium* strains TA97a, TA98 and TA100, showed by doubling the spontaneous reversion rate; the most pronounced response was showed in bacterial strain TA98, with a maximum MI of 5.98 (Table 4). The polymer displayed a reproducible mutagenic response only in TA98 strain (MI from 3.26 to 3.93).

These results indicated the metabolic conversion of these chemicals (cysteine and polymer) to genotoxic intermediates by the enzyme system from the rat hepatic postmitochondrial

supernatant (S9 mix). Thus, cysteine and the polymer can be considered as indirect-acting mutagens.

Cysteine mutagenicity is described in the literature (GLATT, 1989; GLATT; PROTIC-SABLJIĆ; OESCH, 1983) as the result of the formation of the thiyl free radicals, product of its metabolism (CARTER; JOSEPHY, 1986) when tested at very high doses, as found here. This result does represent an isolated effect when used directly, at high concentration, with these bacterial strains, and it does not represent any problem to human or animal health, as also described in the literature (DE FLORA, 1990). In addition, the effect of the metabolism just could be considered for the materials that could be used inside the body, or as food, indicating the safety of the materials for the conventional application as polymer, outside the body.

Table 4 Revertants/plate, standard deviation, and mutagenicity index (in brackets) in the strains TA98, TA100, TA102 and TA97a of *S. typhimurium* after treatment with various doses of L-cysteine, maleic anhydride furan adduct and cys-DA polymer, in experiments with (+S9) and without (-S9) metabolic activation

		Number of revertents (M ± SD)/ plate and MI							
		TA98		TA100		TA102		TA97a	
		- S9	+ S9	- S9	+ S9	- S9	+ S9	- S9	+ S9
NC		35 ± 4	29 ± 9	145 ± 10	119 ± 14	262 ± 31	316 ± 48	162 ± 14	129 ± 10
PC		822 ± 76** _a	1189 ± 114** _d	1409 ± 106** _b	1290 ± 95** _d	1744 ± 212** _c	1688 ± 172** _c	1068 ± 84** _a	1318 ± 70** _d
mg/plate		L-cysteine (mg/plate)							
0.62		41 ± 9 (1.17)	164 ± 20** (5.66)	152 ± 20 (1.05)	209 ± 21* (1.75)	261 ± 21 (1.00)	330 ± 22 (1.04)	184 ± 8 (1.14)	347 ± 22** (2.69)
1.25		38 ± 8 (1.07)	173 ± 21** (5.97)	168 ± 29 (1.16)	218 ± 15** (1.83)	251 ± 32 (0.96)	336 ± 27 (1.06)	166 ± 11 (1.02)	430 ± 30** (3.33)
2.5		39 ± 6 (1.11)	174 ± 38** (5.98)	194 ± 16 (1.34)	235 ± 20** (1.97)	263 ± 16 (1.00)	302 ± 14 (0.95)	163 ± 17 (1.01)	433 ± 21** (3.36)
3.75		33 ± 6 (0.94)	173 ± 22** (5.95)	205 ± 26 (1.41)	249 ± 12** (2.09)	261 ± 36 (0.99)	293 ± 31 (0.93)	145 ± 21 (0.90)	447 ± 14** (3.47)
5		31 ± 7 (0.89)	167 ± 15** (5.76)	209 ± 21 (1.44)	247 ± 27** (2.08)	242 ± 48 (0.92)	312 ± 35 (0.99)	156 ± 25 (0.96)	487 ± 26** (3.78)
mg/plate		Maleic anhydride furan adduct							
0.62		38 ± 8 (1.09)	32 ± 4 (1.09)	151 ± 14 (1.04)	130 ± 11 (1.09)	283 ± 27 (1.08)	334 ± 19 (1.06)	169 ± 17 (1.04)	137 ± 13 (1.06)
1.25		34 ± 7 (0.97)	30 ± 3 (1.03)	143 ± 21 (0.98)	123 ± 13 (1.03)	288 ± 14 (1.10)	329 ± 21 (1.04)	155 ± 27 (0.95)	134 ± 10 (1.04)
2.5		36 ± 6 (1.03)	33 ± 1 (1.14)	158 ± 13 (1.09)	126 ± 16 (1.06)	279 ± 28 (1.06)	341 ± 24 (1.08)	152 ± 12 (0.94)	135 ± 25 (1.04)
3.75		38 ± 8 (1.07)	35 ± 4 (1.19)	153 ± 27 (1.06)	121 ± 19 (1.01)	273 ± 32 (1.04)	313 ± 21 (0.99)	156 ± 16 (0.96)	122 ± 12 (0.94)
5		32 ± 1 (0.91)	29 ± 4 (1.00)	141 ± 14 (0.97)	122 ± 18 (1.03)	254 ± 29 (0.97)	325 ± 14 (1.03)	146 ± 23 (0.90)	132 ± 11 (1.02)
mg/plate		Cys-DA Polymer							

0.62	35 ± 7 (1.00)	114 23** (3.93)	±	152 ± 21 (1.05)	110 ± 18 (0.92)	279 ± 24 (1.06)	287 ± 27 (0.91)	160 ± 23 (0.99)	143 ± 11 (1.11)
1.25	38 ± 4 (1.09)	111 18** (3.83)	±	148 ± 23 (1.02)	129 ± 7 (1.08)	240 ± 14 (0.92)	331 ± 16 (1.05)	159 ± 11 (0.98)	140 ± 14 (1.08)
2.5	35 ± 6 (1.00)	104 15** (3.57)	±	153 ± 27 (1.06)	131 ± 13 (1.10)	308 ± 23 (1.18)	326 ± 16 (1.03)	153 ± 10 (0.94)	128 ± 11 (0.99)
3.75	38 ± 1 (1.07)	95 29** (3.26)	±	150 ± 10 (1.03)	129 ± 11 (1.08)	237 ± 34 (0.90)	286 ± 37 (0.91)	150 ± 14 (0.93)	125 ± 8 (0.97)
5	34 ± 6 (0.97)	101 18** (3.48)	±	135 ± 11 (0.93)	118 ± 17 (0.99)	248 ± 37 (0.95)	310 ± 22 (0.98)	145 ± 10 (0.90)	126 ± 18 (0.97)

* $p < 0.05$ (ANOVA); ** $p < 0.01$ (ANOVA); M ± SD = mean and standard deviation; Negative Control (buffer): rate of spontaneous reversion; Positive Control (C+); ^a 4-nitro-o-phenylenediamine (10.0 µg/plate - TA98 and TA97a); ^b sodium azide (1.25 µg/plate - TA100); ^c mitomycin (0.5 µg/plate - TA102), in the absence of S9; and ^d 2-anthramine (1.25 µg/plate—TA98, TA100 and TA97a); ^e 2-aminofluorene (10.0 µg/plate—TA102), in the presence of S9. Values in brackets (MI) ≥ 2 indicate mutagenicity.

The polymer based on the furan maleic anhydride adduct and cysteine was synthesized and its structure confirmed by FTIR, ¹H NMR, and ¹³C NMR, aiming to study its safety for human handling by cytotoxicity tests. The features of the purified solvent-free polymer is a transparent hard and fragile film. The fragile feature is probably because its structure rich in rings from the furan maleic anhydride adduct, that infer rigidity to the material.

The thermo-reversibility of the polymer was tested and confirmed by ¹H NMR and ¹³C NMR, as well as by rheology. The formation of polymer networks increases viscosity during the polymerization process, and when these networks are broken by the rDA reaction, the viscosity decreased, as expected. The objective of showing the DA and rDA reactions for this polymer is just to confirm its Diels Alder features, and the success of the click chemistry reaction, leading the monomers to easily polymerize. We did not aim to show the thermo-reversibility of the reaction, neither the number of cycles by DA and rDA because its use in biological system will not reach higher temperatures then the body temperature, once it is the purpose of this work.

The biological characterization indicated that both the precursors and the resulting polymer were not mutagenic or cytotoxic to the tested cells. This confirms the harmless of using the furan maleic anhydride adduct to synthesize polymers. Here we have used the amino acid cysteine as the second building block for the synthesis because its harmless, once it is present in most the live organisms and it is not expected to show cytotoxic affects. Even the Cys-DA

polymer was synthesized for this specific purpose, to the best of our knowledge, it was not described in the literature.

4 CONCLUSIONS

The results reported in this study showed the easy and fast synthesis of the polymer based on furan maleic anhydride adduct and cysteine as an interesting and potential route that can open opportunities for the development of molecules for a wide range of applications, including new monomers and polymers. The high reactivity of the thiol-ene and amine-anhydride reactions led the amino acid to be simultaneously modified in its both functional groups. The sequence of the reaction could not be determined, as well the monomer isolation, because of the fast kinetics of this system. The proposed polymerization reaction was performed with success, generating a new polymer based on cysteine and furan-maleic anhydride DA adduct, and its chemical structure, as well its rDA reaction, were confirmed by FTIR and ^1H NMR spectroscopy and rheological tests. In addition, the biological characterization (genotoxicity and cytotoxicity tests) showed that this new polymer, as well all its precursors did not decrease cell viability at the tested concentrations in *in vitro* cell culture with human keratinocytes. The precursors and the polymer did not induce direct mutagenicity as showed by Ames tests. Mutagenic effect was found for cysteine and for the polymer after their metabolic activation (+S9), indicating that the polymer is safe for conventional use outside the body.

CHAPTER IV

*LYSINE GRAFTED POLY(LACTIC ACID): AN INTRINSICALLY ANTIMICROBIAL POLYMER*³

1 INTRODUCTION

1.1 Biomaterials in the medical field

In the field of biomedical science, biomaterials, often biodegradable and/or bioabsorbable, are used as tools to help to restore the body homeostasis. Although, these biomaterials that improve the patient life quality and the medical treatments, can also contribute to the emergence of nosocomial infections. Thus, there is an increasing demand for new biomaterials for application in the development of medical devices such as implantable materials (heart valves and bone substitutes) and devices used in hospitalizations or procedures, such as nasal cannulas, catheters and others (PIRES; BIERHALZ; MORAES, 2015), that could avoid or decrease the spread of nosocomial infections.

1.2 Nosocomial infections

Nosocomial infections represent a challenge to patient safety and public health, as they can lead to increased morbidity, mortality, and healthcare costs (REVELAS, 2012). The most common types of nosocomial infections include respiratory infections, urinary tract infections, surgical site infections, bloodstream infections, and gastrointestinal infections, and can be caused by bacteria, viruses, fungi, or other microorganisms (KAECH et al., 2006). These infections result mainly from the use of polymer-based materials in healthcare settings and represents a great challenge to be solved (ZANDER; BECKER, 2018). The relationship of polymer devices and the nosocomial infections is a global reality, mainly because the surface properties of these biomaterials, used for wound dressings, medical tubing, implants, among others (USCATEGUI; DÍAZ; VALERO, 2018). These surfaces can allow the protein adhesion when

³ This chapter was accepted as an article in the International Journal of Biological Macromolecules, on June 13th,2024 and is available to be consulted at <https://doi.org/10.1016/j.ijbiomac.2024.133181>.

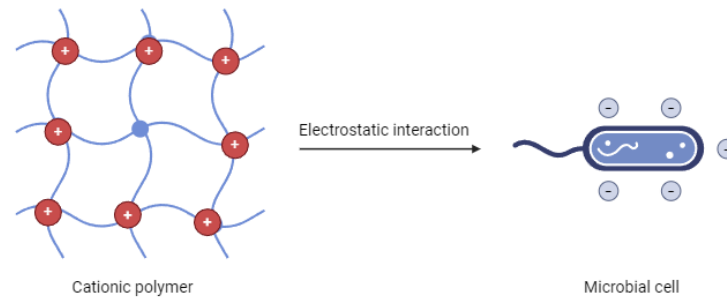
in contact with body fluids and trigger the bacterial adhesion and biofilm formation on the device's surface. Bacteria within the biofilm can detach and enter the bloodstream, leading to infections that can compromise the well-being and health of the patient (ZANDER; BECKER, 2018).

The main agents of nosocomial infections include *Klebsiella pneumoniae*, *Serratia marcescens*, *Escherichia coli*, *Enterobacter* spp., and *Pseudomonas aeruginosa* (KAECH et al., 2006; WEINER-LASTINGER et al., 2020). Moreover, the indiscriminate use of antibiotics has contributed to the emergence and spreading of new resistant bacterial strains that are highly disseminated and difficult to control, such as methicillin-resistant *Staphylococcus aureus* (MRSA), strains resistant to oxacillin, nafcillin, cefazolin, cephalexin, among others (GREMA, 2015; LEE et al., 2018). This problem became even more evident during the COVID-19 pandemic, with a high rate of hospitalizations and an increase of procedures such as intubation, and the use of medical devices like probes and catheters (BARDI et al., 2021).

1.3 Biomaterials with antimicrobial properties

Antimicrobial biomaterials have been designed and emerged to actively inhibit the growth of microorganisms and prevent nosocomial infections. This antimicrobial property can be achieved by materials that release the antimicrobial agents (or substances that prevent microbial colonization), or by materials in which the antimicrobial activity is inherent to the polymer structure, ie, which acts by contact and is not released from the material. This particular property is of great interest for manufacturing devices to be used in body, as they can reduce or inhibit the growth of microorganisms on their surface, decreasing the rate of nosocomial infections. Polymers such as chitosan, halamines, and poly(L-lysine) exhibit antimicrobial properties intrinsically provided by their structures (JAIN et al., 2014), specifically by the free amine groups attached to their main chain, capable of destabilizing the outer membrane of microorganisms (Figure 34). However, other desired properties, such as good mechanical strength, processability, and solubility (or lack thereof) limit their application. For instance, chitosan's processability is restricted by its solubility, since it does not behave like a thermoplastic; poly(L-lysine) is soluble in water, which hampers its application in physiological environments (CLARO et al., 2016; LI et al., 2014).

Figure 34. Scheme of the antimicrobial action mechanism involving electrostatic interactions. Adapted from Babutan et al, 2021. (BABUTAN; LUCACI; BOTIZ, 2021)



Created in BioRender.com 

In this scenario, there is a great demand for new materials with intrinsic antimicrobial activity for the effective industrial manufacturing of medical devices. Thus, the demand for chemical modification of polymers with good mechanical and thermal properties, such as thermal and chemical stability, mechanical strength, elasticity, among others, such as PLA, stands out. To mimic the structure of antimicrobial aminated polymers, amino acids can be grafted to polymers structure. Lysine, in particular, is an excellent anchor for grafting to polymers due to its amino group available for chemical reactions. Hydrophilic polymers such as polyethylene glycol (PEG) were grafted to lysine or poly-L-lysine to enhance its solubility and the half-life of drugs, thereby enhancing their therapeutic efficacy (CHOI et al., 1998; KAMINSKAS et al., 2008). Lysine grafted to poly(ethylene terephthalate) was developed to improve hemocompatibility and anti-biofouling properties (ZHI et al., 2014). Additionally, lysine grafted to poly(glycidyl methacrylate) structure can be applied in the adsorption of organic dyes in aquatic environments (JING; WANG; TAN, 2018). Direct grafting is often not possible, so an intermediate reaction is necessary, and the polymer maleation represents a reliable alternative for such purposes (BSHENA et al., 2011). To the best of our knowledge, the grafting of lysine to polymers such as PLA and its application as a biomaterial with antimicrobial properties have not been described in the literature.

1.4 Poly(lactic acid)

PLA is an aliphatic polyester widespread use in the industry due to its thermoplastic properties (ILYAS et al., 2021). Furthermore, it is synthesized from renewable natural sources, making it advantageous compared to conventional petroleum-based polymers (RAJESHKUMAR et al., 2021). PLA is both biodegradable and biocompatible, with good processability, enabling it to be molded according to specific application (FARAH; ANDERSON; LANGER, 2016). Common processing techniques for PLA include extrusion and injection molding. Due to these characteristics, PLA has found extensive applications in the industry, particularly in packaging, textile fibers, and as filaments for 3D printing. Thus, its utilization has been growing within the medical field, where it serves as a material for various devices, including cannulas, catheters, sutures, implants, stents, bone fixation screws, among others (DESTEFANO; KHAN; TABADA, 2020).

Therefore, the development of new materials based on PLA for the manufacture of medical devices that displays intrinsic antimicrobial properties and processability is crucial. With this in mind, this work focuses on grafting lysine to PLA structure, aiming that the free amine group from the grafted amino acid could infer the intrinsic antimicrobial activity to PLA. To achieve this, PLA was chemically modified in two steps, first, maleation, followed by the reaction with the amino acid lysine.

2 MATERIALS AND METHODS

2.1 Materials

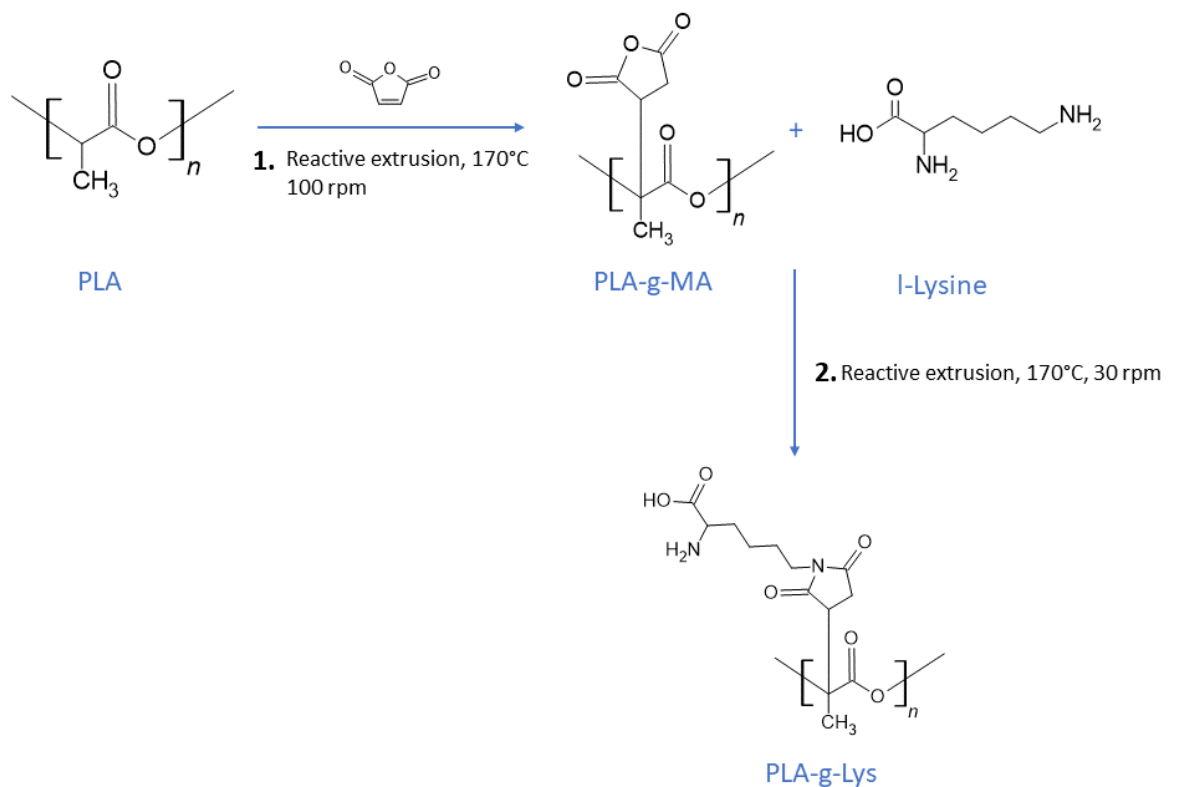
Commercial poly(lactic acid) pellets of Ingeo Biopolymer 3D850 from NatureWorks (purchased from 3D Lab, Brazil), maleic anhydride and benzoyl peroxide (Êxodo Científica), L-lysine monohydrochloride and chloroform (Synth). Nutrient broth (beef extract 1.0; yeast extract 2.0; peptone 5.0; sodium chloride 5.0 g/L⁻¹, Kasvi), Agar (Dinâmica), *Escherichia coli* (ATCC 43895) and *Staphylococcus aureus* (ATCC 25923). Deuterated chloroform (Sigma). L929 mouse fibroblast, Dulbecco's modified Eagle's medium (DMEM), fetal bovine serum (FBS), dimethyl sulfoxide and MTT (3-(4,5-dimethylthiazol-2-yl)-2,5 diphenyltetrazolium bromide), all purchased from Sigma-Aldrich.

2.2 Methods

2.2.1 Poly(lactic acid) modification by two- step reactive extrusion

PLA (100 g), maleic anhydride (2 g) and benzoyl peroxide (0.5 g) were mixed in a beaker and then transferred to a benchtop extruder (AX Plásticos, model Lab-16) with a 16 mm L/D 26 single screw operating at 100 rpm. The temperature profile of the extruder was, respectively, from the feeding zone to die, 170 °C, 180 °C and 185 °C. The extruded product was collected and ground in a mill, resulting in a mass of 89 g. 60 g of the product was used for the following extrusion, mixed with 2.6 g of L-lysine. This procedure was carried out using two zones, with the die set at 170 °C and a rotation speed of 30 rpm. The intermediary (PLA-g-MA) and the end product (PLA-g-Lys) were dissolved in chloroform (three times) to remove residual non-bonded lysine, then dried in an oven at 50 °C for three hours and stored for analysis. The chemical reactions for PLA chemical modification are represented in Figure 35.

Figure 35. Scheme of the maleation reaction of PLA (reaction 1) and extrusion with lysine (reaction 2).



2.3 Characterization

2.3.1 Fourier Transform Infrared Spectroscopy (FTIR)

L-lysine, PLA, PLA-g-MA and PLA-g-Lys were analyzed using a Perkin-Elmer Spectrum 100 FT-IR Spectrometer equipped with an attenuated total reflectance (ATR) device of diamond coated with zinc selenide crystal. The spectra were in the range of 600 to 4000 cm^{-1} , with 4 cm^{-1} resolution and 16 scans, the spectral outputs were recorded in transmittance.

2.3.2 ^1H Nuclear magnetic resonance (^1H NMR)

^1H spectra were acquired at 14.1 T, 600.13 MHz for ^1H , using Bruker Avance II HD equipment. PLA, PLA-g-MA and PLA-g-Lys samples were dissolved in deuterated solvent (CDCl_3) at 1 % wt. (w/v). For ^1H spectra observation: 90° pulse of 11.02 ms; recycle delay 1s; acquisition time 2.73 s; 64 scans, spectral width 20 ppm, number of points 65536.

2.3.3 Thermal Analysis

The thermal properties were investigated by Differential Scanning Calorimetry (DSC) in a DSC25 equipment from TA Instruments. The sample was conditioned at 40°C for 24h before testing. Dry samples (7 mg) were placed in a hermetically sealed aluminum pan. The tests were conducted with a nitrogen purge gas (50 mL/ min) at a heating rate of 10 °C/ min from 25°C to 200° C (isothermal for 10 min), and cooling to -65 °C at a rate of 20 °C/ min, followed by a second heating until 200 °C at rate 10°C/ min. The melting temperature (T_m), glass transition temperature (T_g), and cold crystallization temperature (T_{cc}) were determined by the second heating scan, and crystallization temperature (T_c) by the cooling scan. The enthalpies of the transition temperatures were determined, too. The crystallinity degree (X_c , %) was calculated by the equation (1) (BATTEGAZZORE; BOCCHINI; FRACHE, 2011)

$$X_C(\%) = \frac{\Delta H_m - \Delta H_{cc}}{\Delta H_m^0 \times w} \times 100 \% \quad (1)$$

Note: X_c was crystallinity. ΔH_m was the enthalpy of melting. ΔH_{cc} was the cold crystallization enthalpy. ΔH_m^0 was the melting enthalpy of PLA 100% crystalline, considered the value of 93.6 J/g. And w was the weight fraction of PLA in the sample.

The thermal decomposition behavior of the sample was estimated using thermogravimetric analysis conducted in TGA55 equipment from TA Instruments at a heating rate of 10°C/ min from 25° to 600° C.

2.3.4 Mechanical analysis

The samples were cut (approximately 30 mm length) and their ends were glued with double-sided tape on a foam of ethylene vinyl acetate surface in order to avoid concentration of stresses in the fixation of the specimen in the device. The tensile testing samples were conditioned in Mg (NO₃)₂ saturated solution inside a glass desiccator (to generate nearly 52 % RH) for 2 weeks prior to tests, in accordance with ASTM E104. Mechanical tensile test was performed on a universal testing machine EMIC DL30000 at room temperature, using 1 kN load cell and knurled fastening device with spring closure. The tensile test was performed at a 1 mm.min⁻¹ with a preload of 15 N. The test was performed on five specimens for each sample, the stress x strain curves show the average of the specimens, and the maximum tensile strength, and the strain were determined until failure.

2.3.5 Antimicrobial activity

The antibacterial activity of PLA and PLA-g-Lys samples was tested using the Dynamic Shake Flask Test Method (ASTM E2149-10) against *E. coli* and *S. aureus*. Bacteria were inoculated in nutrient agar, grown for 18 hours at 37 °C and then suspended in a 0.85 % sterile sodium chloride solution to reach a turbidity equivalent to McFarland standard 0.5 (~1.5x 10⁸ CFU/ mL⁻¹). Further dilutions were performed with sterile 0.85 % sodium chloride solution to reach a bacterial concentration of 1x10⁵ CFU/ mL⁻¹.

PLA and PLA-g-Lys (30 mg) were sterilized in an autoclave. Then, 300 µL of the bacterial suspension (1x 10⁵ CFU/ mL⁻¹) was added to the samples and incubated at 37 °C under continuous shaking for 18 hours. The bacterial suspension was diluted using the serial dilution method and 100 µL was spread on the surface of nutrient agar and incubated at 37 °C for 24

hours. The number of colonies forming units (CFU) was determined by counting the colonies. The bacterial suspension (1×10^5 CFU/ mL⁻¹) was used as control. All procedures were carried out under sterile conditions.

2.3.6 Cell Viability

The materials were analyzed following ISO 10993-5 (2009) (Biological evaluation of medical devices, Part 5: Tests for in vitro cytotoxicity), using their aqueous liquid extract.

Cell culture - L-929 mouse fibroblasts were seeded in DMEM culture medium supplemented with 10 % FBS and maintained at 37 °C with 5 % CO₂ atmosphere until the cells reached 90 % confluence. The cells were then cultured in 96-well plates (1×10^4 /well) in DMEM supplemented with 10 % FBS and incubated for 24 hours at 37 °C with a 5 % CO₂ atmosphere for cell adhesion.

To prepare the liquid extract, PLA, PLA-g-MA and PLA-g-Lys (15 mg each) were placed into 1 mL of DMEM culture medium supplemented with 10 % fetal bovine serum (FBS) in a 2 mL centrifuge microtube. The tubes were kept at 37 °C with 5 % CO₂ for 24 hours. After the incubation period, the supernatant culture medium was removed and used in the MTT test.

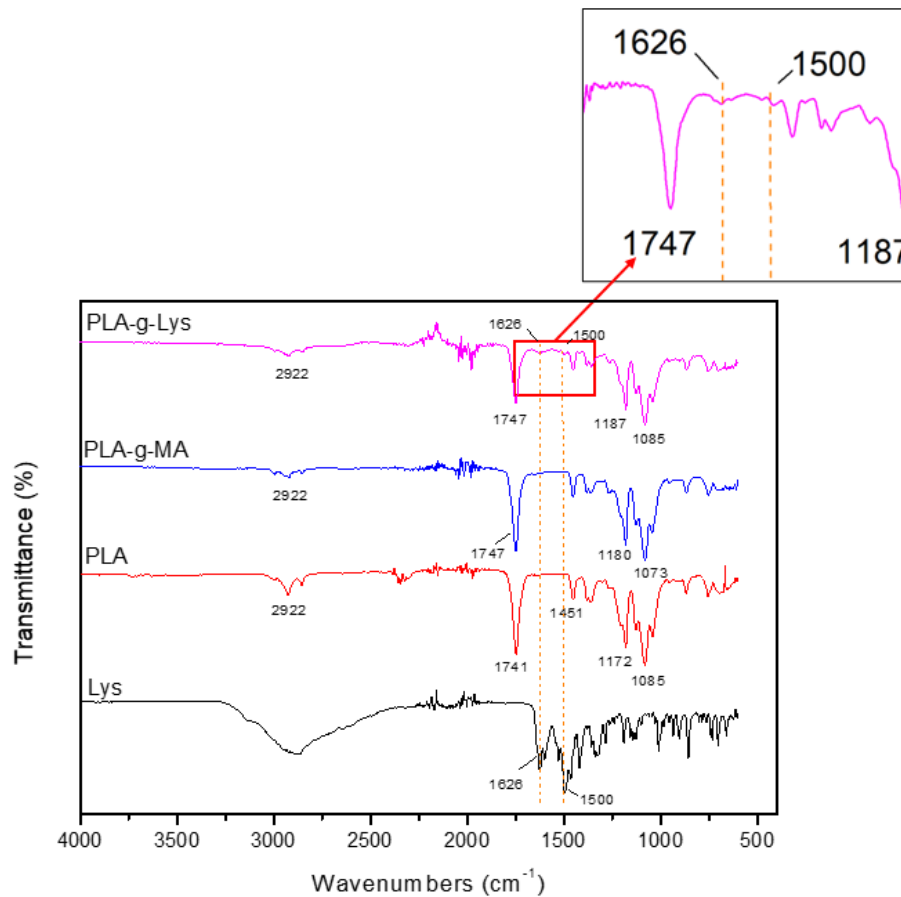
The cytotoxicity was determined using the MTT assay. To evaluate the cytotoxicity of PLA, PLA-g-MA and PLA-g-Lys samples, L929 cells were cultured in 96-well plates (1×10^4 /well), in triplicate and filled with 100 µL of conditioned medium from each material for 24 h at 37 °C. The negative control was the culture medium, and the positive control was the dimethyl sulfoxide (70 wt %) water solution. After 24 h of contact with the liquid extract, the wells were washed with 150 µL of PBS. MTT solution (50 µL, 5 mg/mL) was added to each well, and the plate was incubated for 4 h at 37° C, protected from the light. The MTT solution was then removed, and the formazan crystals were solubilized using 50 µL of DMSO. The absorbance was measured at 570 nm using a SPECTRAMax Gemini XS (Molecular Devices) microplate reader. The test was performed in three independent runs on different days, each run being done in triplicate. The cell viability was calculated following ISO 10993-5 (2009) recommendations.

3 RESULTS AND DISCUSSION

3.1 Fourier Transform Infrared Spectroscopy (FTIR)

The FTIR spectra of the samples are shown in Figure 36. The bands related to PLA at 2934 cm^{-1} (C-H) and 1454 cm^{-1} (CH_3) [24] are preserved in the PLA-g-Lys spectrum. The band corresponding to the C=O at 1741 cm^{-1} in the PLA spectrum was shifted to 1747 cm^{-1} in the spectrum of the maleated sample, as the result of the maleimide C=O vibration bands overlapping the PLA C=O bands. This band is also shifted in PLA-g-Lys sample. Two new weak bands appeared in the PLA-g-Lys spectrum, at 1626 and 1500 cm^{-1} , corresponding to the C=O from lysine after chemical modification, and its N-H deformation vibrations, respectively (SZYC; PILORZ; CZARNIK-MATUSEWICZ, 2008).

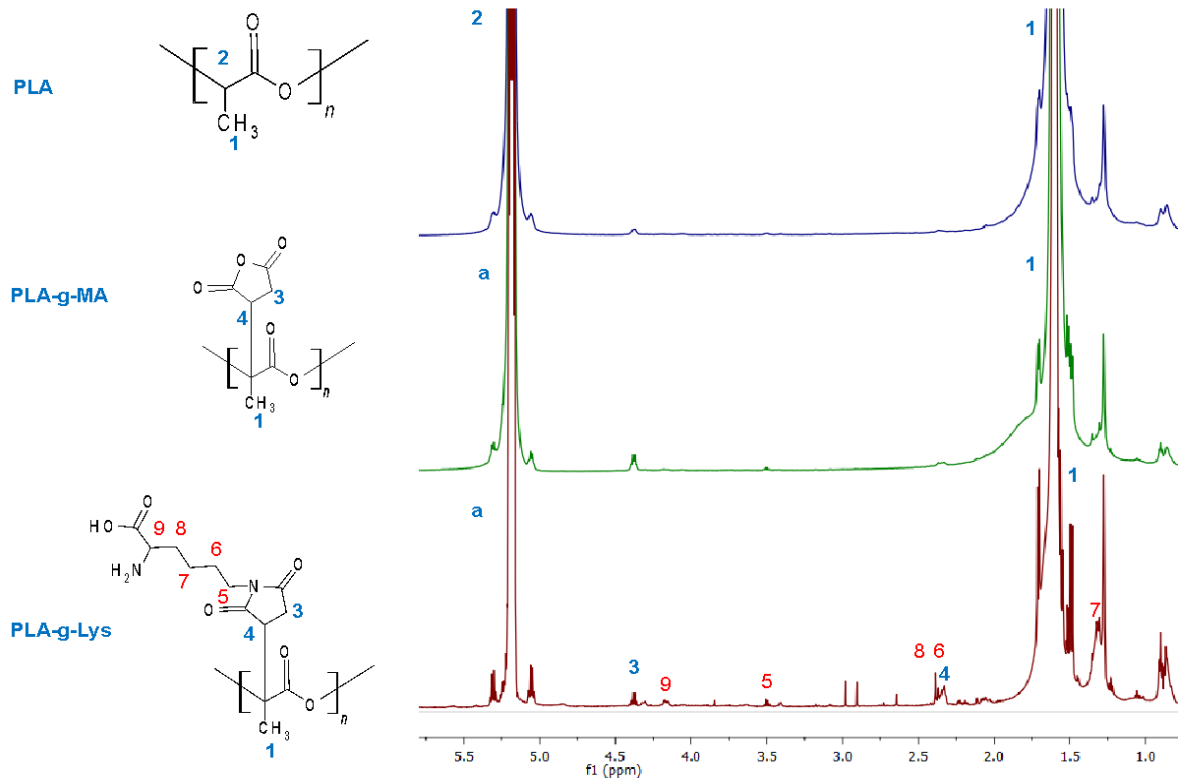
Figure 36. FTIR spectra of PLA, PLA-g-MA and PLA-g-Lys samples.



3.2 ^1H NMR

The samples were also analyzed by ^1H NMR spectroscopy, and the spectra of PLA, PLA-g-MA and PLA-g-Lys are shown in Figure 37. The PLA spectrum shows two high intensity peaks at 1.52 ppm and 5.27 ppm, corresponding to the methine and methyl protons of PLA, respectively (GARDELLA; CALABRESE; MONTICELLI, 2014). After the maleation of PLA, the spectrum showed a decrease in the integration value of the peak at 5.27 ppm, where the reaction took place. The integration values can be seen at Table 5. The PLA-g-Lys spectra, showed the new peaks corresponding to the lysine structure at 1.32, 1.95, 2.07, 3.51 (methylene protons) and 4.17 ppm (methine protons), indicating the grafting of the amino acid to PLA-g-MA. Very weak peaks at 2.3 and 4.3 ppm, corresponding to the methine and methylene protons from the succinic anhydride ring, respectively (PENG; DING; XUE, 2012), appeared in the spectra of PLA-g-Lys. The peak at 5.27 ppm in the PLA-g-MA and PLA-g-Lys spectra correspond to the methyl protons from PLA that did not react with maleic anhydride. This peak was represented by “a” in their respective spectra in Figure 37.

Figure 37. ^1H NMR spectra of PLA, PLA-g-MA and PLA-g-Lys samples. “a” represents the unreacted peak 2 from PLA, considering that the structures of PLA-g-MA and PLA-g-Lys in the figure did not show peak 2.



The integration peaks of PLA, PLA-g-MA and PLA-g-Lys are shown in Table 5. The integration results indicated that the maleation reaction led to the grafting of about 4.1 % of maleic anhydride to the PLA structure. The content of grafted lysine was smaller, approximately 1.3 %. The degree of substitution was primarily confirmed by changes in the integration peaks at the reaction site, which may be seen as a limitation of this work. Thus, we propose using this method as a new strategy to determine the degree of substitution in PLA.

Table 5. ^1H NMR peak assignments and integrations for PLA, PLA-g-MA and PLA-g-Lys.

PLA		PLA-g-MA		PLA-g-Lys	
Shift (ppm)	Integration	Shift (ppm)	Integration	Shift (ppm)	Integration
1.52	3	1.52	3	1.52	3
5.27	0.97	5.27	0.93	5.27	0.93
				1.32	0.03
				1.95, 2.07	0.06
				3.51	0.03
				4.17	0.01

3.3 Thermal Analysis

Figure 38 shows the DSC curves for PLA, PLA-g-MA, and PLA-g-Lys, and Table 6 shows the values of thermal transitions, enthalpies, and crystallinity degrees generated from the DSC curves. Figure 38(a) shows the transition in the heating, in which PLA glass transition temperature (T_g) appears at 58.34 °C, cold crystallization temperature (T_{cc}) at 107.62 °C, and the melting temperature (T_m) at 175.96 °C. The endothermic melting peaks can be seen in all samples, however, a bimodal peak has appeared in the curves of PLA-g-MA and PLA-g-Lys (T_{m1} and T_{m2}). This pattern can be associated with the formation of different crystalline structures (HUANG et al., 2021; JIMÉNEZ; PELTZER; RUSECKAITE, 2014). In addition, the melting temperature of the modified samples have decreased, PLA-g-MA displayed T_{m1} at 156.27 and T_{m2} at 161.30 °C, and PLA-g-Lys T_{m1} was 158.67 and T_{m2} was 163.15 °C. The enthalpies were also increased with the incorporation of lysine, indicating the increased degree of crystallization of the material.

Figure 38(b) shows the curves generated in the cooling. The cooling lines of the PLA indicated that it did not crystallize at cooling (no crystallization peaks at cooling). A small crystallization can be seen at the heating curve, closely to the melting temperature. PLA-g-MA and PLA-g-Lys showed crystallization peaks at T_c of 91.48 and 96.61 °C, respectively. The degree of crystallization (X_c) calculated from the enthalpy values of the second heating curve was 1.8 % for the PLA, 57.62 % for the PLA-g-MA, and 65.08 % for the PLA-g-Lys.

Figure 38. DSC thermograms of PLA, PLA-g-MA, and PLA-g-Lys for (a) second heating at 10°C/min and (b) cooling at 10°C/min.

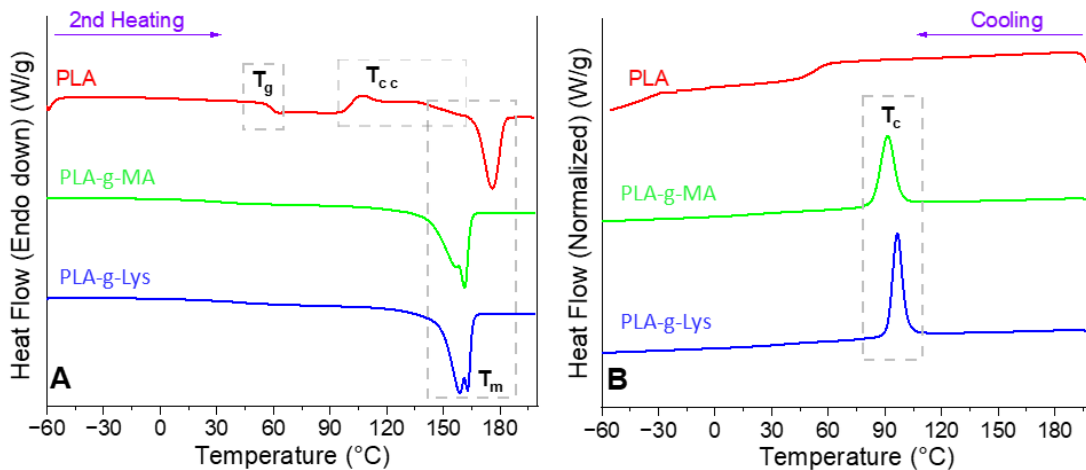


Table 6. Thermal Transitions of DSC data from heating and cooling process to PLA, PLA-g-MA, and PLA-g-Lys.

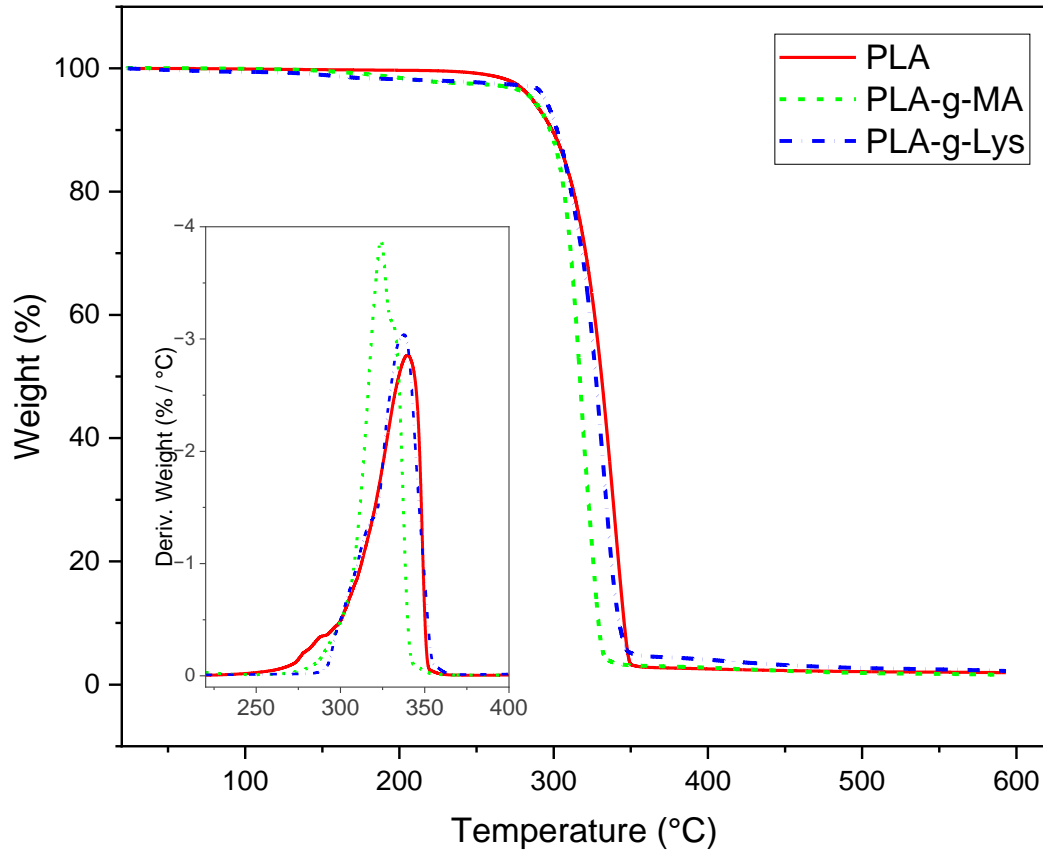
Sample	Thermal Transitions (°C)					ΔH_{cc} (J/g)	ΔH_c (J/g)	ΔH_m (J/g)	X_c (%)
	T_g	T_{cc}	T_c	T_{m1}	T_{m2}				
PLA	58.34	107.62	-	175.96	-	9.31	-	38.38	1.8
PLA-g-MA	-	-	91.48	156.27	161.30	-	38.48	52.62	57.62
PLA-g-Lys	-	-	96.61	158.67	163.15	-	42.76	56.94	65.08

PLA displays relatively low crystallinity that can hinder its processing and application. Branched structures inserted into PLA chains can increase its crystallization, improving its processing efficiency (LI et al., 2022a; TIWARY; KONTOPOULOU, 2018). The unmodified PLA used in the study is sensitive to nucleation, and the inclusion of additives may increase the crystallization kinetics. This feature enhances the effectiveness of PLA filaments for 3D printing improving processing at high-speed production without compromising mechanical properties (SCHIAVONE; VERNEY; ASKANIAN, 2020).

The double melting peaks and reduced T_m found for PLA-g-MA and PLA-g-Lys suggests that the grafted groups affected the formation of PLA crystals, leading to different degrees of crystallinity. Furthermore, crystallization can be affected by variations in molar mass. Some authors report a reduction in molecular weight during the grafting process (OLIVER-ORTEGA et al., 2022; RIGOLIN et al., 2019) . This change influences the increase in the mobility of the PLA molecular chain and the promotion of crystallization (JANG et al., 2022; LI et al., 2022b).

The DSC results showed that the temperature and the degree of crystallization of both modified samples PLA-g-MA, and PLA-g-Lys increased considerably, reducing its melting temperature and improving their processability. The improvement in PLA crystallization performance is more pronounced with the incorporation of lysine because of its longer branched chain structure (when compared to maleic anhydride) that possibly acted as nucleation site.

The thermal stability of the materials was analyzed by thermogravimetric analysis and the results are shown in Figure 39. Table 7 shows the results from the curves where T_{onset} represents the onset decomposition temperature, T_{end} is the end decomposition temperature, and T_{dmax} is the peak degradation temperature from the derivative weight curves. When comparing the samples, the PLA-g-MA curve was shifted to the left, with lower temperatures than the others. PLA-g-Lys behavior was similar to PLA, with T_{dmax} of 324.74 °C, close to 339.29 °C of PLA. The mass loss at the maximum composition temperature was about 27.81 % for PLA, 49.63 % for PLA-g-MA and 56.84 % for PLA-g-Lys. PLA-g-Lys showed a slightly higher degradation temperature than PLA-g-MA, however its considerably higher weight at the maximum degradation temperature (Table 7), suggests its higher thermal stability.

Figure 39. Thermogravimetric analysis of PLA, PLA-g-MA and PLA-g-Lys.**Table 7.** TGA data of PLA, PLA-g-MA, and PLA-g-Lys.

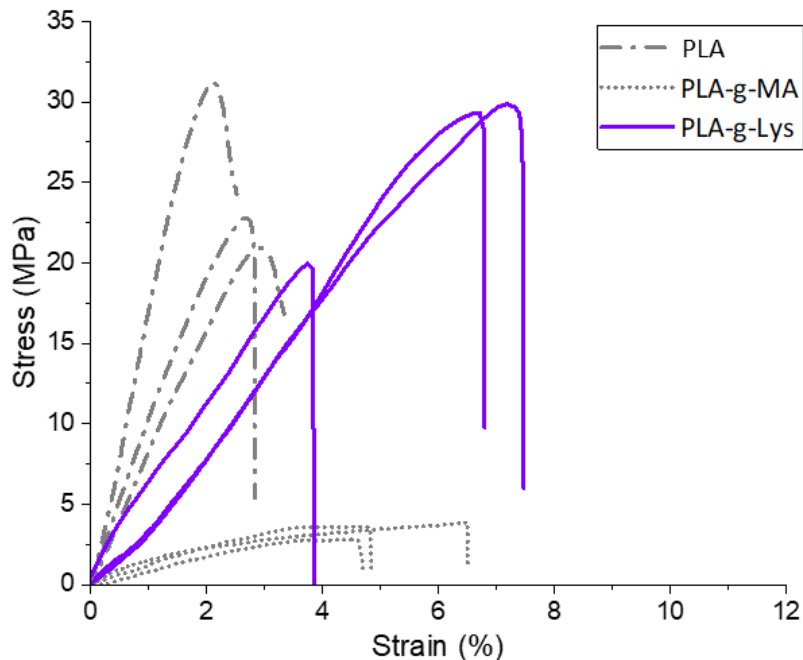
Sample	T _{onset} (°C)	T _{end} (°C)	T _{dmax} (°C)	Weight at T _{dmax} (%)
PLA	314.02	348.25	339.29	27.81
PLA-g-MA	304.07	329.27	317.07	49.63
PLA-g-Lys	311.63	332.89	324.74	56.84

3.4 Mechanical properties

The results of the mechanical properties products of the reactive extrusion with maleic anhydride and lysine were studied and the stress-strain curves of the PLA, PLA-g-MA and

PLA-g-Lys are shown in Figure 40. The extruded PLA showed the maximum tensile strength of 28.8 ± 8.9 MPa, elongation until the warping 2.9 ± 0.6 %, and Young's modulus of 1.3 ± 0.4 GPa. The PLA-g-MA extruded showed the maximum tensile strength of 3.0 ± 0.77 MPa, elongation at break of 4.3 ± 1.81 %, and Young's modulus of 0.1 ± 0.06 GPa. The maleation reaction clearly decreased the mechanical performance of PLA-g-MA when compared to PLA. This effect was already described in the literature, and even for low degree PLA maleation, the mechanical properties were considerably reduced when compared to PLA (CLASEN; MÜLLER; PIRES, 2015). However, after the reaction with lysine the curves clearly show an interesting increase in all the mechanical properties. PLA-g-Lys displayed increased maximum tensile strength when compared with PLA-g-MA, with a tensile stress of 26.7 ± 4.7 MPa, close to PLA, elongation at break about 7.6 ± 2.9 %, and Young's modulus of 0.5 ± 0.04 GPa. After the mechanical tests, the broken specimens of PLA-g-Lys showed several cracks along its length, a feature that can be attributed to the increased crystallization.

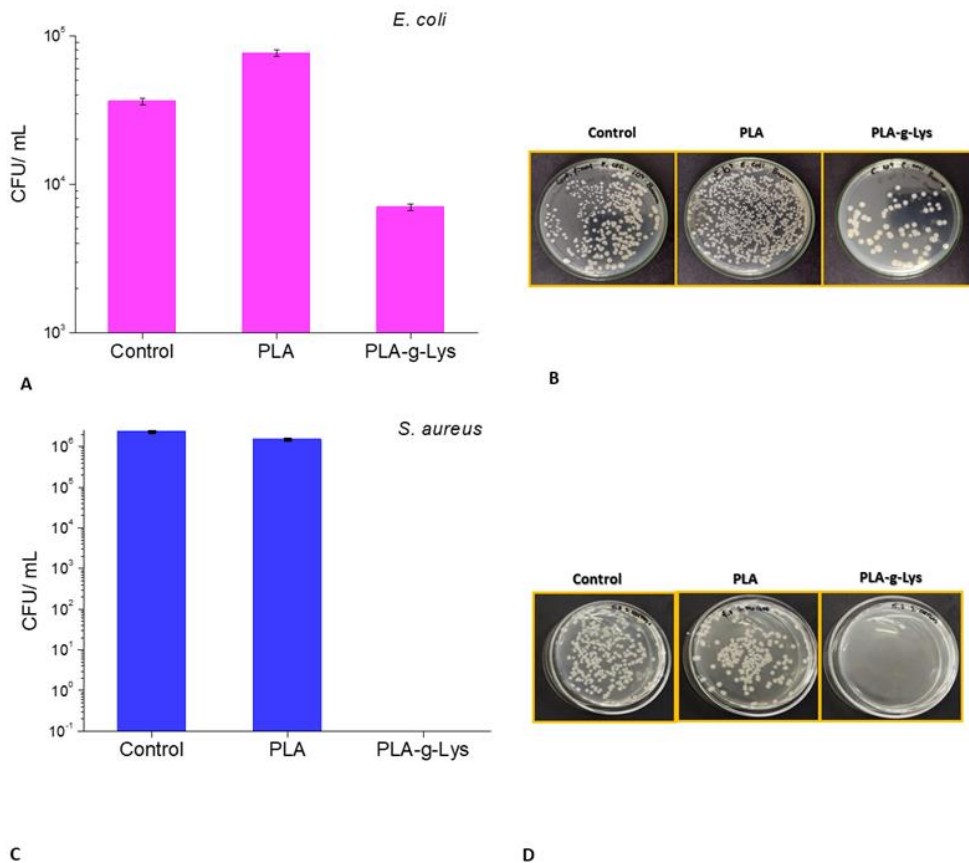
Figure 40. Stress-strain curves of the extruded filament samples of PLA, PLA-g-MA and PLA-g-Lys.



3.5 Antimicrobial Activity

The results of antimicrobial activity assay for the control, PLA and PLA-g-Lys, and the corresponding images displaying the countable colonies, are presented in Figure 41. These results indicate a decrease in bacterial growth after contact with PLA-g-Lys for both tested bacteria. Specifically, PLA-g-Lys inhibited approximately 80 % (equivalent to 7×10^3 CFU) of *E. coli* growth when compared to the control (3.6×10^4 CFU) and 92 % (7.6×10^4 CFU) compared to unmodified PLA (Fig 7 a and b). Notably, PLA-g-Lys inhibited more than 99 % of *S. aureus* growth compared to unmodified PLA (2.2×10^5 CFU) and the control (3.5×10^5 CFU) (Fig 7 a and c).

Figure 41. Antimicrobial assay demonstrating the growth inhibition of *E. coli* and *S. aureus* by the control, PLA, and PLA-g-Lys samples (A and C, respectively), and the corresponding colony-forming unit counts for *E. coli* (B) and *S. aureus* (D).



The higher inhibition of bacterial growth exhibited by the PLA-g-Lys sample, compared to the control or PLA, can be attributed to the grafting of the amino group (NH₂) into the PLA structure. It is well known that polymers with pendant amines, such as chitosan, exhibit antimicrobial properties. In an aqueous medium, the amino group in their structure becomes protonated and interacts with the negatively charged membrane of microbial cells (KONG et al., 2010). This interaction can interfere with membrane properties in two ways: by altering the membrane's permeability, leading to internal osmotic imbalances that inhibit the microbial growth, and by hydrolyzing the peptidoglycans of the microbial cell wall, resulting in the leakage of intracellular electrolytes such as potassium ions, proteins, nucleic acids, glucose, and other essential components for cell function (GOY; BRITTO; ASSIS, 2009).

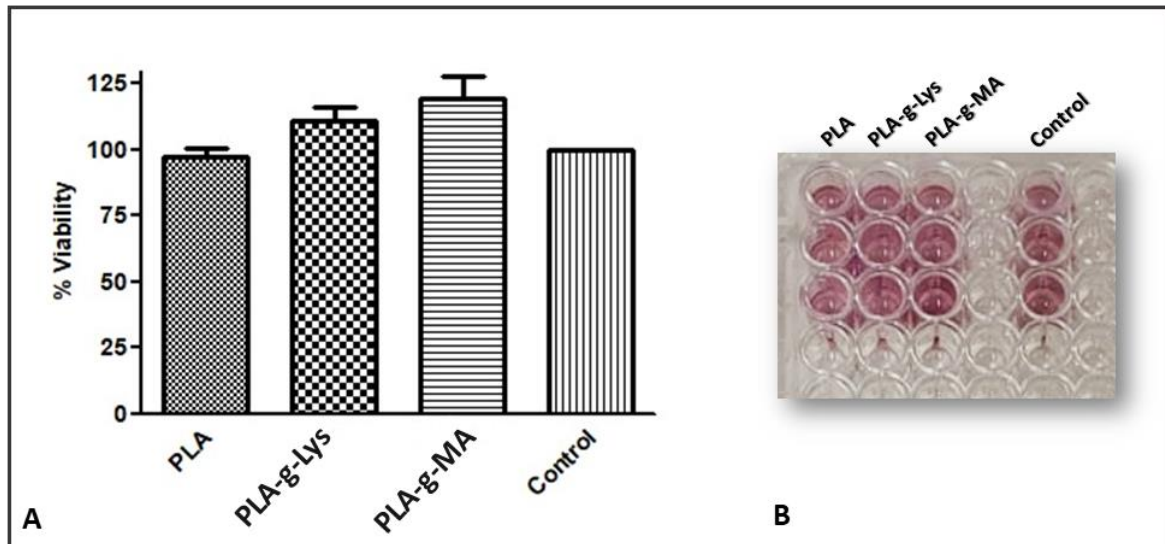
The increased inhibition in *S. aureus* is consistent with the literature, where it is observed that polymers with exposed amines, particularly chitosan, exhibit higher antimicrobial activity against these gram-positive bacteria (COSTA et al., 2017; RODRÍGUEZ-NÚÑEZ et al., 2012).

3.6 Cell Viability

PLA, PLA-g-MA, and PLA-g-Lys samples were evaluated for cytotoxicity using the MTT test on L929 cells. In this test, the cell viability is determined by MTT reduction by live organisms, as the result of their mitochondrial activity. MTT is metabolized by mitochondrial dehydrogenases, changing its yellowish color to blue or purple, the color of the reduced product formazan, indicating the respiratory chain activity.

The results of the test are shown in Figure 42. All tested samples showed cell viability equal to or greater than the control, indicating that the tested materials did not kill the cells (Fig 42 a). Figure 42 b shows the purple color on the plate wells, corresponding to the formation of formazan product for PLA, PLA-g-Lys, PLA-g-MA, and Control, respectively, indicating that the cells were alive and metabolically active.

Figure 42. (A) Cell viability (%) for the tested samples. All tested samples showed cell viability equal to the control ($p < 0,05$). (B) Plates with purple color, representing the cell viability.



The cell viability of L929 cells exposed to PLA is consistent with the literature. Therefore, the results with PLA-g-MA and PLA-g-Lys were expected, as PLA is generally not toxic to cells (HOVEIZI et al., 2014; SIQUEIRA et al., 2015).

In summary, the structure-properties relationship of the new PLA-g-Lys derivative represents a significant advancement in the development of new materials for medical and biological applications. The method used for grafting the molecules to PLA, namely reactive extrusion, is advantageous for industrial production, as it can be prepared on a large scale and is a common processing method in the plastics sector. Additionally, reactive extrusion generated an efficient grafting of maleic anhydride and lysine to PLA. The resulting material PLA-g-Lys derivative can be processed on a large scale without degradation, which is crucial for the industrial manufacture of several types of devices. Therefore, PLA-g-Lys shows high potential for implementation in the industrial sector. Moreover, the antimicrobial properties of PLA-g-Lys are very desirable for developing devices for use in contact with the body, aiming to decrease or avoid the infection rate and spreading among the patients within the hospital. The material also exhibited no cytotoxic effect on eukaryotic cells, indicating its biocompatibility, which is

another advantageous property supporting its industrial production for use in medical devices fabrication.

4 CONCLUSION

Reactive extrusion was used to modify PLA. The first step involved the maleation of PLA with maleic anhydride, followed by grafting L-lysine into PLA structure. The resulting product was characterized by FTIR, ¹H NMR, thermal, and mechanical analyses. FTIR and ¹H NMR confirmed the grafting of the amino group into the PLA structure. The cold crystallization peak of PLA disappeared, and an exothermic crystallization peak emerged during the cooling of modified PLA samples, showing improved crystallization of PLA-g-Lys, reducing its melting temperature, and improving the processability of the material. Biological characterization showed that PLA-g-Lys inhibited *E. coli* and *S. aureus* growth, with particularly strong inhibition of *S. aureus*. Moreover, both unmodified and modified PLA did not affect cell viability in the tested cells, indicating their harmless. In summary, the results suggest the successful preparation of a novel material derivative from PLA, exhibiting robust antimicrobial properties and enhanced processability. These findings suggest that the modified PLA is as a promising candidate for applications such as the manufacturing of medical devices.

CHAPTER V

CHEMICAL MODIFICATION OF STARCH AND CHITOSAN FOR THE PREPARATION OF POLYSACCHARIDE CONJUGATES FOR BIOMEDICAL APPLICATIONS⁴

1 INTRODUCTION

Antimicrobial biomaterials for biomedical applications have been developed to actively inhibit the growth of microorganisms and prevent or treat infections. These materials achieve antimicrobial properties either by releasing antimicrobial agents or by inherent properties of the material structure, which act on contact without releasing substances. More details of these type of biomaterials are given at **Chapter IV, section 1.3**.

1.1 Chitosan

Chitosan is the second most abundant polysaccharide, after cellulose and it is derived by partial deacetylation of chitin ((1→4)-2-acetamino-2-deoxy-β-D-glucopyranose) (YOUNES; RINAUDO, 2015). Chitosan is frequently used in the preparation of films and coatings due to its properties of biocompatibility, biodegradability (DÍAZ BUKVIC; ROSSI; ERREA, 2023), ability to form flexible and transparent films, adhesion to various types of surfaces, release potential controlled medication, in addition to intrinsically presenting antimicrobial properties (SAHARIAH; MÁSSON, 2017). Due to all these characteristics, chitosan has been used in several areas, such as food, biomedical engineering, regenerative medicine, among others.

⁴ This chapter is the result of a work developed during an internship at Instituto Tecnológico de Buenos Aires, Argentina. This work was improved with more synthesis and characterizations and was submitted as an article in the International Journal of Biological Macromolecules, on March 25, 2024 and it's status in June 18, 2024 is: In revision.

1.2 Starch

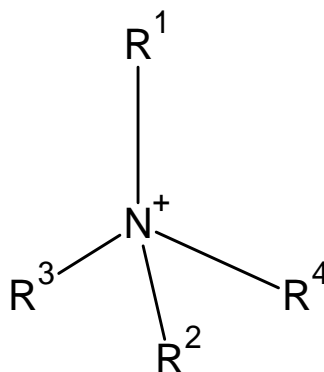
Starch is a natural polysaccharide, abundant and inexpensive widely used in industries like food and pharmaceuticals. This polymer is derived from renewable plant sources such as corn and potatoes. Starch is inherently biocompatible, non-toxic, and biodegradable, making it suitable for various biomedical applications (TORRES; COMMEAUX; TRONCOSO, 2013).

Starch structure consists predominantly of two polysaccharides: amylose, a linear polymer of glucose units linked by α (1 \rightarrow 4) glycosidic bonds and amylopectin, a branched polymer with α (1 \rightarrow 4) and α (1 \rightarrow 6) glycosidic linkages. Interesting properties of starch include: biodegradability, varying mechanical strengths and flexibility, suitable for different applications and gel formation, that allows that this polymer have application in drug delivery systems, wound dressings, biodegradable implants, among others (FALUA et al., 2022). Starch holds promise as a biomaterial due to its natural origin, biocompatibility, and versatile properties. However, in some cases, to improve its properties regarding be used in a specific application, chemical modification is needed, and most of the modification involves the hydroxyl groups present in its structure (Wei et al., 2020).

1.3 Quaternary ammonium compounds

Quaternary ammonium compounds (QACs) are compounds that have a structure with a central nitrogen atom linked to four alkyl or aryl groups, forming a positive ion (cation) (Figure 43). This cation is always accompanied by an anion, such as chloride or bromide. Due to this cationic nature, QACs are surfactants. QACs are highly effective antimicrobial agents, targeting a wide range of microorganisms including bacteria, viruses, and fungi (BUREŠ, 2019). These compounds function primarily by membrane disruption, as QACs are cationic surfactants that interfere with microbial cell membranes, similar to the action of chitosan. Additionally, QACs can lead protein denaturation and DNA damage by disrupting hydrogen bonds and hydrophobic interactions (ZHANG et al., 2015). QACs find extensive application in various fields like: healthcare, food industry and water treatment, since these compounds are good disinfectants, antiseptics and sanitizers (JIAO et al., 2017).

Figure 43. General scheme of a quaternary ammonium.



1.4 Thiol Michael Addition

Thiol- Michael addition is a type of Click Chemistry reaction which, in addition to have efficiency, selectivity, and mild reaction conditions, such as Click reactions, present a mechanism involving nucleophilic addition of a thiol to an activated alkene or alkyne (such as an α,β -unsaturated carbonyl compound). The thiol attacks the β -carbon of the activated double or triple bond, forming a carbon-sulfur bond. This reaction can be catalyzed by bases, acids, or proceed via a radical mechanism in some cases and typically proceeds under mild to moderate temperatures. Thiol-Michael addition is typically utilized in bioconjugation, polymer functionalization, and advanced material design (NAIR et al., 2014).

Polysaccharides, like starch and chitosan, are biodegradable, biocompatible, hydrophilic and contain several functional groups available for conjugation (BASU et al., 2015). Besides, conjugated polysaccharides have been proved to be useful for biomedical applications, like drug delivery and vaccine carrier (CHEN; MA; EDGAR, 2021). Thus, the study of feasible synthetic pathways to obtain these conjugated polymers is very important in the biomedical field.

Cysteine is a natural amino acid with a thiol (-SH) group in its side chain (DORM et al., 2024). The thiol nucleophilic properties can be used to insert cysteine in the polysaccharide chains. Besides, cysteine could be transformed in its quaternary ammonium salt (QA- Cysteine) with potential antimicrobial activity (CHEN; MA; EDGAR, 2021).

Based in literature (CASETTARI et al., 2012; RODRÍGUEZ-FÉLIX et al., 2023; XIAO et al., 2011), there are only a few documented instances of producing hydrogels by grafting chitosan with α -amino acids. Notably, even in these cases, the hydrogels have not been thoroughly characterized regarding key physicochemical properties essential for wound dressing applications, such as viscoelastic properties, long-term stability, and the nature of the water contained within the gels (i.e., freezable or non-freezable water). Furthermore, there are no existing reports in the literature on permethylation reactions of amino acid-grafted chitosans to create fully quaternized derivatives.

Considering the above discussion, this work was aiming to the obtention of new antimicrobial agents by chemical modifications of starch and chitosan which include the insertion of cysteine in the polysaccharide's chains and the further quaternization of their amino groups in an attempt to give antimicrobial properties to the product.

2 MATERIALS AND METHODS

2.1 Materials

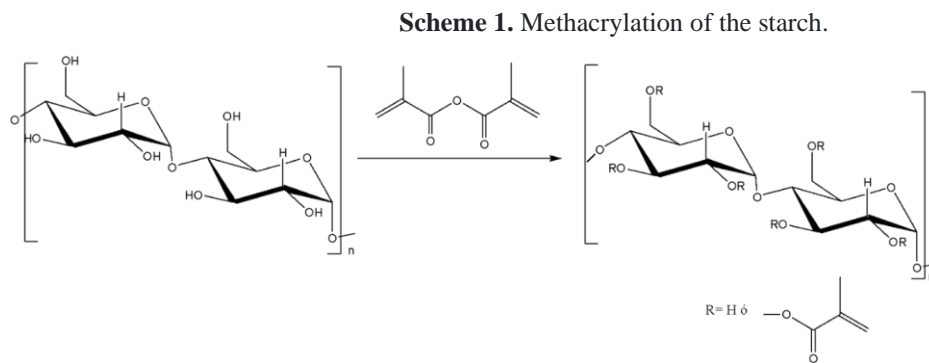
Deionized water, Starch (S9765, Sigma Aldrich), Chitosan (medium molecular weight Sigma Aldrich 448877), triethylamine, methacrylic anhydride, DMSO, THF, pyridine, methyl iodide, diethyl ether, methanol and NaBH₄. All the solvents and reagents (Sigma Aldrich) were all analytical grade and used as received without further purification. Dialysis tubing (MWCO 3500 g/mol) was purchased from Unitek (Spectra/Por). Nutrient broth (Beef extract 1.0; yeast extract 2.0; peptone 5.0; sodium chloride 5.0 g.L⁻¹) was purchased from Kasvi. Agar (Dinâmica), Escherichia coli (ATCC 43895) and Staphylococcus aureus (ATCC 25923).

2.2 Methods

2.2.1 Starch's Chemical Modifications

2.2.1.1 Methacrylation

The reaction (scheme 1) was carried out in five different conditions looking forward to the product with the highest substitution degree (DS). The experimental conditions are described in the next topics.



Conditions:

-Soluble starch (1 g), previously dried in a vacuum oven (100 °C, 24 h), was dissolved in DMSO (20 mL) under argon atmosphere, with magnetic stirring at 60°C overnight. Then, a solution of pyridine (4 mL) and methacrylic anhydride (4.2 mL) was prepared. One- third of this solution was slowly added to the reaction mixture at 8-h intervals, reaching a final molar ratio of: anhydroglucose: pyridine: methacrylic acid; 6.2: 12.4: 12.4. The reaction mixture was always protected from light by covering the whole system with aluminum foil and stirred at room temperature, under argon atmosphere, until reaching a total time of 72 h. Then, the solution was dialyzed against deionized water containing small amounts of sodium azide for 48 h. Finally, the product (MS3) was freeze-dried (1.16 g).

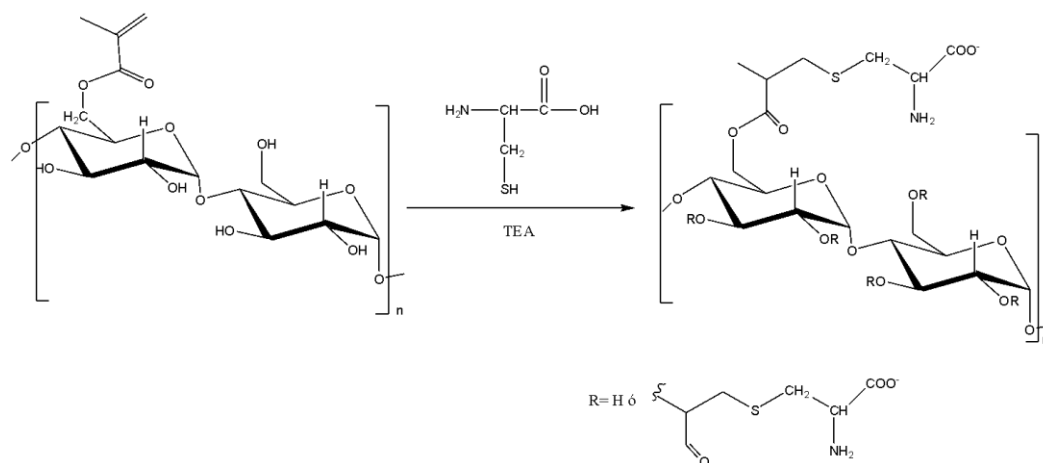
-Soluble starch (2 g), previously dried in a vacuum oven (100 °C, 24 h), was dissolved in DMSO (20 mL) under argon atmosphere, with magnetic stirring at 60 °C overnight. Then TEA (3.45 mL) and methacrylic anhydride (4 mL) was slowly added to the reaction mixture, under N₂ atmosphere (anhydro glucose: TEA: methacrylic acid; 6.2: 12.4: 12.4; molar ratio). The reaction

mixture was protected from light by covering the whole system with an aluminum foil and left at room temperature for 72 h with continuous stirring. Then, the solution was dialyzed against deionized water containing small quantities of sodium azide for 48 h. Finally, the product (MS5) was freeze-dried (2.3 g).

2.2.1.2 Thiol-Michael Reaction

The methacrylated products obtained under reactions conditions 3 (MS3) and 5 (MS5) were submitted to the Michael Reaction (Scheme 2)

Scheme 2. Thiol-Michael reaction over the starch' methacrylic derivative.

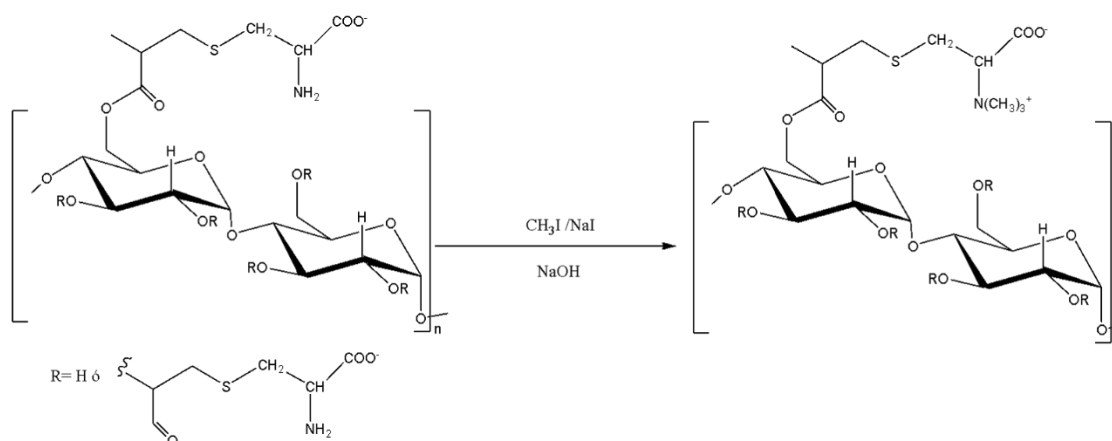


- MS3 (0.5 g) was dissolved in DMSO (20 mL) under argon atmosphere. Then, cysteine (0.48 g) and triethylamine (0.55 mL) were added, and the reaction mixture was left at room temperature, under argon atmosphere, for 1 h with continuous stirring. After that, the solution was dialyzed against deionized water containing small quantities of sodium azide, for 72h and then freeze-dried (MS3TM; 0.29 g).
- MS5 (1 g), was dissolved in DMSO (40 mL) under argon atmosphere. Then, cysteine (1.05 g) and triethylamine (1.2 mL) were added, and the reaction mixture was left at room temperature, under argon atmosphere, for 1 h with continuous stirring. After that, the solution was dialyzed against deionized water containing small quantities of sodium azide, for 72 h and then freeze-dried (MS5TM; 1.07 g).

2.2.1.3 Methylation of MS3TM and MS5TM

MS3TM and MS5TM were methylated (scheme3) under the conditions described in the next topics.

Scheme 3. Methylation of the Thiol-Michael Products.



- MS3TM (220 mg) was suspended in *N*-methyl-2-pyrrolidone (10 mL). To this suspension, 1 mL of a sodium hydroxide solution (15 %) was added together with 1 mL of iodomethane and 0.31 g of sodium iodide. After 2 h, the pH of the reaction medium was 6, and the decrease in the pH was taken as indication that the methylation reaction was proceeding. NaOH (150 mg) and 1 mL of iodomethane were added at 2, 4 and 6 h of reaction. After the last addition, the reaction was kept for 1 more hour with continuous stirring. Then, in order to exchange I^- by Cl^- , the reaction mixture was sequentially dialyzed against ultrapure water, NaCl (0.1 M) and ultrapure water and finally freeze-dried (MS3TMM; 0.08 g).
- MS5TM (750 mg) was suspended in *N*-methyl-2-pyrrolidone (30 mL). To this suspension, 8.69 mL of a sodium hydroxide solution (15 %) was added together with 6 mL of iodomethane and 2.53 g of sodium iodide. After 2 h, the pH of the reaction medium was 6, and the decrease in the pH was taken as indication that the methylation reaction was proceeding. NaOH (150 mg) and 1 mL of iodomethane were added at 2, 4 and 6 h of reaction. After the last addition, the reaction was kept for 1 more hour with continuous stirring. Then, to exchange I^- by Cl^- , the reaction mixture was sequentially dialyzed against ultrapure water, NaCl (0.1 M) and ultrapure water and finally freeze-dried (MS5TMM; 0.29 g).

2.2.2 Chitosan's Chemical Modifications

2.2.2.1 Modification of Chitosan with Cysteine using EDC-NHS

To a solution of L-cysteine hydrochloride (340.9 mg, 1.94 mmol) in 25 mL of water, chitosan (400 mg, 1.94 mmol of deacetylated units) was added. Then, pH was adjusted to 6.5 by addition of NaOH (0.1 M, about 10 mL) and the resulting solution was cooled in an ice bath.

EDC (1.116 g, 5.82 mmol) was added to a solution of NHS (670 mg, 5.82 mmol) in water (about 3 mL), previously cooled in an ice bath. The mixture was added to the chitosan and L-Cysteine solution with energetic mechanical stirring.

The reaction mixture was left with mechanical stirring in an ice bath until gelation was observed (about 8 h) and then it was kept at 4 °C for 16 h. Finally, a 10 % NaOH aqueous solution was added to quench the reaction (50 mL), the product was separated by centrifugation (5000 rpm, 10 min) and then washed sequentially with HCl (0.1 M, x2), NaOH (0.1 M, x2), and finally water until neutral pH was reached. The product obtained as a gel was freeze-dried to give 0.51 mg of a white powder.

The procedure was repeated three times, yielding in all the cases a water insoluble product in all ranges of pH. Furthermore, the products gelled on contact with water regardless of the pH of the water (ROSSI; RAMÍREZ; ERREA, 2020).

2.2.2.2 Methylation of Chitosan- Cysteine derivative

Chitosan-Cys (500 mg) was suspended in *N*-methyl-2-pyrrolidone (40 mL). To this suspension, 5.5 mL of a sodium hydroxide solution (15 %) was added together with 5,7 mL of iodomethane and 2.4 g of sodium iodide. After 2.30 h, 0.3 g of solid NaOH and 1 mL of iodomethane were added to the reaction medium. The addition of these reagents was repeated at 5 h, 7.30 h and 24h and then the reaction was left for 6 more hours with continuous stirring.

After this time, the pH was adjusted to 7.5 and, in order to exchange I- by Cl-, the reaction mixture was sequentially dialyzed against ultrapure water, NaCl (0.1 M) and ultrapure water. Then, the samples were freeze-dried (methylated Chitosan-Cys, 0.41 g) (ZARIFPOUR,2013)

2.2.2.3 Methylation of native chitosan

Chitosan (254.5 mg) was suspended in *N*-methyl-2-pyrrolidone (20 mL). To this suspension, 2.75 mL of a sodium hydroxide solution (15 %) was added together with 2.85 mL of iodomethane and 1.2 g of sodium iodide. After 2.30 h, 150 mg of solid NaOH and 0.5 mL of iodomethane were added to the reaction medium. The addition of these reagents was repeated at 5 h, 7.30 h and 24h h and then the reaction was left for 6 h more hours with continuous stirring.

After this time, pH was adjusted to 7.5 and, in order to exchange I- by Cl-, the reaction mixture was dialyzed sequentially against ultrapure water, NaCl (0.1 M) and ultrapure water. Then, samples were freeze-dried (Methylated chitosan, 0.31 g).

2.3 Characterization

2.3.1 Fourier transformed infrared spectra (FTIR)

Spectra were acquired on a Thermo Scientific Nicolet 6700 spectrometer in transmission mode. The samples were mixed with KBr (Grade FT-IR 99+%, Thermo Spectra-Tech) at 1:100 ratio (sample:KBr) and an aliquot was pressed into a disc of 5 mm using a Hand Press accessory PIKE Technologies. Samples were scanned 32 times at a spectral resolution of 4 cm⁻¹ in the range of 400 to 4000 cm⁻¹.

2.3.2 Nuclear magnetic resonance (NMR) spectra (¹H- and ¹³C-NMR)

Spectra were recorded on a Bruker AMX-500 spectrometer. According to the sample's solubility, experiments were carried out either in DMSO-D₆ or in D₂O.

2.3.3 Conductometric titration

Lyophilized samples according to their solubility were either suspended or dissolved in 10 mL of HCl aqueous solution (0.1 M) with vigorous stirring and then titrated with NaOH aqueous solution (0.1 M). Conductivity values were registered each 0.05 mL using a Hanna Instruments HI-2300 conductometer.

2.3.4 Measurements of Zeta potential as function of pH

The isoelectric points of the samples were determined by measuring the Zeta potential as function of pH using a Zetasizer Nano ZS coupled with MPT-2 autotitrator (Malvern Panalytical).

2.3.5 Ellman's Assay

5 mg of the polymer to be assayed was added to a volumetric flask (50 mL). Then, 1 mL of an aqueous solution of NaBH₄ (6 %) and 5 mL of distilled water were also added. In parallel, 5 mg of polymer was added in another volumetric flask with 6 mL of distilled water. The assays were carried out in duplicates. The mixtures were magnetically stirred overnight at room temperature, protected from light. Then, HCl 1M (5 mL) and Ellman's reagent solution (25 mL) were added to each flask. After two hours, samples were diluted to a final volume of 50 mL with a phosphate buffer solution. The absorbance was read at 410 nm in a UV-spectrophotometer. Blank experiments were also carried out in duplicates (KRAULAND; GUGGI; BERNKOP-SCHNÜRCH, 2004).

Calibration curve: A 100 ppm solution of cysteine in distilled water was prepared. Then, aliquots of different volumes were taken from this solution and added to test tubes. After that, a phosphate buffer was added to each tube to a final volume of 5 mL, reaching concentrations of 6, 10, 14, 20, 26, 30 and 34 ppm, respectively. The Ellman's reagent solution (5 mL) was then added to the tubes and then the tubes were kept at room temperature (protected from light) for two hours. A blank experiment was carried out adding only phosphate buffer and Ellman's reagent to the tube test. The absorbance was read at 410 nm in a UV-spectrophotometer.

2.3.6 Antimicrobial activity

Antibacterial activity of chitosan and starch and their derivative samples were tested by the Dynamic Shake Flask Test Method (ASTM E2149-10) against *E. coli* and *S. aureus*. The bacteria were inoculated in Nutrient agar and grown for 18 hours at 37 °C. The microorganisms were then suspended into 0.85 % sterile sodium chloride solution to reach a turbidity equivalent

to McFarland standard 0.5 ($\sim 1.5 \times 10^8$ CFU. mL⁻¹). Further dilutions were performed with sterile 0.85 % sodium chloride solution to reach a bacterial concentration of 1×10^5 CFU. mL⁻¹.

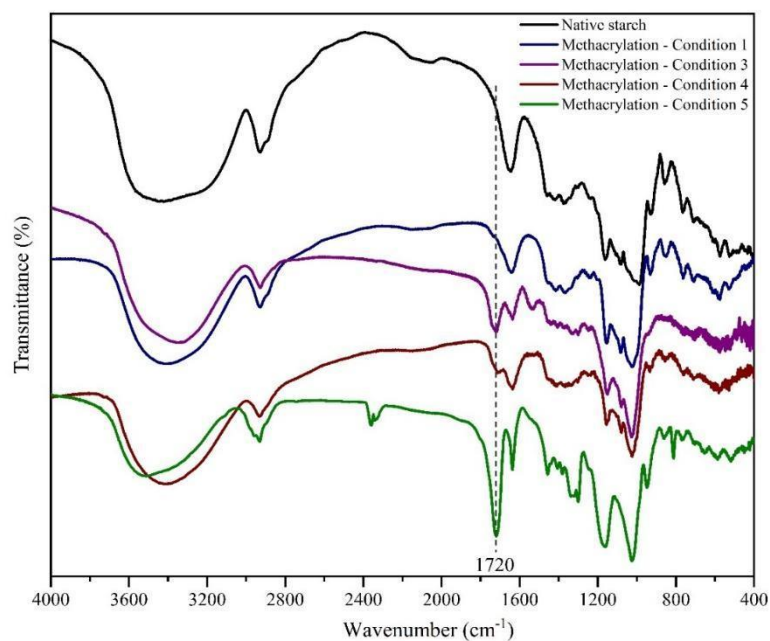
Chitosan and starch (30 mg) and its derivative samples were sterilized in the autoclave. 300 μ L of the bacterial suspension (1×10^5 CFU. mL⁻¹) was added to the samples and incubated at 37 °C under continuous shaking for 18 hours. The bacterial suspension was diluted (serial dilution method), 100 μ L was spread on the surface of Nutrient Agar and incubated at 37 °C for 24 hours. The number of colonies forming units (CFU) was determined by counting the colonies. The control was the bacterial suspension treated as the samples. All the procedures were carried out under sterile conditions.

3 RESULTS AND DISCUSSION

3.1 Starch's Chemical Modifications

The products of the reactions carried out under conditions 1, 3, 4 and 5 were analyzed by FTIR spectroscopy. In Figure 44 the spectra of these products are compared with the *FT-IR* spectrum of the native starch. As it can be seen in the figure, the spectra of the products from conditions 3, 4 and 5 showed the expected signal about 1720 cm⁻¹, corresponding to the stretching vibration of the conjugated ester carbonyl group, indicating that the product had been successfully obtained in these three cases. However, the highest intensity of this signal was observed when the reaction occurred under conditions 5, suggesting that under these conditions higher substitution degree was achieved (NOË et al., 2020).

Figure 44. FT-IR spectra of both native and methacrylated starch.



The products from conditions 3 and 5 (MS3 and MS5, respectively), were analyzed by NMR spectroscopy and the spectra are shown in Figures 45 and 46.

Figure 45. ¹H-NMR spectra of native and methacrylated starches.

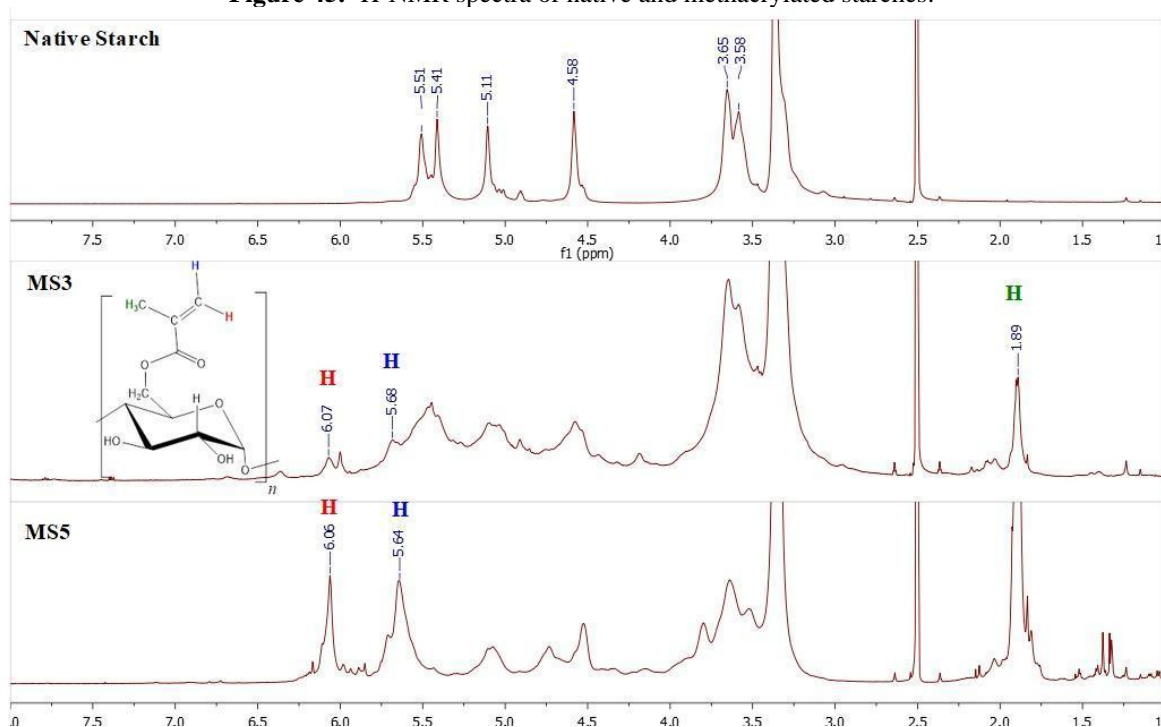
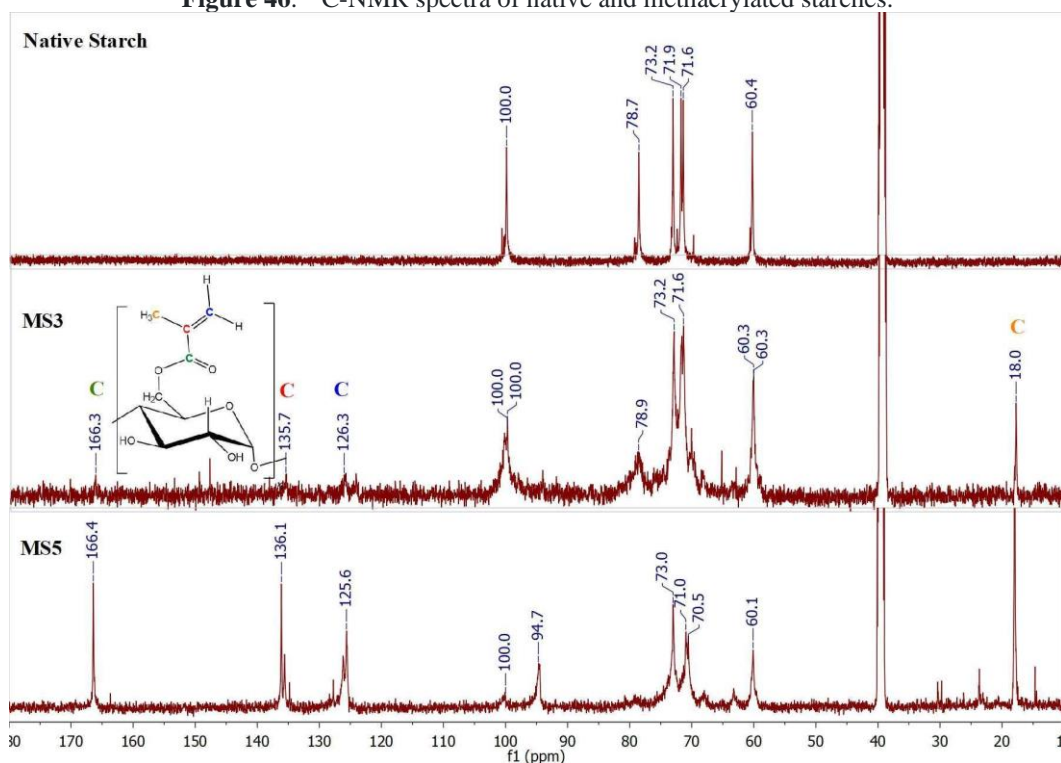


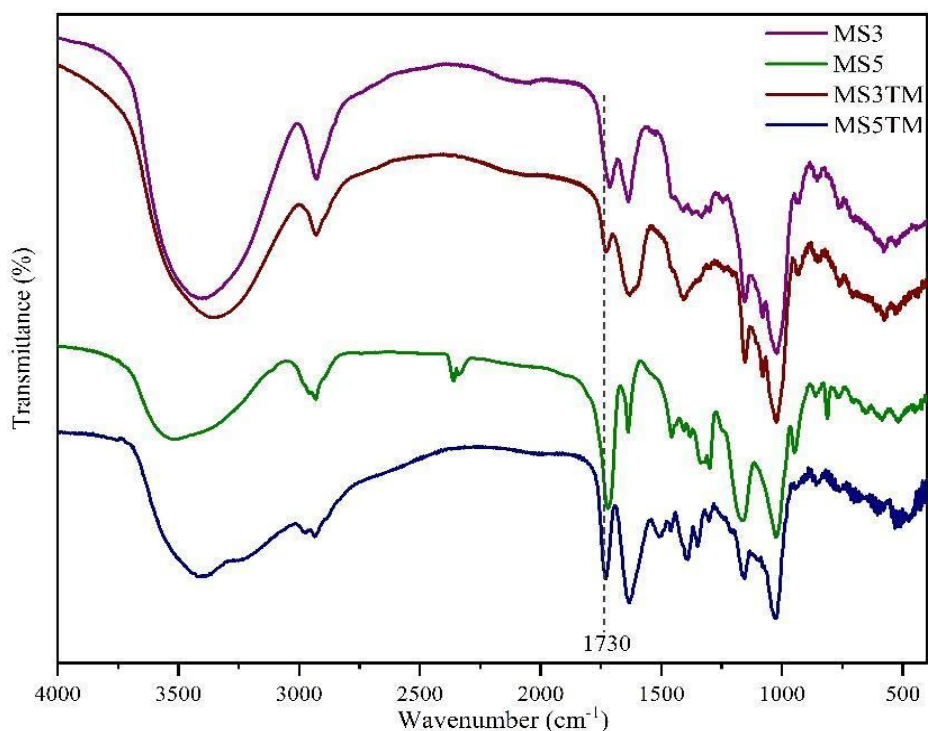
Figure 46. ^{13}C -NMR spectra of native and methacrylated starches.

In the ^1H -NMR spectra, signals corresponding to the hydrogens of the methylene and methyl group of the methacrylic ester were observed, confirming that the reaction had been proceeded successfully. The fact that the area of this signal in the MS5 spectrum is larger than in the spectrum of MS3 is consistent with a higher substitution degree in MS5 (BRAVO-OSUNA; FERRERO; JIMÉNEZ-CASTELLANOS, 2005; NOÈ et al., 2020). This result agrees with the IR analysis of these samples.

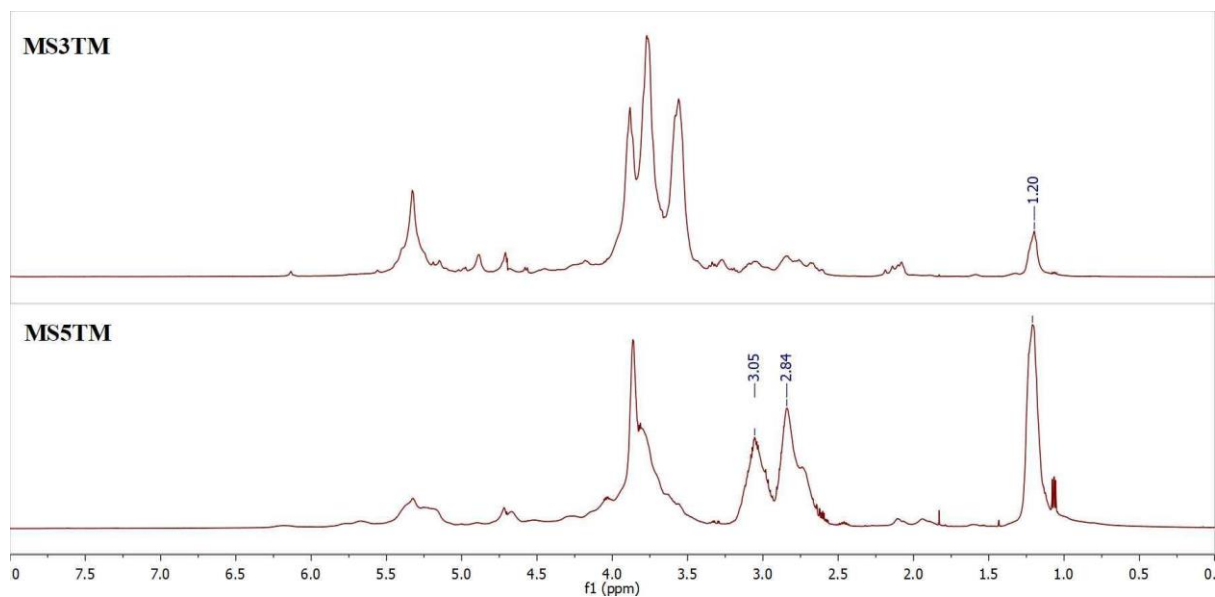
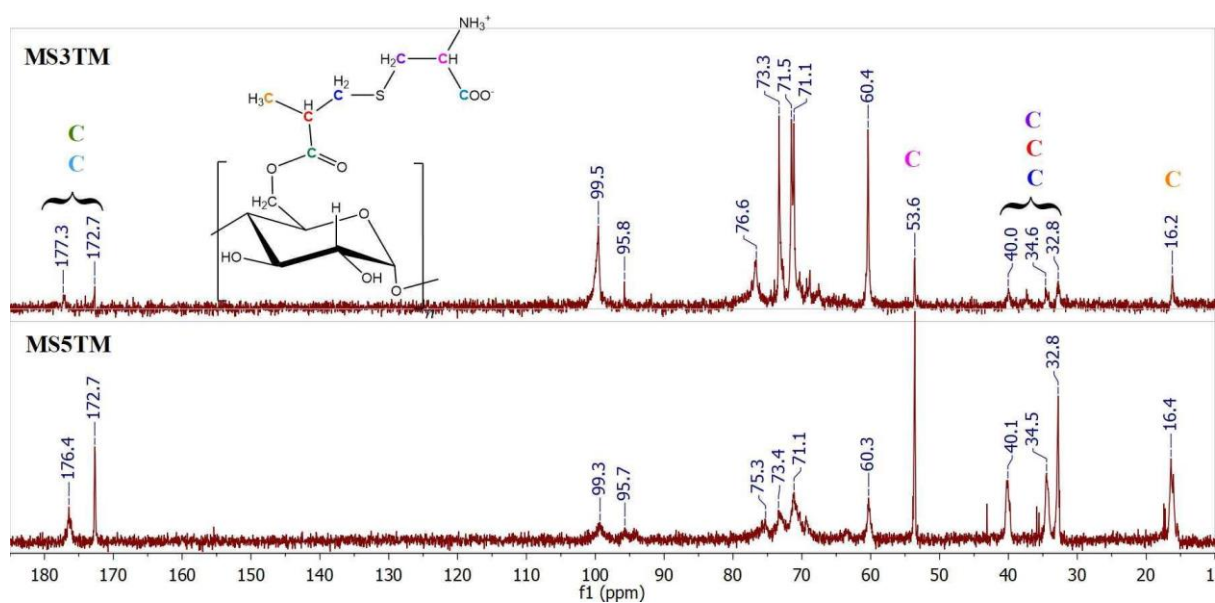
Besides, the expected signals corresponding to the carbons linked to the double bond of the methacrylic moiety, as well as those of the carbonyl and methyl group were observed in the ^{13}C -NMR spectra.

The *FT*-IR spectra of the Thiol Michael products are shown in Figure 47.

Figure 47. FT-IR spectra of MS3 and MS5 and their corresponding Thiol-Michael products (MS3TM and MS5TM).



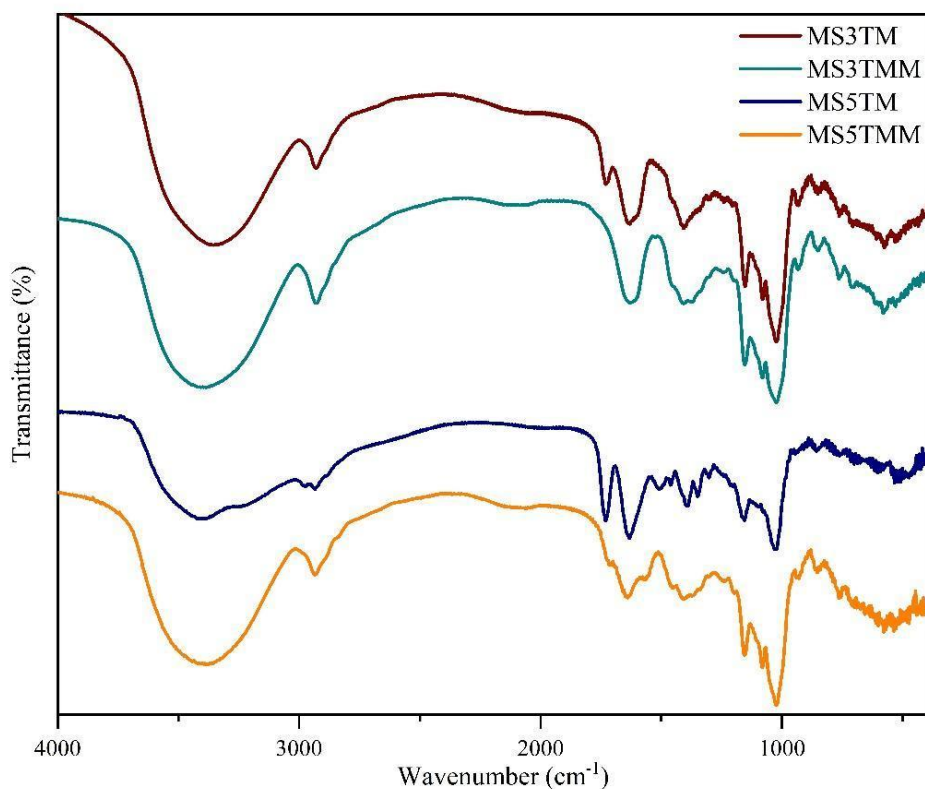
The displacement of the signal corresponding to the stretching of the carbonyl group towards higher wavenumbers (from 1720 to 1730 cm⁻¹) is consistent with the loss of conjugation of that group after the Thiol-Michael addition, which suggests that the reaction occurred successfully. This result is in agreement with the observation of the signals corresponding to the carbonyl, methylene and methyl groups in the ¹³C-NMR spectra of the MS3TM and MS5TM (Figures 48 and 49).

Figure 48. $^1\text{H-NMR}$ spectra of MS3TM and MS5TM.**Figure 49.** $^{13}\text{C-NMR}$ spectra of MS3TM and MS5TM

The substitution degrees of the samples were determined by titration as was described in the Methods and Materials Section: TS3TM: DS=0.32; TS5TM: DS= 1.27.

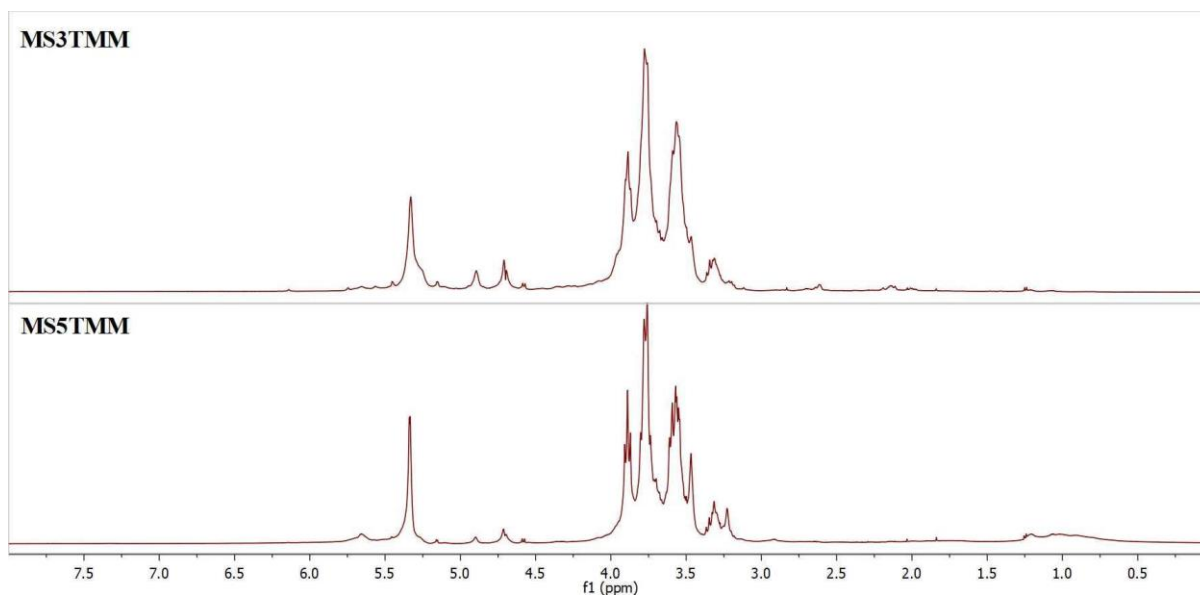
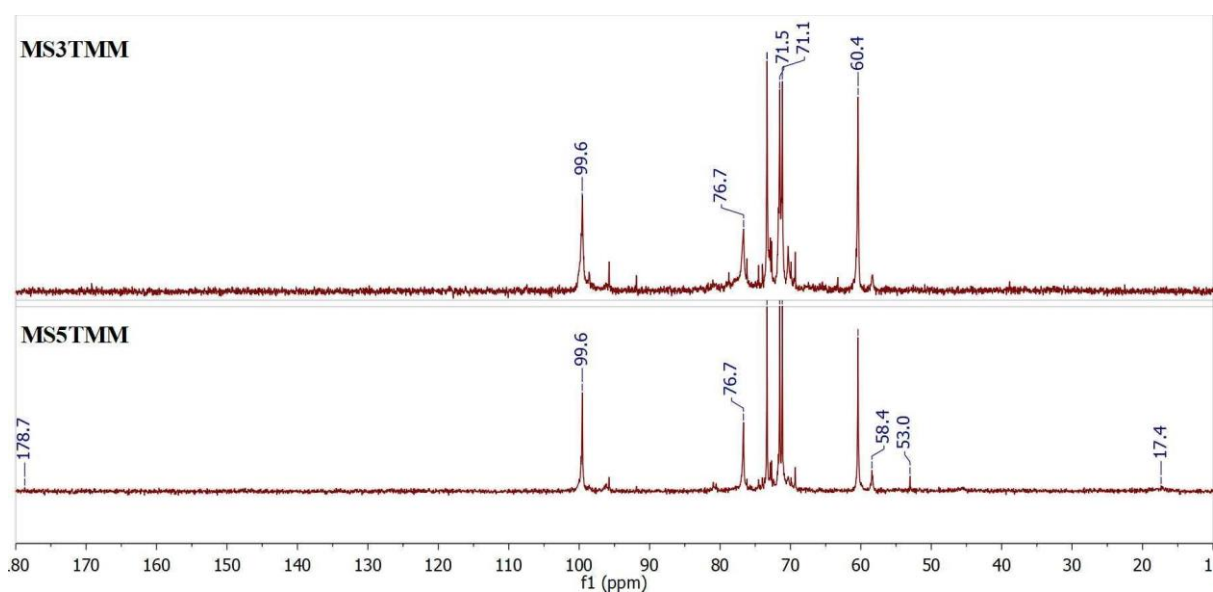
In Figure 50, the *FT-IR* spectra of the Thiol-Michael product are compared with those obtained for the product from methylation treatment.

Figure 50. FTIR spectra of the Thiol-Michael products and their methylated derivatives.



As was observed in Figure 50, the signal corresponding to the stretching of the carbonyl group was not observed in the MS3TMM spectrum, while in the MS5TMM spectrum, this signal exhibited a significant decrease in its area, with respect to that observed in the spectrum of MS5TM. These results are consistent with at least a partial hydrolysis of the ester group under the methylation conditions (PIGORSCH, 2009).

To confirm these results ¹H NMR and ¹³C NMR studies were also carried out (Figure 51 and 52).

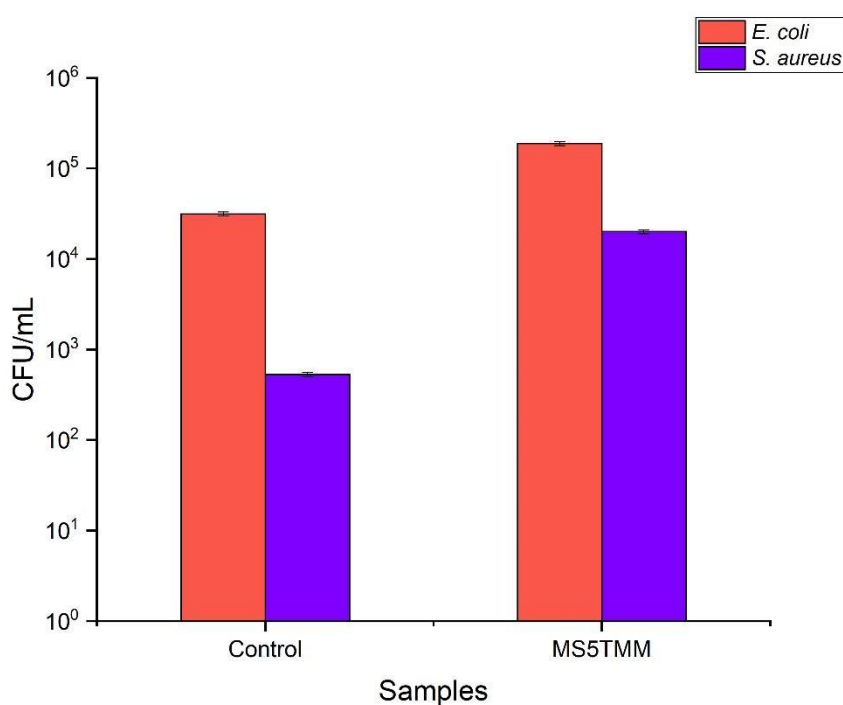
Figure 51. $^1\text{H-NMR}$ spectra of MS3TMM and MS5TMM.**Figure 52.** $^{13}\text{C-NMR}$ spectra of MS3TMM and MS5TMM.

As it was observed in the IR spectrum, in the $^{13}\text{C-NMR}$ spectrum of MS3TMM, the signals corresponding to the carbonyl groups were not observed, while in the $^{13}\text{C-NMR}$ spectrum of MS5TMM a small signal at 178 ppm as well as one at 17.4 ppm were observed, indicating that in contrast to what had happened in MS3TMM, the hydrolysis of the ester group was not total in this sample.

This result encourages us to continue working in the search of methylation conditions that minimize the hydrolysis of the ester group.

The results of the antibacterial activity test for starch and its derivative sample is shown in Figure 53. After 24 h of incubation, the control samples showed $\sim 5 \cdot 10^4$ and $7 \cdot 10^3$ CFU.mL⁻¹ for *E. coli* and *S. aureus*, respectively. The starch samples (MS5TMM) showed a bacterial growth 10 times higher than the controls. This result can be attributed to the fact that the starch, as indicated by the FTIR and NMR analyses, did not undergo successful methylation, and it did not show antimicrobial properties. Furthermore, the native starch can be used as the substrate for bacterial growth, which could explain the higher number of CFU.mL⁻¹ found for starch samples (LIU et al., 2013).

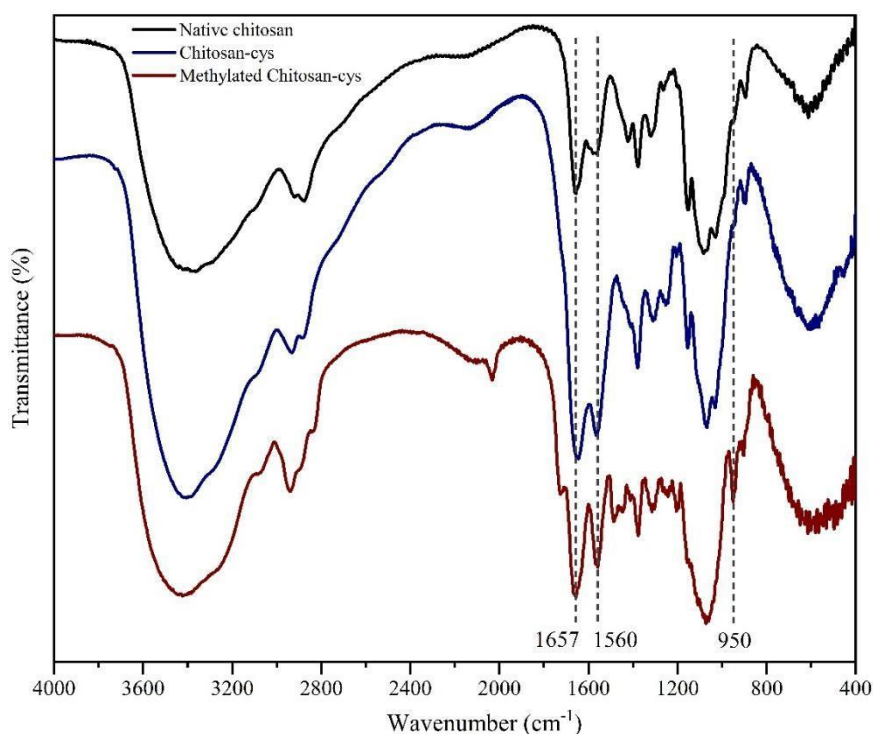
Figure 53: Antibacterial activity on *E. coli* and *S. aureus* of modified starch (MS5TMM). The results are compared with a control sample (bacterial suspension).



3.2 Chitosan's Chemical Modifications

The products were analyzed by FT-IR spectroscopy and in all of the spectra the same signals were observed. The products of the 3 syntheses were then mixed because they were considered to be identical (Chitosan-Cys). The FT-IR spectrum of Chitosan-Cys is shown in Figure 54.

Figure 54: FTIR spectra of native Chitosan, Chitosan-Cys and Methylated Chitosan-Cys.



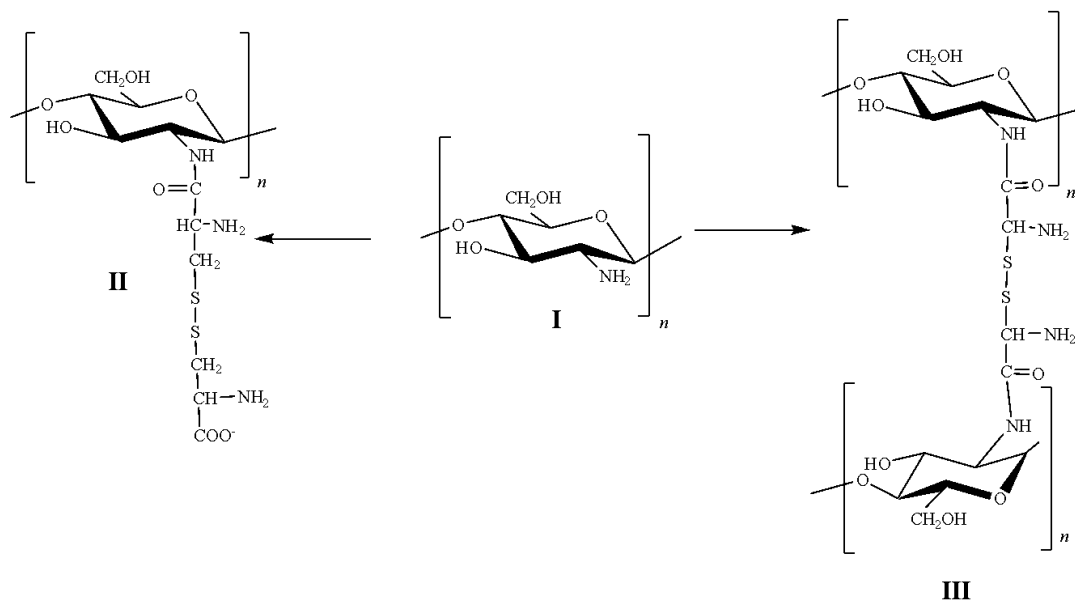
In addition, the thiol content of this sample was analyzed by Ellman's method, as was described in the Methods and Materials Section.

In the IR spectrum of the Chitosan-Cys, an increase in the intensity of the signal corresponding to the N-H bond flexion of the secondary amides was observed (1560 cm⁻¹), (ROSSI; RAMÍREZ; ERREA, 2020) consistent with the attachment of cysteine via an amide bond to the chitosan's chain (Scheme 4).

On the other hand, according to the results of the Ellman's assay, there were no thiols in the sample, and that meant that all the cysteine's thiol groups had been oxidized to disulfide. This result was in agreement with the water insolubility of this product in all the pH range (KRAULAND; GUGGI; BERNKOP-SCHNÜRCH, 2004).

Considering the above discussion, the structures that must be present in the Chitosan-Cys are summarized in scheme 4.

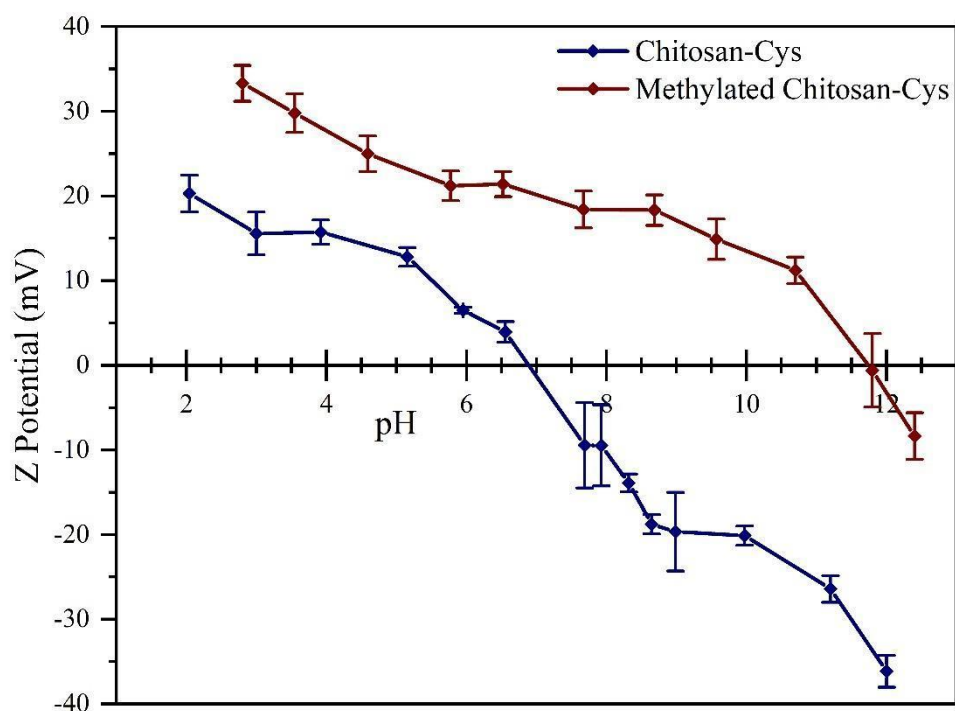
Scheme 4. Chitosan's Chemical Modifications.



In the FT-IR spectra of the methylated sample (Fig. 11) the characteristic signal of quaternary ammonium salts was observed at 950 cm^{-1} .

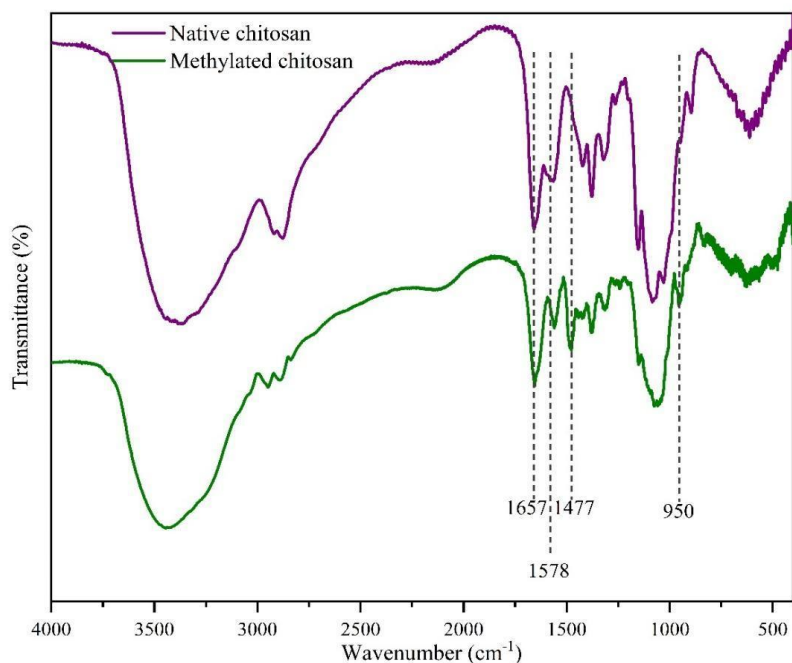
Figure 55 shows the curves by measuring the Z-potential of both, Chitosan-Cys and Methylated Chitosan-Cys, as a function of pH. At low pH values, since both ammonium and carboxyl groups were protonated, the Z-potential was positive. When pH increased, carboxyl groups began to deprotonate, achieving the isoelectric point when the amount of carboxylate groups equaled that of ammonium groups. Then, the Z-potential became negative. As it was expected the isoelectric point of the Methylated Chitosan-Cys was higher (12) than that of Chitosan-Cys (7).

Figure 55: Measurements of Z-potential of Chitosan-Cys and Methylated Chitosan-Cys



In the FTIR spectrum of the methylated chitosan the characteristic signal of quaternary ammonium at 950 cm^{-1} was observed, together with that corresponding to the bending vibration of the methyl groups linked to the nitrogen after the methylation treatment (BOTTGER; GEDDES, 1965; GÖKCE; BAHÇELI, 2013; SOWMYA; MEENAKSHI, 2013). (Figure 56).

Figure 56. FTIR spectra of both, native and Methylated Chitosan.



Besides, in the ¹³C-NMR and the ¹H-NMR spectra of the methylated chitosan (Figures 57 and 58), the signal of the methyl group linked to the amino group were clearly observed at 41.6 ppm. and 3.27 ppm, respectively.

Figure 57. ¹³C-NMR spectra of both, native and Methylated Chitosan.

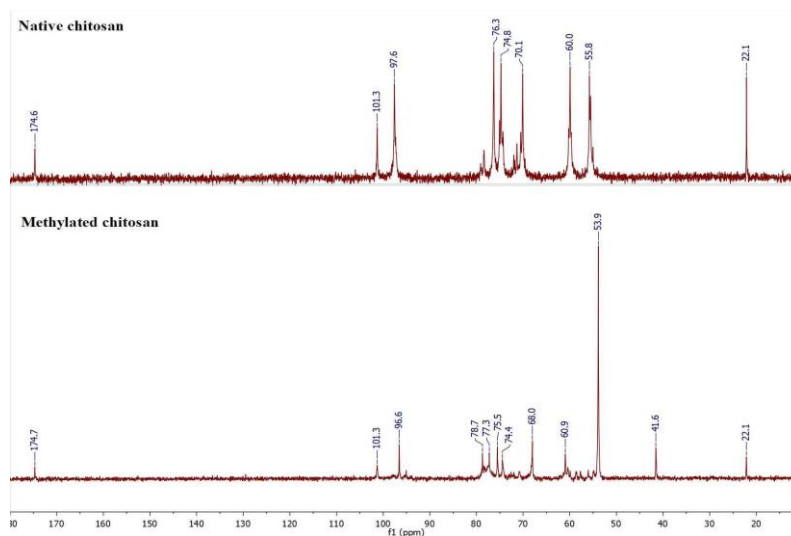
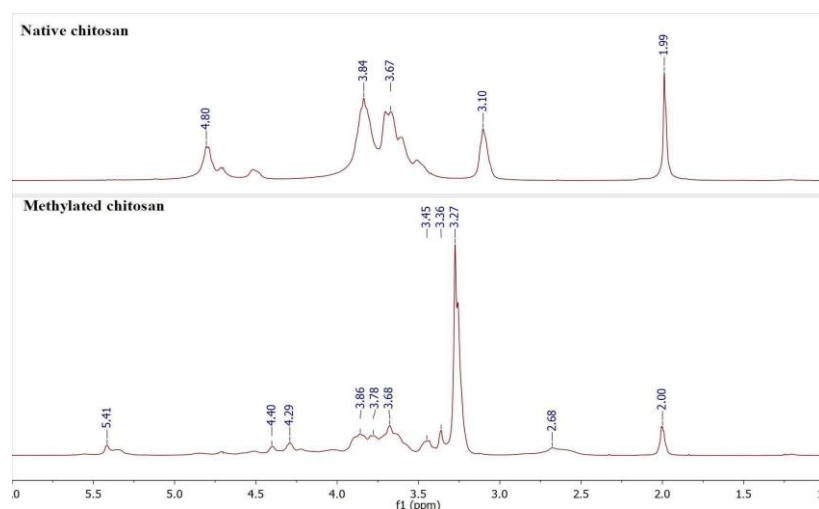
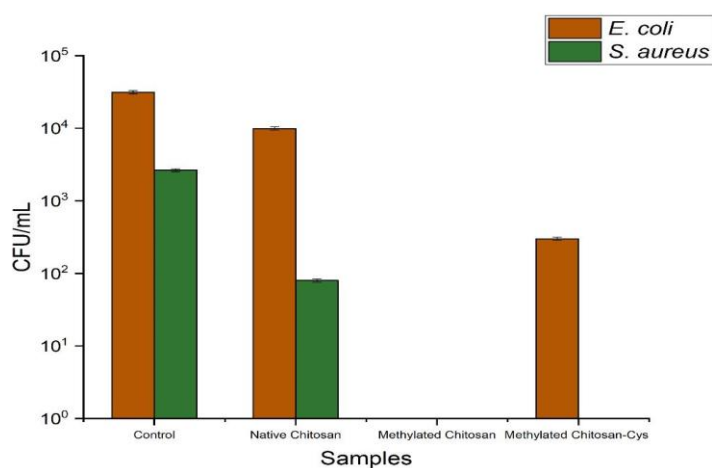


Figure 58. $^1\text{H-NMR}$ spectra of both, native and Methylated Chitosan.



Antibacterial activity tests for native chitosan, methylated chitosan and methylated Chitosan-Cys are shown in Figure 59. As expected, native chitosan showed significant antibacterial activity against *E. coli* and *S. aureus*. The antibacterial activity of methylated chitosan and methylated Chitosan-Cys was higher than that of native chitosan against both microorganisms. The increased bactericidal effect of the methylated samples compared to unmodified chitosan is associated with the presence of quaternary ammonium groups in the chitosan backbone, which are well known to induce higher antibacterial activity.

Figure 59. Antibacterial activity on *E. coli* and *S. aureus* of chitosan, methylated chitosan and methylated chitosan-Cys. The results are compared with a control sample (bacterial suspension).



The results of the antimicrobial activity of the chitosan- based films are in agreement with the literature (HOSSEINNEJAD; JAFARI, 2016; KALAYCIOĞLU et al., 2017), including its highest activity against Gram positive microorganisms (NO, 2002; TORLAK; NIZAMLIOĞLU, 2011). Regarding to the increased antimicrobial activity of chitosan against Gram-positive bacteria it can be explained by the electrostatic interactions between the positive charges of chitosan with the negative teichoic acid backbone in their cell wall, leading to the membrane disruption (FERNANDEZ-SAIZ; LAGARON; OCIO, 2009; KONG et al., 2010).

Similarly, the antibacterial action of chitosan quaternary ammonium salt is known (MIN et al., 2020; YAO et al., 2020). Therefore, the results found in this work are in agreement with the literature

4 CONCLUSIONS

Chemical modifications of chitosan and starch were successfully carried out.

In particular, quaternary ammonium salts of both, chitosan modified with cysteine and native chitosan were obtained. On the other hand, the methacrylation as well as the Thiol-Michael reaction carried out over the starch proceeded successfully, and the goal of synthesize conjugated starch products was achieved. However, the methylation step of the Thiol-Michael products requires further studies to avoid the hydrolysis of the ester under the methylation conditions.

Furthermore, antimicrobial studies were conducted on *Escherichia coli* and *Staphylococcus aureus*, which showed that methylated chitosan and methylated chitosan-Cys had better bactericidal effects than native chitosan and modified starch. Therefore, they are an interesting material for use in surfaces that require antibacterial properties, such as biomedical application materials.

In general, it is considered that the objectives of this work were achieved, with the synthesis of conjugated starch derivatives by starch methacrylation and the Thiol-Michael addition. Besides, a new line was started, in which, after activating the carboxyl group of cysteine with EDC/NHS, joined this amino acid to the chitosan chains, via amide bonds. The new derivative was then submitted to an exhaustive methylation reaction, synthesizing its quaternary ammonium salt successfully. In addition, the quaternary ammonium salt of the native chitosan was also successfully obtained and the results of antimicrobial activity tests of these products are promising.

CHAPTER VI

SYNTHESIS AND BIOLOGICAL PROPERTIES OF ALANINE GRAFTED HYDROXYAPATITE NANOPARTICLES⁵

1 INTRODUCTION

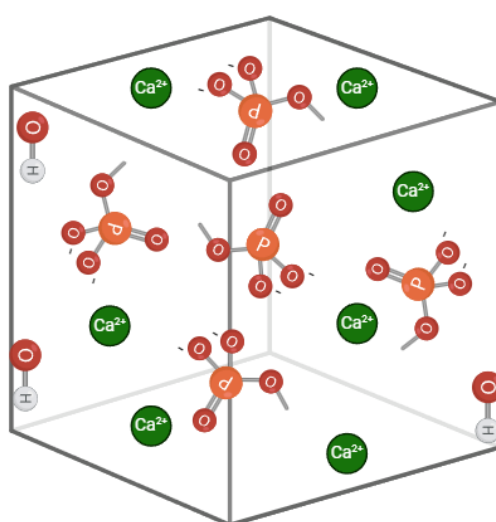
1.1 Hydroxiapatite as a biomaterial for bone regeneration

Hydroxyapatite (HAp) is calcium phosphate material with unit cell formula $\text{Ca}_{10}(\text{PO}_4)_6(\text{OH})_2$ (Figure 60). Due to chemical composition and crystal structure similar to bone and dental phosphates, HAp is considered to be of a great interest for synthesis in pure and composite forms. There are many techniques for hydroxyapatite synthesis, such as solid-state (JAVADINEJAD; EBRAHIMI-KAHRIZSANGI, 2021), chemical precipitation (YELTEN-YILMAZ; YILMAZ, 2018), hydrolysis (SINITSYNA et al., 2005), hydrothermal (ZHANG et al., 2009), pyrolysis (AGUILAR-FRUTIS; KUMAR; FALCONY, 2009), combustion (BATISTA et al., 2020) and electrospinning (LEE; KIM, 2014). By choosing the method and the synthesis conditions, various morphologies were achieved, such as spheres, rods, needles, wires, etc. (WANG et al., 2010). Besides pure hydroxyapatite, ions substitution was shown to be beneficial for achieving different HAp functionality. To increase similarity with natural bones, cations such as (Fe^{3+} , Mn^{2+} , Zn^{2+} , Sr^{2+} , Cu^{2+} , Na^+ , etc.) and anions e.g., CO_3^{2-} , SiO_4^{4-} and F^- , were successfully incorporated in HAp without affecting its crystal structure, but influencing crystallinity, morphology and solubility (LAVANYA; VIJAYAKUMARI, 2018; MOHD PU'AD et al., 2020). For better tracking of bone and dental implants behavior, doping with rare earth ions Yb^{3+} , Tm^{3+} , Eu^{3+} , Gd^{3+} and Ho^{3+} was also applied (IGNJATOVIĆ et al., 2019; LI; CHEN, 2016; WIGLUSZ et al., 2015). It was also shown that HAp marked with radioactive isotopes like $^{99\text{m}}\text{Tc}$ is a good indicator for osteogenesis process (GROSSNER; HABERKORN; GOTTERBARM, 2021). Besides favorable osteoinductivity (WANG et al., 2021) and osteoconductivity (KOZUMA et al., 2019), there is a number of shortages associated with a low strength and toughness, brittleness and poor mechanical strength of HAp (MA, 2019; VEIGA et al., 2020). These lacks could be

⁵ Note: This chapter was published as an article in the journal Life, on December 31, 2022 and can be founded at: <https://doi.org/10.3390/life13010116>

overcome by surface functionalization of HAp with different organic materials. For example, when poly-(lactic-co-glycolic acid) (PLGA) was used for HAp grafting, material with enhanced biocompatibility and increased tensile strengths was obtained (PARK et al., 2019) . Modification of HAp crystal surface toward increasing proteins uptake was accomplished by using bisphosphonates, polyphosphates, carboxyl groups or pyrophosphate ions (LEE et al., 2012a). Lately, compounds that contain both amino and carboxylic acid functional groups, like amino acids, were shown to be perspective for achieving this goal (COMEAU; WILLETT, 2018; JOGIYA et al., 2017).

Figure 60. Scheme of Hydroxyapatite. Adapted from Bystrov et al, 2021 (BYSTROV et al., 2021)



Created in BioRender.com 

1.2 Amino acids to improve cell adhesion and proliferation

Several strategies have been adopted to functionalize the surface of biomaterials such as hydroxyapatite (HAp) and poly(l-lactic-co-glycolic acid) (PLGA) with the objective to improve protein adsorption and cell adhesion. A classic strategy involves plasma surface-modification (PSM) techniques (CHU, 2002). Interactions involving the surface of biomaterials and proteins include van der Waals, electrostatic, hydrogen bonding and hydrophobic interactions. In this sense, the functionalization of the surface of materials such as HAp by the incorporation of

amino acids into their structure has been an interesting strategy, since amino acids are intrinsically biocompatible and are derived from natural and renewable sources. (LEE et al., 2012b)

Amino acids grafted HAp could be obtained by several manners, including mixing of previously prepared HAp and amino acids (COMEAU; WILLETT, 2018), surfactant mediated approach (JOGIYA et al., 2017), hydrothermal treating (GAO; RUAN; CHEN, 2007; GONZALEZ-MCQUIRE et al., 2004a), precipitation with HAp seed crystals (MATSUMOTO et al., 2006) and *in situ* grafting (LEE et al., 2015).

Considering the choice of an amino acid to be grafted to the hydroxyapatite structure, alanine stands out for its simple structure and high commercial availability. The modesty of data related to success of L-alanine amino acid grafting on HAp nanoparticles was the motivation for exploring different grafting procedures and to test biological properties of obtained grafted materials. Three different procedures of grafting were applied, i.e. simple mixing, thermal induction and *in situ*, using two different L-alanine precursors. Results of detailed structural, chemical, morphological and biological analyses served as an instrument for the revealing grafting efficiency and biocompatibility of these materials. The aim of this study was also to choose the best method for grafting of nano HAp with alanine toward creating materials with optimized biological properties.

2 MATERIALS AND METHODS

2.1 HAp Synthesis

All chemicals used were of analytical grade and purchased from Sigma Aldrich. Hydroxyapatite was synthesized using aqueous solutions A and B in accordance with procedure described in (IGNJATOVIĆ et al., 2014), where solution A was a mixture of $\text{Ca}(\text{NO}_3)_2 \times 4\text{H}_2\text{O}$ and NH_4OH and solution B comprised H_3PO_4 and NH_4OH . Solution B was preheated to 50 °C and solution A was added dropwise under stirring. Then the heater was turned off and the mixture was stirred during next 24h at room temperature, after which the obtained gel-like product was rinsed with distilled water three times by centrifugation (5000 rpm, 2 min), collected and freeze dried.

2.2 Grafting procedures

2.2.1 Simple mixing

Simple mixing was performed by homogenization of L-alanine or L-alanine methyl ester hydrochloride with HAp nanopowder in 1:1 mass ratio, vortexing for 20 min, rinsing by centrifugation (5000 rpm/2 min) and drying at 60 °C for 1 h. Obtained nanopowders are marked as SMA, for sample prepared with alanine precursor, and SME - for sample prepared with ester precursor.

2.2.2 Thermal induction

In thermal induction procedure the same reactants as described above were homogenized in 2:1 mass ratio and after 20min of vortexing, obtained mixtures were subjected to the heat treatments at: 200 °C (1h) in the case of L-alanine; and 140 °C (1h) in the case of L-alanine methyl ester hydrochloride. After heating, nanopowders are naturally cooled down to room temperature and rinsed once by centrifugation (5000 rpm/2 min). Drying is performed at 60 °C for 1 h. Obtained samples are marked as TTA and TTE, depending on the used alanine precursor.

2.2.3 In situ grafting

In situ grafting procedure was performed according to the stated steps for hydroxyapatite synthesis, with the addition of L-alanine or L-alanine methyl ester hydrochloride precursor to the solution A in 1:1 mass ratio. Obtained samples are marked as ISA and ISE, depending on the used alanine precursor.

2.3 Characterization

2.3.1 Powder characterization

All synthesized powders were analyzed by: X-ray powder diffraction (XRPD) in a range of 10-70° (Philips PW 1050); Fourier transform infrared spectroscopy (FTIR) in the spectral range from 400 to 4000 cm⁻¹ (Nicolet iS10 FTIR Spectrometer, Thermo Scientific); thermogravimetric analyses up to 500°C, with a heating rate of 10°C/min in air atmosphere (SETSYS Evolution 24000 Setaram Instrumentation); differential scanning calorimetry up to 250°C, with heating rate of 10°C/min in N₂ atmosphere (Evo 131 Setaram Instrumentation); field emission scanning electron microscopy (Carl Zeiss ULTRA Plus FESEM).

2.3.2 Protein Adsorption

The protein adsorption was determined by incubating the samples (5 or 10 mg) in 1 mL of albumin solution (0.25mg/mL, in distilled water, pH 7.4), for 10 and 30 min at room temperature. After the incubation, the samples were centrifuged at 5000 rpm for 5 min. The protein concentration in the supernatant was determined by UV absorption at 280 nm using a Bel UV-Vis (V-M5) spectrophotometer. The protein adsorbed at the surface of the samples was calculated from the difference between the initial and the final mass of protein in solution and the results were shown in percentage.(NEFFE et al., 2014)

2.3.3 Cell adhesion

Samples (10 mg) were spread on the surface of a round coverslip (1.3 cm diameter), glued with superglue (3M) and sterilized under UV radiation for 30 min. MG-63 human osteoblastic cellline (purchased from Rio de Janeiro Cell Biobank, Brazil) was used to study the cell attachment to the samples and cell viability assay. The cells were maintained in Dubelcco's Modified Eagle's Medium – DMEM with 10% of fetal bovine serum (Nutricell, Gibco/Thermofisher)) and antibiotics (penicillin 100 U/mL; streptomycin 0.1mg/mL, from Sigma Aldrich) in a humidified atmosphere of 5 % CO₂ and 95 % air at 37 °C. For the cell adhesion assay, the samples (coated coverslip) were inserted into the wells, the cells (5x10⁵ cells per well, in 1 mL of DMEM supplemented culture medium) were seeded on the samples and cultured in 5% CO₂ and 95% air atmosphere at 37 °C. After culturing the cells for 24 hours, each sample was rinsed with phosphate buffer saline (PBS), then fixed with paraformaldehyde (2 % vol in PBS) at room temperature for 20 minutes, and washed with PBS three times. Each sample was stained with 40,60-diamidino-2-phenylindole (DAPI, Merck, US) for 10 min, for nuclei labeling. The cells, in five random fields on each sample were observed using a fluorescence microscope (Leica MDi8, Germany).

2.3.4 Cell viability

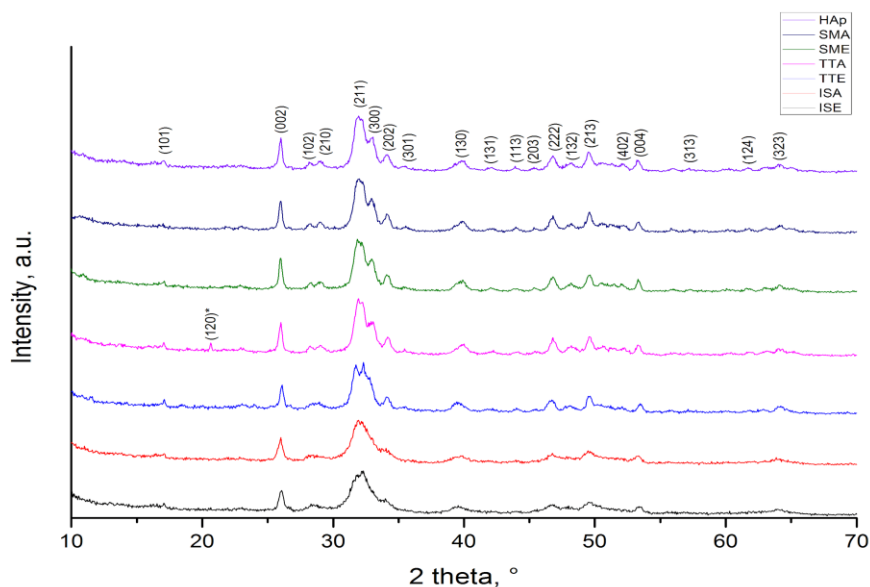
Cell viability was investigated using the standard resazurin reduction method. The cell culture was maintained at 37 ± 2 °C in 5% CO₂ atmosphere and trypsinized when reached confluence of 80–90%. The cell suspension was then centrifuged for 5 min at 1200 g, and 1 mL (1×10⁶cells) was seeded into a 24-well plate filled with the coated coverslip (samples). The cells also seed into an empty well and cultivated at the same conditions and used as the negative control (to

ensure the cell grow free of sample). At predetermined time points (24 and 48 h), the culture medium was removed and the cells were washed with PBS. Resazurin solution (10% vol in DMEM supplemented medium) was added to each well and the microplates were incubated at $37\pm 2^\circ\text{C}$ for 4h and 5% CO_2 atmosphere. 100 μL of each sample was transferred to the 96 wells microplate. Resazurin was removed and the wells were filled with 1mL of culture medium and incubated again at the culture conditions. The fluorescence was read at 570 nm excitation and 590 nm emission wavelengths in a microplate reader (CaryEclipse Agilent Technologies, Santa Clara, CA, USA). The cell viability was reported as fluorescence intensity. The results are reported as mean values \pm SD.

3 RESULTS AND DISCUSSION

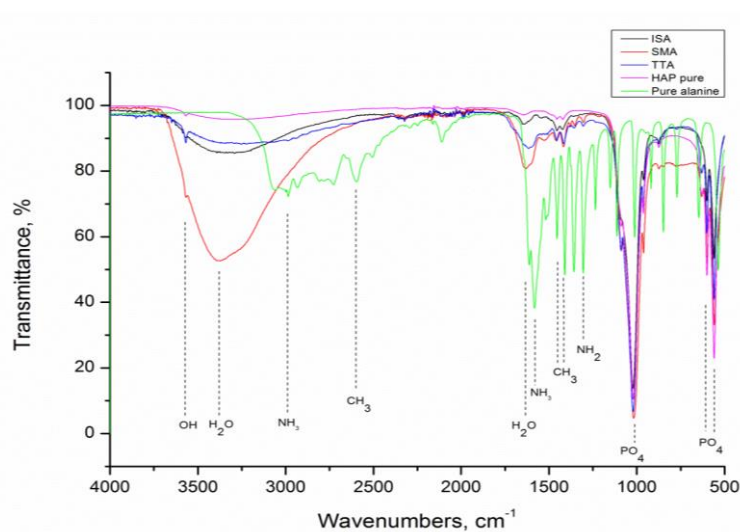
3.1 Structural, morphological and physic-chemical characterization

XRPD patterns of HAp before and after grafting are presented in Fig. 1. As indicated by indexed Bragg reflections, identified maxima in all samples belongs to the hexagonal hydroxyapatite which crystallizes in $P6_3/m$ space group (JCPDS No. 89-6440). Evident broadening of the reflections is associated with nanocrystalline size of HAp particles, while emergence of a weak reflection at 20.67° in TTA diffractogram implicates presence of L-alanine (JCPDS No. 28-1508). According to the Debye-Scherrer equation, determined crystallite size of HAp, SMA, SME and TTA is 30 nm. Slight decrease of crystallite size to 25 nm in TTE sample is provoked by heat treatment of powder at temperature which is higher than melting temperature of L-alanine methyl ester hydrochloride, so Cl^- ion from melt adhere at HAp surface inhibiting further crystal growth. For ISA and ISE samples, the smallest crystallite size of 18 nm is calculated. According to the literature, dissolved amino acids could chelate Ca^{2+} and PO_4^{3-} ion and bind to the HAp nuclei inhibiting their further growth (GONZALEZ-MCQUIRE et al., 2004b; TAVAFOGHI; CERRUTI, 2016). Although Tanaka et al. shown that alanine establishes the weakest interaction with HAp in comparison to other amino acids (TANAKA et al., 1989) , it is obvious that level of interaction achieved here was sufficient to suppress the crystallites growth in ISA and ISE samples.

Figure 61. XRPD patterns of HAp and HAp grafted samples

HAp grafting with alanine was confirmed by FTIR analysis, Figure 62. The following vibrational modes of HAp were identified in spectra: PO_4^{3-} v₄ out of plane bending at 550 and 598 cm^{-1} , PO_4^{3-} v₁ symmetric stretching at 1006 cm^{-1} , OH^- stretching at 3570 cm^{-1} and adsorbed water stretching at 1634 and 3320 cm^{-1} (MICHELOT et al., 2015). Besides, L-alanine shows characteristic vibrational modes of NH_2 bending at 1309 cm^{-1} , CH_3 bending at 1421 and 1447 cm^{-1} , NH_3 bending and stretching at 1585 and 2976 cm^{-1} respectively, CH_3 stretching at 2600 cm^{-1} and H_2O at 1600 cm^{-1} (BRYM, 2017; GHEORGHE et al., 2014; GROWTH AND CHARACTERIZATION OF L-ALANINE CRYSTALS USING FT-IR, UV VISIBLE SPECTRA, [s. d.]). The characteristic L-alanine mode of NH_2 bending at about 1300 cm^{-1} is present in spectra of all grafted samples. Its intensity is strongest for SMA sample. A few other L-alanine modes are detectable in spectra of grafted samples but with weaker intensity. For all grafted samples the presence of adsorbed H_2O is prominent.

Figure 62. FTIR spectra of HAP, L-alanine, SMA, TTA and ISA samples

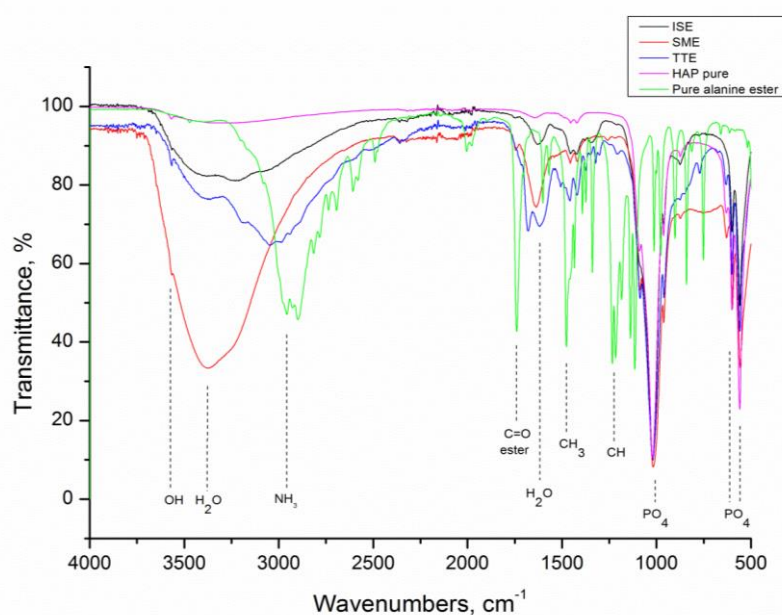


FTIR spectrum of methyl ester hydrochloride, presented together with spectra of HAP, SME, TTE and ISE, Fig. 63, shows that besides characteristic modes of L-alanine (NH_3 and CH_3), this compound has additional modes of CH bending at 1229 cm^{-1} and C=O bending at 1740 cm^{-1} (BRYM, 2017)(EFFECTS OF ALANINE METHYL ESTER HYDROCHLORIDES ON THERMAL BEHAVIOUR OF BIODEGRADABLE POLY(L-LACTIC ACID), 2013). As it can be seen, all of these are present in grafted samples related spectra too, but with weaker intensities.

Comparative thermal analyses of the samples were also performed in order to evaluate the level of grafting, Figs. 64 and 65. As observed in Fig. 64a, thermal decomposition of L-alanine occurs at about $310\text{ }^\circ\text{C}$, which correspond well to the literature (OLAFSSON; BRYAN, 1970; RODANTE; MARROSU; CATALANI, 1992; YABLOKOV et al., 2009). Similar temperature range is observed for L-alanine methyl hydrochloride decomposition (Fig. 64b). Both alanine precursors exhibit higher weight loss than HAp in the same temperature range, so the differences among detected weight loss in HAp (of about 5 wt%) and grafted samples were attributed to the quantity of alanine retained in these. Considering simple mixing, both samples decrease in their weight for

about 8 wt%. Weight loss of 16 wt% observed for TTA sample corresponds well to twice larger mass of alanine precursor used for grafting by thermal induction. On the other hand, the higher content of alanine is present in TTE judging on the 25 wt% loss observed. Same trend is detected for ISA and ISE, where losses of 10 and 14 wt% were measured.

Figure 63. FTIR spectra of HAP, L-alanine methyl ester hydrochloride, SME, TTE and ISE samples



The results of DSC analyses, Fig. 64, implicate that desorption of water near 100 °C is the most prominent endothermic processes caused by grafting. Judging from the steepness of the slopes, it is obvious that water release is slower in grafted samples obtained by thermal induction than in their counterparts obtained by simple mixing. Moreover, the process of water desorption in ISA and ISE samples takes place at higher temperatures than in others, meaning that more energy is required for this process.

Figure 64. TGA diagrams of: a) SMA, TTA, ISE; b) SME, TTE, ISE grafted samples

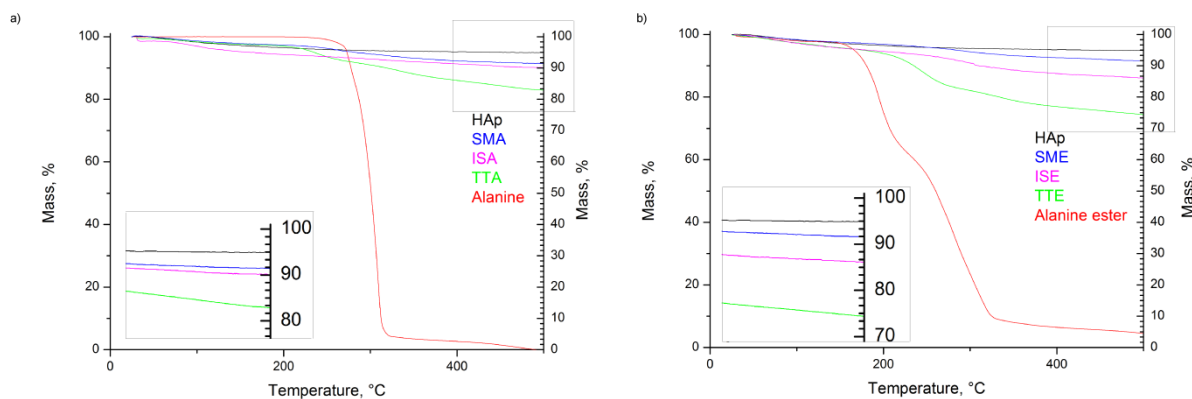
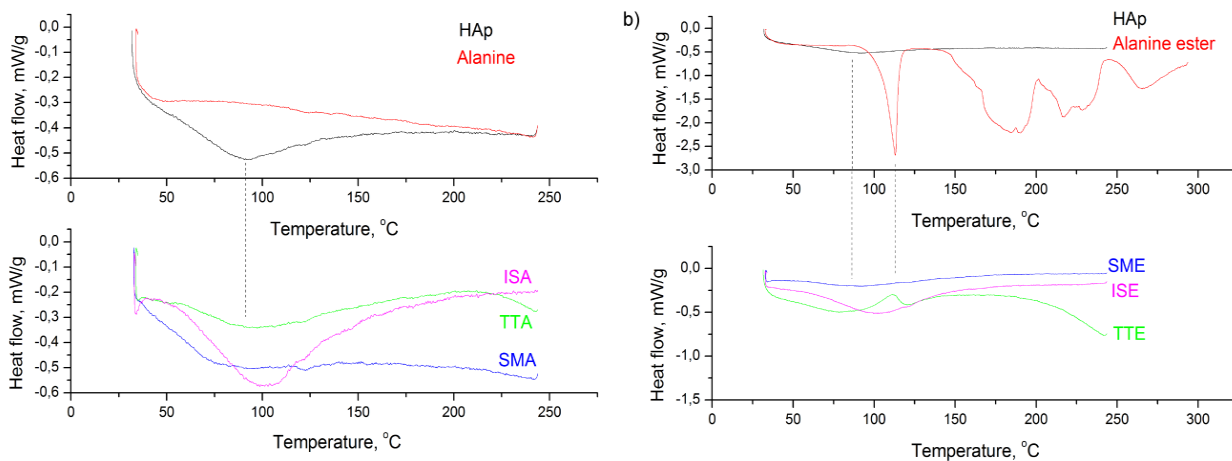
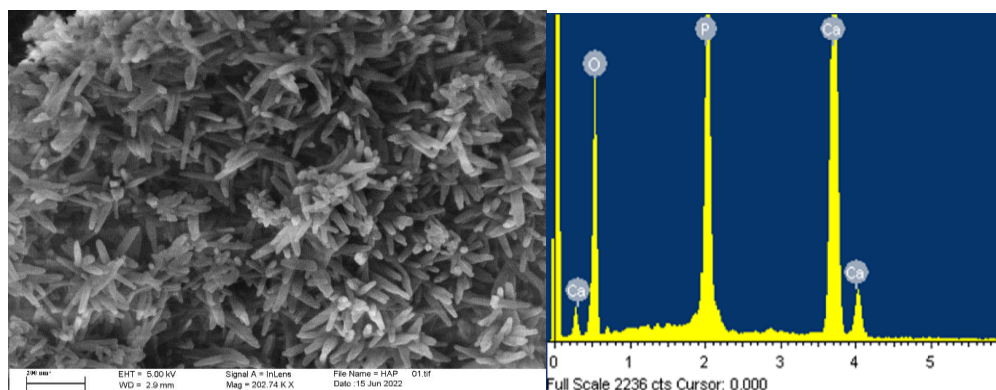


Figure 65. DSC diagrams of samples grafted with: a) L-alanine; b) L-alanine methyl ester hydrochloride



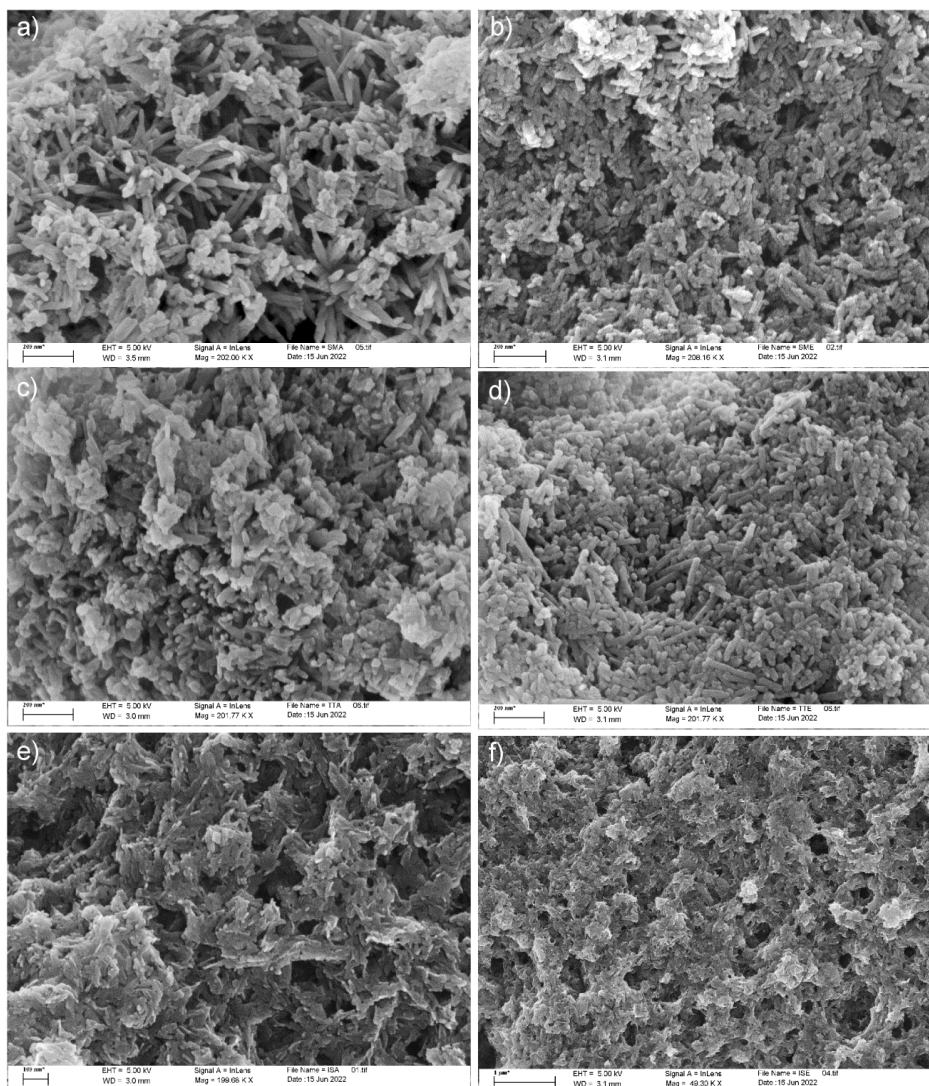
Modification of the HAp powders morphology due grafting is revealed by FESEM analysis, Figs. 66 and 67. The well dispersed rod-like HAp particles with average length about 100 nm and diameter of 10 nm are clearly distinguished in Fig. 66. The Ca/P ratio of 1.5 calculated directly from the EDS result is lower than theoretical value of 1.67, so Ca-deficient HAp is obtained during precipitation. With grafting, HAp particles become more prone to agglomeration, but without change in their morphology.

Figure 66. FESEM micrograph of HAp powder and corresponding EDS analysis



It is evident that agglomeration (SCHACHSCHAL; PICH; ADLER, 2007), increases gradually in a following way: simple mixing, thermal induction, in situ grafting, and is generally more intense in all samples obtained by grafting with L-alanine methyl ester hydrochloride. This indicates a higher level of reactivity of L-alanine methyl ester hydrochloride for grafting, in comparison to L-alanine.

Figure 67. FESEM micrographs of grafted samples: a) SMA; b) SME; c) TTA; d) TTE; e) ISA; f) ISE



3.2 Protein adsorption

Figure 68 shows the results of the protein adsorption test. The interactions between cells and grafted HAp particles were measured after 10 and 30min. When 5 mg of grafted samples were tested after 10 min, the beginning of the protein adsorption at the particles surfaces is observed. With the prolongation of time to 30 min, the mass of protein adsorbed to the surface of SME, ISA and ISE samples abruptly increased, reaching the maximum of ~35% for ISE. Doubling the samples mass (10 mg) also enhances adsorption in these samples for both tested times. The

mass of protein adsorbed after 30min at SME, ISA and ISE surface reached 33%, 36% and 50%, respectively. The negative values observed for HAp, SMA, TTA and TTE with prolongation of time indicate that these nanoparticles remain trapped in protein solutions due to formation of stable suspension which could not be removed by centrifugation. The value obtained for the ISA at a concentration of 10mg and time of 10 minutes was zero, since the measured absorbance value for this sample was the same obtained for the standard albumin solution.

Figure 68. Protein adsorption test

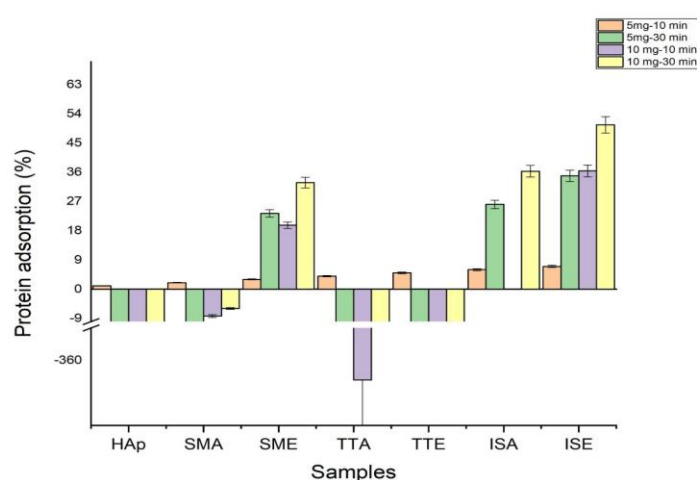


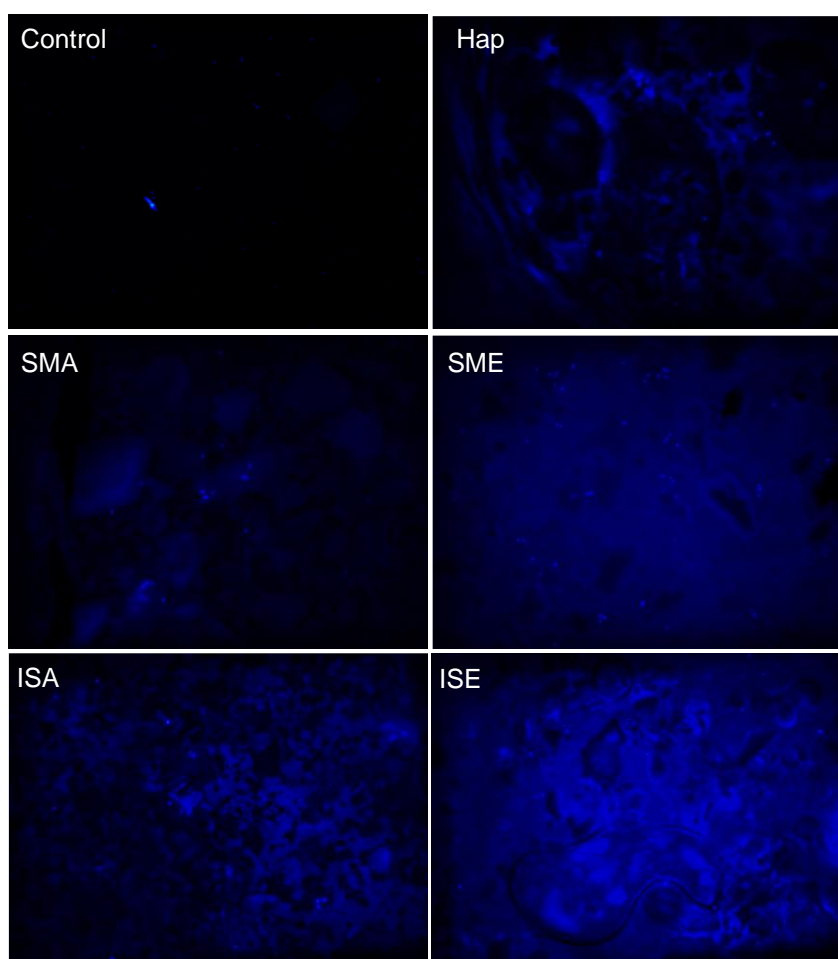
Table 8. Protein adsorption (%) values.

Sample	Protein adsorption (%)			
	5mg-10 min	5mg-30 min	10mg-10 min	10mg-30 min
HAp	-20.16	-50.08	-147.4	-118.36
SMA	-8.12	-16.75	-8.28	-5.96
SME	14.15	23.32	19.68	32.8
TTA	-279.92	-280.16	-366	-329.8
TTE	-48.28	-25.72	-98.8	-84.48
ISA	16.2	26.08	0	36.32
ISE	26.16	34.88	36.4	50.6

3.3 Cell adhesion

The cell adhesion at the surface of the samples was visualized by DAPI labeling of their nuclei, as shown in Figure 69. The light blue spots indicating the cells nuclei were found in HAp, SMA, SME, ISA and ISE. The heat-treated samples TTA and TTE did not display any cell at their surface, confirming results presented in Table 8.

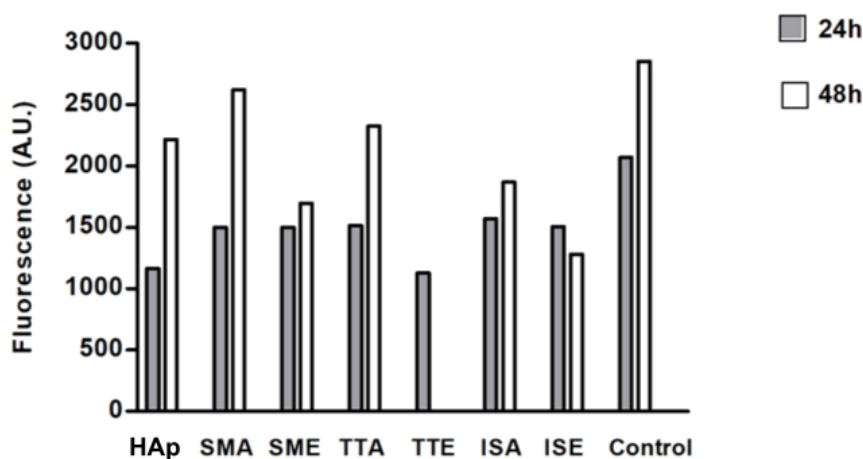
Figure 69. Cell adhesion at the surface of HAp and alanine grafted HAp samples. The visualization of cells nuclei with DAPI staining is shown as light blue spots at samples surface. The blur blue background is due to autofluorescence of samples. Control shows cells at the surface of well without sample.



3.4 Cell viability

The cell viability results determined by resazurin test are shown in Figure 70. The metabolization of resazurin by live cells generates the fluorescent resofurin which is used to estimate the cell viability by measurement of the fluorescence intensity. Although lower than in control, cell viability is preserved after 24h hours in all samples. Furthermore, clear tendency of cell growth after 48 h of incubation is confirmed for all samples, except for TTE which has been dispersed into the medium and was not read at 48 h time point.

Figure 70. Cells viability at the surface of the samples



Alanine is the simplest molecule used as the constructive block of proteins, with one carboxylic acid, one amine group, few carbons and hydrogens. Its grafting to HAp nanoparticles should contribute to the biocompatibility and osseointegration of implants based on them. Ca-deficient HAp rod-like nanoparticles with aspect ratio of 10, obtained in this work by simple precipitation, have better crystallinity (crystallite size of 30nm) than nanoparticles from *in-situ* grafting (crystallite size of 18nm). This implies that presence of alanine (either in form of acid or ester) during HAp precipitation suppress its crystal growth. Inhibition of HAp growth in the presence of some other poly(amino acids) containing amine and carboxylate groups is already reported in literature, and is usually associated with the chelation of Ca^{2+} and PO_4^{3-} ions by dissolved amino acids (SHAN et al., 2013). With grafting, HAp nanoparticles become more prone to agglomeration, but their morphology stay unchanged. The most intense agglomeration is characteristic of ISA and ISE samples in which HAp nanoparticles were cross-linked *in situ* by alanine forming porous nanostructures with low degrees of long-range order. For these, 10 and 14 wt% of alanine is calculated based on TGA. Somewhat smaller alanine content of 8 wt% is detected in samples from simple mixing, while 25 wt% of alanine is estimated from weight loss of TTE sample. The presence of the characteristic modes of L-alanine (NH_3 and CH_3) is confirmed in all grafted samples by FTIR spectroscopy. The characteristic L-alanine mode of NH_2 bending at about 1300 cm^{-1} is strongest for SMA sample, while additional modes of CH bending at 1229 cm^{-1} and C=O bending at 1740 cm^{-1} are most pronounced in spectra of SME and ISE sample. Their presence on the HAp nanoparticles surface provides additional binding

sites, which is confirmed by protein adsorption test. Namely, increase of about 50% for protein adsorption at SME and ISE surfaces is detected with prolongation of time from 10 to 30min, Table 8. The capability of binding body proteins from blood serum is extremely important property of biomaterials in generally. When the artificial biomaterial is inserted into the body, the first response of the body is to trigger the innate protective immune system, i.e., to cover its surface with proteins from blood serum. Thus, the protein adsorption rapidly changes the biomaterial surfaces influencing on that way inflammatory response and wound healing process in body (Peptides and Proteins as Biomaterials for Tissue Regeneration and Repair, 2018). Beside adhesion, cytotoxicity test is the most frequently utilized for ensuring the safety of biomaterial use. As it is shown at Figure 70, the viability of MG-63 human osteoblastic cells following 24 h incubation with the alanine grafted HAp samples is well preserved, being in all cases above viability of cells incubated with HAp. The viability of cells was even higher after 48 h exposure in all cases, excluding ISE. Most intense cell proliferation with a prolongation of the exposure is observed for cells incubated with SMA. Similar trend of MG-63 cells growth is determined after 3 days of their incubation with composites based on HAp and aspartic/glutamic acid (BOANINI et al., 2006) Same study shows that composites were able to support better the growth of MG63 cells during long-time exposure of 7 days, contributing to osteoblast activation and extra-cellular matrix mineralization processes.

4 CONCLUSIONS

Presented results demonstrate successful grafting of alanine at HAp nanoparticles by all synthesis methods explored. Two alanine precursors were used for grafting: L-alanine and L-alanine methyl ester hydrochloride. Higher content of alanine in samples from *in situ* grafting contributes to higher protein adsorption in comparison to other samples, while greater content of NH_3 , NH_2 and CH_3 moieties at surface of SMA enables superior proliferation of MG-63 human osteoblastic cells after exposure of 48h. Based on this, these samples could be considered as the most promising for application in bone graft.

REFERENCES

- ABUSHAHEEN, Manar Ali et al. Antimicrobial resistance, mechanisms and its clinical significance. **Disease-a-Month**, [*S. l.*], v. 66, n. 6, p. 100971, 2020. DOI: 10.1016/j.disamonth.2020.100971.
- ADELNIA, Hossein; TRAN, Huong D. N.; LITTLE, Peter J.; BLAKEY, Idriss; TA, Hang T. Poly(aspartic acid) in Biomedical Applications: From Polymerization, Modification, Properties, Degradation, and Biocompatibility to Applications. **ACS Biomaterials Science & Engineering**, [*S. l.*], v. 7, n. 6, p. 2083–2105, 2021. DOI: 10.1021/acsbiomaterials.1c00150.
- AGUILAR-FRUTIS, M.; KUMAR, S.; FALCONY, C. Spray-pyrolyzed hydroxyapatite thin-film coatings. **Surface and Coatings Technology**, [*S. l.*], v. 204, n. 6–7, p. 1116–1120, 2009. DOI: 10.1016/j.surfcoat.2009.07.021.
- AHMAD, Zubair; SALMAN, Saad; KHAN, Shahid Ali; AMIN, Abdul; RAHMAN, Zia Ur; AL-GHAMDI, Youssef O.; AKHTAR, Kalsoom; BAKHSH, Esraa M.; KHAN, Sher Bahadar. Versatility of Hydrogels: From Synthetic Strategies, Classification, and Properties to Biomedical Applications. **Gels**, [*S. l.*], v. 8, n. 3, p. 167, 2022. DOI: 10.3390/gels8030167.
- ALDANA, Ana A.; HOUBEN, Sofie; MORONI, Lorenzo; BAKER, Matthew B.; PITET, Louis M. Trends in Double Networks as Bioprintable and Injectable Hydrogel Scaffolds for Tissue Regeneration. **ACS Biomaterials Science & Engineering**, [*S. l.*], v. 7, n. 9, p. 4077–4101, 2021. DOI: 10.1021/acsbiomaterials.0c01749.
- ALTAMIMI, Mohammad A.; NEAU, Steven H. A study to identify the contribution of Soluplus® component homopolymers to the solubilization of nifedipine and sulfamethoxazole using the melting point depression method. **Powder Technology**, [*S. l.*], v. 338, p. 576–585, 2018. DOI: 10.1016/j.powtec.2018.07.027.
- ANJUM, Muna F. et al. The potential of using E. coli as an indicator for the surveillance of antimicrobial resistance (AMR) in the environment. **Current Opinion in Microbiology**, [*S. l.*], v. 64, p. 152–158, 2021. DOI: 10.1016/j.mib.2021.09.011.
- ANTUNES, Bruna Fernandes; FERREIRA, Antonio Gilberto; AMARAL, André Capaldo; CARVALHO, Antonio José Felix; GANDINI, Alessandro; TROVATTI, Eliane. Crosslinking starch with Diels–Alder reaction: water-soluble materials and water-mediated processes. **Polymer International**, [*S. l.*], v. 71, n. 11, p. 1340–1346, 2022. DOI: 10.1002/pi.6438.
- BABUTAN, Iulia; LUCACI, Alexandra-Delia; BOTIZ, Ioan. Antimicrobial Polymeric Structures Assembled on Surfaces. **Polymers**, [*S. l.*], v. 13, n. 10, p. 1552, 2021. DOI: 10.3390/polym13101552.
- BARDI, Tommaso; PINTADO, Vicente; GOMEZ-ROJO, Maria; ESCUDERO-SANCHEZ, Rosa; AZZAM LOPEZ, Amal; DIEZ-REMESAL, Yolanda; MARTINEZ CASTRO, Nilda; RUIZ-GARBAJOSA, Patricia; PESTAÑA, David. Nosocomial infections associated to COVID-19 in the intensive care unit: clinical characteristics and outcome. **European Journal**

of **Clinical Microbiology & Infectious Diseases**, [*S. l.*], v. 40, n. 3, p. 495–502, 2021. DOI: 10.1007/s10096-020-04142-w.

BASHIR, Shahid; HINA, Maryam; IQBAL, Javed; RAJPAR, A. H.; MUJTABA, M. A.; ALGHAMDI, N. A.; WAGEH, S.; RAMESH, K.; RAMESH, S. Fundamental Concepts of Hydrogels: Synthesis, Properties, and Their Applications. **Polymers**, [*S. l.*], v. 12, n. 11, p. 2702, 2020. DOI: 10.3390/polym12112702.

BASU, Arijit; KUNDURU, Konda Reddy; ABTEW, Ester; DOMB, Abraham J. Polysaccharide-Based Conjugates for Biomedical Applications. **Bioconjugate Chemistry**, [*S. l.*], v. 26, n. 8, p. 1396–1412, 2015. DOI: 10.1021/acs.bioconjchem.5b00242.

BATISTA, Hudson A.; SILVA, Francisco N.; LISBOA, Hugo M.; COSTA, Ana Cristina F. M. Modeling and optimization of combustion synthesis for hydroxyapatite production. **Ceramics International**, [*S. l.*], v. 46, n. 8, p. 11638–11646, 2020. DOI: 10.1016/j.ceramint.2020.01.194.

BATTEGAZZORE, D.; BOCCHINI, S.; FRACHE, A. Crystallization kinetics of poly(lactic acid)-talc composites. **Express Polymer Letters**, [*S. l.*], v. 5, n. 10, p. 849–858, 2011. DOI: 10.3144/expresspolymlett.2011.84.

BATTIGELLI, Alessia; ALMEIDA, Bethany; SHUKLA, Anita. Recent Advances in Bioorthogonal Click Chemistry for Biomedical Applications. **Bioconjugate Chemistry**, [*S. l.*], v. 33, n. 2, p. 263–271, 2022. DOI: 10.1021/acs.bioconjchem.1c00564.

BERNSTEIN, Leslie; KALDOR, John; MCCANN, Joyce; PIKE, Malcolm C. An empirical approach to the statistical analysis of mutagenesis data from the Salmonella test. **Mutation Research/Environmental Mutagenesis and Related Subjects**, [*S. l.*], v. 97, n. 4, p. 267–281, 1982. DOI: 10.1016/0165-1161(82)90026-7.

BHAT, Sumrita; KUMAR, Ashok. Biomaterials in Regenerative Medicine. **Journal of Postgraduate Medicine, Education and Research**, [*S. l.*], v. 46, n. 2, p. 81–89, 2012. DOI: 10.5005/jp-journals-10028-1018.

BOANINI, E.; TORRICELLI, P.; GAZZANO, M.; GIARDINO, R.; BIGI, A. Nanocomposites of hydroxyapatite with aspartic acid and glutamic acid and their interaction with osteoblast-like cells. **Biomaterials**, [*S. l.*], v. 27, n. 25, p. 4428–4433, 2006. DOI: 10.1016/j.biomaterials.2006.04.019.

BORMIO NUNES, Julia Helena; DE PAIVA, Raphael Enoque Ferraz; CUIN, Alexandre; LUSTRI, Wilton Rogério; CORBI, Pedro Paulo. Silver complexes with sulfathiazole and sulfamethoxazole: Synthesis, spectroscopic characterization, crystal structure and antibacterial assays. **Polyhedron**, [*S. l.*], v. 85, p. 437–444, 2015. DOI: 10.1016/j.poly.2014.09.010.

BOTTGER, G. L.; GEDDES, A. L. The infrared spectra of the crystalline tetramethylammonium halides. **Spectrochimica Acta**, [*S. l.*], v. 21, n. 10, p. 1701–1708, 1965. DOI: 10.1016/0371-1951(65)80082-0.

BRAVO-OSUNA, I.; FERRERO, C.; JIMÉNEZ-CASTELLANOS, M. R. Water sorption–desorption behaviour of methyl methacrylate–starch copolymers: effect of hydrophobic graft

and drying method. **European Journal of Pharmaceutics and Biopharmaceutics**, [*S. l.*], v. 59, n. 3, p. 537–548, 2005. DOI: 10.1016/j.ejpb.2004.10.003.

BRYM, Szczepan. Comparison IR spectra of alanine $\text{CH}_3\text{CH}(\text{NH}_2)\text{COOH}$ and alanine $\text{CD}_3\text{CH}(\text{NH}_2)\text{COOH}$. **Journal of Physics: Conference Series**, [*S. l.*], v. 810, p. 012026, 2017. DOI: 10.1088/1742-6596/810/1/012026.

BSHENA, Osama; HEUNIS, Tiaan DJ; DICKS, Leon MT; KLUMPERMAN, Bert. Antimicrobial fibers: therapeutic possibilities and recent advances. **Future Medicinal Chemistry**, [*S. l.*], v. 3, n. 14, p. 1821–1847, 2011. DOI: 10.4155/fmc.11.131.

BUREŠ, Filip. Quaternary Ammonium Compounds: Simple in Structure, Complex in Application. **Topics in Current Chemistry**, [*S. l.*], v. 377, n. 3, p. 14, 2019. DOI: 10.1007/s41061-019-0239-2.

BYSTROV, Vladimir; PARAMONOVA, Ekaterina; AVAKYAN, Leon; COUTINHO, José; BULINA, Natalia. Simulation and Computer Study of Structures and Physical Properties of Hydroxyapatite with Various Defects. **Nanomaterials**, [*S. l.*], v. 11, n. 10, p. 2752, 2021. DOI: 10.3390/nano11102752.

CADAMURO, Francesca; RUSSO, Laura; NICOTRA, Francesco. Biomedical Hydrogels Fabricated Using Diels–Alder Crosslinking. **European Journal of Organic Chemistry**, [*S. l.*], v. 2021, n. 3, p. 374–382, 2021. DOI: 10.1002/ejoc.202001042.

CAO, Xuan Thang; KIM, Yong Hun; PARK, Jong Myung; LIM, Kwon Taek. One-pot syntheses of dual-responsive core cross-linked polymeric micelles and covalently entrapped drug by click chemistry. **European Polymer Journal**, [*S. l.*], v. 78, p. 264–273, 2016. DOI: 10.1016/j.eurpolymj.2016.03.039.

CAO, Xuan Thang; VU-QUANG, Hieu; DOAN, Van-Dat; NGUYEN, Van Cuong. One-step approach of dual-responsive prodrug nanogels via Diels–Alder reaction for drug delivery. **Colloid and Polymer Science**, [*S. l.*], v. 299, n. 4, p. 675–683, 2021. DOI: 10.1007/s00396-020-04789-z.

CARTER, Margaret H.; JOSEPHY, P. David. Mutagenicity of thionitrites in the ames test. **Biochemical Pharmacology**, [*S. l.*], v. 35, n. 21, p. 3847–3851, 1986. DOI: 10.1016/0006-2952(86)90674-X.

CASSETTARI, Luca; VLLASALIU, Driton; LAM, Jenny K. W.; SOLIMAN, Mahmoud; ILLUM, Lisbeth. Biomedical applications of amino acid-modified chitosans: A review. **Biomaterials**, [*S. l.*], v. 33, n. 30, p. 7565–7583, 2012. DOI: 10.1016/j.biomaterials.2012.06.104.

CHAI, Qinyuan; JIAO, Yang; YU, Xinjun. Hydrogels for Biomedical Applications: Their Characteristics and the Mechanisms behind Them. **Gels**, [*S. l.*], v. 3, n. 1, p. 6, 2017. DOI: 10.3390/gels3010006.

CHEN, Junyi; MA, Xutao; EDGAR, Kevin J. A Versatile Method for Preparing Polysaccharide Conjugates via Thiol–Michael Addition. **Polymers**, [*S. l.*], v. 13, n. 12, p. 1905, 2021. DOI: 10.3390/polym13121905.

CHOI, Young Hun; LIU, Feng; KIM, Jin-Seok; CHOI, Young Kweon; JONG SANG PARK; KIM, Sung Wan. Polyethylene glycol-grafted poly-L-lysine as polymeric gene carrier. **Journal of Controlled Release**, [S. l.], v. 54, n. 1, p. 39–48, 1998. DOI: 10.1016/S0168-3659(97)00174-0.

CHU, P. Plasma-surface modification of biomaterials. **Materials Science and Engineering: R: Reports**, [S. l.], v. 36, n. 5–6, p. 143–206, 2002. DOI: 10.1016/S0927-796X(02)00004-9.

CHUNG, Man-Chin; SILVA, Antonio Távora de Albuquerque; CASTRO, Lúcia Fioravanti; GÜIDO, Rafael Victório Carvalho; NASSUTE, José Carlos; FERREIRA, Elizabeth Igne. Latenciação e formas avançadas de transporte de fármacos. **Revista Brasileira de Ciências Farmacêuticas**, [S. l.], v. 41, n. 2, p. 155–180, 2005. DOI: 10.1590/S1516-93322005000200004.

CLARO, P. I. C.; NETO, A. R. S.; BIBBO, A. C. C.; MATTOSO, L. H. C.; BASTOS, M. S. R.; MARCONCINI, J. M. Biodegradable Blends with Potential Use in Packaging: A Comparison of PLA/Chitosan and PLA/Cellulose Acetate Films. **Journal of Polymers and the Environment**, [S. l.], v. 24, n. 4, p. 363–371, 2016. DOI: 10.1007/s10924-016-0785-4.

CLASEN, Samuel H.; MÜLLER, Carmen M. O.; PIRES, Alfredo T. N. Maleic Anhydride as a Compatibilizer and Plasticizer in TPS/PLA Blends. **Journal of the Brazilian Chemical Society**, [S. l.], 2015. DOI: 10.5935/0103-5053.20150126.

COFELICE, Martina; MESSIA, Maria Cristina; MARCONI, Emanuele; CUOMO, Francesca; LOPEZ, Francesco. Effect of the xanthan gum on the rheological properties of alginate hydrogels. **Food Hydrocolloids**, [S. l.], v. 142, p. 108768, 2023. DOI: 10.1016/j.foodhyd.2023.108768.

COMEAU, Patricia; WILLETT, Thomas. Impact of Side Chain Polarity on Non-Stoichiometric Nano-Hydroxyapatite Surface Functionalization with Amino Acids. **Scientific Reports**, [S. l.], v. 8, n. 1, p. 12700, 2018. DOI: 10.1038/s41598-018-31058-5.

COSTA, E. M.; SILVA, S.; TAVARIA, F. K.; PINTADO, M. M. Insights into chitosan antibiofilm activity against methicillin-resistant *Staphylococcus aureus*. **Journal of Applied Microbiology**, [S. l.], v. 122, n. 6, p. 1547–1557, 2017. DOI: 10.1111/jam.13457.

D'AMICO, Francesco et al. Chemical constitution of polyfurfuryl alcohol investigated by FTIR and Resonant Raman spectroscopy. **Spectrochimica Acta Part A: Molecular and Biomolecular Spectroscopy**, [S. l.], v. 262, p. 120090, 2021. DOI: 10.1016/j.saa.2021.120090.

DE FLORA, Silvio. Letter to the Editor. **Mutagenesis**, [S. l.], v. 5, n. 3, p. 301–302, 1990. DOI: 10.1093/mutage/5.3.301.

DESTEFANO, Vincent; KHAN, Salaar; TABADA, Alonzo. Applications of PLA in modern medicine. **Engineered Regeneration**, [S. l.], v. 1, p. 76–87, 2020. DOI: 10.1016/j.engreg.2020.08.002.

DHARUN, P.; ISMAIL, Y.; VIJAYA, VARA PRASAD M. Latentiated prodrug approach of drugs: an overview. **Int J Appl Pharm**, v. 13, n. 6, 2021.

DÍAZ BUKVIC, Gema Díaz; ROSSI, Ezequiel; ERREA, María Inés. Polysaccharides as Economic and Sustainable Raw Materials for the Preparation of Adsorbents for Water Treatment. **Polysaccharides**, [S. l.], v. 4, n. 3, p. 219–255, 2023. DOI: 10.3390/polysaccharides4030016.

DISPINAR, Tugba; SANYAL, Rana; SANYAL, Amitav. A Diels-Alder/retro Diels-Alder strategy to synthesize polymers bearing maleimide side chains. **Journal of Polymer Science Part A: Polymer Chemistry**, [S. l.], v. 45, n. 20, p. 4545–4551, 2007. DOI: 10.1002/pola.22299.

DORM, Bruna Carolina; JUNIOR, José Alberto Paris; DA SILVA, Lucas Henrique Domingos; FORATO, Lucimara Aparecida; DE SOUZA NOSSA, Tamires; CARVALHO, Antonio José Felix; RESENDE, Flávia Aparecida; GANDINI, Alessandro; TROVATTI, Eliane. Synthesis of a cysteine Diels–Alder-based polymer by simultaneous double-click chemistry and its cyto-genotoxicity evaluation. **Macromolecular Research**, [S. l.], v. 32, n. 2, p. 133–144, 2024. DOI: 10.1007/s13233-023-00216-8.

Effects of Alanine Methyl Ester Hydrochlorides on Thermal Behaviour of Biodegradable Poly(L-lactic Acid). **Asian Journal of Chemistry**, [S. l.], v. 25, n. 3, 2013. DOI: 10.14233/ajchem.2013.13014.

FALUA, Kehinde James; POKHAREL, Anamol; BABAEI-GHAZVINI, Amin; AI, Yongfeng; ACHARYA, Bishnu. Valorization of Starch to Biobased Materials: A Review. **Polymers**, [S. l.], v. 14, n. 11, p. 2215, 2022. DOI: 10.3390/polym14112215.

FARAH, Shady; ANDERSON, Daniel G.; LANGER, Robert. Physical and mechanical properties of PLA, and their functions in widespread applications — A comprehensive review. **Advanced Drug Delivery Reviews**, [S. l.], v. 107, p. 367–392, 2016. DOI: 10.1016/j.addr.2016.06.012.

FERNANDEZ-SAIZ, P.; LAGARON, J. M.; OCIO, M. J. Optimization of the biocide properties of chitosan for its application in the design of active films of interest in the food area. **Food Hydrocolloids**, [S. l.], v. 23, n. 3, p. 913–921, 2009. DOI: 10.1016/j.foodhyd.2008.06.001.

FERRAZ, Maria Pia. Bone Grafts in Dental Medicine: An Overview of Autografts, Allografts and Synthetic Materials. **Materials**, [S. l.], v. 16, n. 11, p. 4117, 2023. DOI: 10.3390/ma16114117.

GABANO, Elisabetta; PERIN, Elena; BONZANI, Diego; RAVERA, Mauro. Conjugation between maleimide-containing Pt(IV) prodrugs and furan or furan-containing drug delivery vectors via Diels-Alder cycloaddition. **Inorganica Chimica Acta**, [S. l.], v. 488, p. 195–200, 2019. DOI: 10.1016/j.ica.2019.01.014.

GANDINI, Alessandro. Polymers and Oligomers Containing Furan Rings. *Em*: [s.l: s.n.]. p. 195–208. DOI: 10.1021/bk-1990-0433.ch017.

GANDINI, Alessandro. The furan/maleimide Diels–Alder reaction: A versatile click–unclick tool in macromolecular synthesis. **Progress in Polymer Science**, [S. l.], v. 38, n. 1, p. 1–29, 2013. DOI: 10.1016/j.progpolymsci.2012.04.002.

GANDINI, Alessandro; BELGACEM, Mohamed Naceur. Furan Derivatives and Furan Chemistry at the Service of Macromolecular Materials. *Em: Monomers, Polymers and Composites from Renewable Resources*. [s.l.] : Elsevier, 2008. a. p. 115–152. DOI: 10.1016/B978-0-08-045316-3.00006-5.

GANDINI, Alessandro; BELGACEM, Mohamed Naceur. Furan Derivatives and Furan Chemistry at the Service of Macromolecular Materials. *Em: Monomers, Polymers and Composites from Renewable Resources*. [s.l.] : Elsevier, 2008. b. p. 115–152. DOI: 10.1016/B978-0-08-045316-3.00006-5.

GANDINI, Alessandro; COELHO, Dora; GOMES, Mónica; REIS, Bruno; SILVESTRE, Armando. Materials from renewable resources based on furan monomers and furan chemistry: work in progress. **Journal of Materials Chemistry**, [S. l.], v. 19, n. 45, p. 8656, 2009. DOI: 10.1039/b909377j.

GANDINI, Alessandro; COELHO, Dora; SILVESTRE, Armando J. D. Reversible click chemistry at the service of macromolecular materials. Part 1: Kinetics of the Diels–Alder reaction applied to furan–maleimide model compounds and linear polymerizations. **European Polymer Journal**, [S. l.], v. 44, n. 12, p. 4029–4036, 2008. a. DOI: 10.1016/j.eurpolymj.2008.09.026.

GANDINI, Alessandro; COELHO, Dora; SILVESTRE, Armando J. D. Reversible click chemistry at the service of macromolecular materials. Part 1: Kinetics of the Diels–Alder reaction applied to furan–maleimide model compounds and linear polymerizations. **European Polymer Journal**, [S. l.], v. 44, n. 12, p. 4029–4036, 2008. b. DOI: 10.1016/j.eurpolymj.2008.09.026.

GANDINI, Alessandro; LACERDA, Talita M.; CARVALHO, Antonio J. F.; TROVATTI, Eliane. Progress of Polymers from Renewable Resources: Furans, Vegetable Oils, and Polysaccharides. **Chemical Reviews**, [S. l.], v. 116, n. 3, p. 1637–1669, 2016. DOI: 10.1021/acs.chemrev.5b00264.

GAO, Mengqian et al. Enhanced curcumin solubility and antibacterial activity by encapsulation in PLGA oily core nanocapsules. **Food & Function**, [S. l.], v. 11, n. 1, p. 448–455, 2020. DOI: 10.1039/C9FO00901A.

GAO, Wei Min; RUAN, Cheng Xiang; CHEN, Yun Fa. Effects of Acidic Amino Acids on Hydroxyapatite Morphology. **Key Engineering Materials**, [S. l.], v. 336–338, p. 2096–2099, 2007. DOI: 10.4028/www.scientific.net/KEM.336-338.2096.

GARCÍA-ASTRAIN, Clara; ALGAR, Ixaso; GANDINI, Alessandro; ECEIZA, Arantxa; CORCUERA, María Ángeles; GABILONDO, Nagore. Hydrogel synthesis by aqueous Diels–Alder reaction between furan modified methacrylate and polyetheramine-based bismaleimides. **Journal of Polymer Science Part A: Polymer Chemistry**, [S. l.], v. 53, n. 5, p. 699–708, 2015. DOI: 10.1002/pola.27495.

GARDELLA, Lorenza; CALABRESE, Michela; MONTICELLI, Orietta. PLA maleation: an easy and effective method to modify the properties of PLA/PCL immiscible blends. **Colloid and Polymer Science**, [S. l.], v. 292, n. 9, p. 2391–2398, 2014. DOI: 10.1007/s00396-014-3328-3.

GENG, Zhishuai; SHIN, Jaeman J.; XI, Yumeng; HAWKER, Craig J. Click chemistry strategies for the accelerated synthesis of functional macromolecules. **Journal of Polymer Science**, [S. l.], v. 59, n. 11, p. 963–1042, 2021. DOI: 10.1002/pol.20210126.

GHEORGHE, Daniela; NEACSU, Ana; CONTINEANU, Iulia; TEODORESCU, Florina; TĂNĂSESCU, Speranta. Thermochemical properties of l-alanine nitrate and l-alanine ethyl ester nitrate. **Journal of Thermal Analysis and Calorimetry**, [S. l.], v. 118, n. 2, p. 731–737, 2014. DOI: 10.1007/s10973-014-3996-8.

GIL ALVARADEJO, Gabriela; GLASSNER, Mathias; HOOGENBOOM, Richard; DELAITTRE, Guillaume. Maleimide end-functionalized poly(2-oxazoline)s by the functional initiator route: synthesis and (bio)conjugation. **RSC Advances**, [S. l.], v. 8, n. 17, p. 9471–9479, 2018. DOI: 10.1039/C8RA00948A.

GLATT, Hansruedi. Mutagenicity spectra in *Salmonella typhimurium* strains of glutathione, L-cysteine and active oxygen species. **Mutagenesis**, [S. l.], v. 4, n. 3, p. 221–227, 1989. DOI: 10.1093/mutage/4.3.221.

GLATT, Hansruedi; PROTIĆ-SABLJIĆ, Miroslava; OESCH, Franz. Mutagenicity of Glutathione and Cysteine in the Ames Test. **Science**, [S. l.], v. 220, n. 4600, p. 961–963, 1983. DOI: 10.1126/science.6342137.

GOITI, Eunat; HUGLIN, Malcolm B.; REGO, José M. Some properties of networks produced by the Diels–Alder reaction between poly(styrene-co-furfuryl methacrylate) and bismaleimide. **European Polymer Journal**, [S. l.], v. 40, n. 2, p. 219–226, 2004. DOI: 10.1016/j.eurpolymj.2003.09.017.

GÖKCE, Halil; BAHÇELI, Semiha. The molecular structures, vibrational spectroscopies (FT-IR and Raman) and quantum chemical calculations of n-alkyltrimethylammonium bromides. **Optics and Spectroscopy**, [S. l.], v. 115, n. 5, p. 632–644, 2013. DOI: 10.1134/S0030400X13110076.

GONSALVES, Arlan de Assis; ARAÚJO, Cleônia Roberta Melo; SOARES, Nivaldo Alves; GOULART, Marília Oliveira Fonseca; ABREU, Fabiane Caxico De. Diferentes estratégias para a reticulação de quitosana. **Química Nova**, [S. l.], v. 34, n. 7, p. 1215–1223, 2011. DOI: 10.1590/S0100-40422011000700021.

GONZALEZ-MCQUIRE, Rosanna; CHANE-CHING, Jean-Yves; VIGNAUD, E.; LEBUGLE, A.; MANN, Stephen. Synthesis and characterization of amino acid-functionalized hydroxyapatite nanorods. **Journal of Materials Chemistry**, [S. l.], v. 14, n. 14, p. 2277, 2004. a. DOI: 10.1039/b400317a.

GONZALEZ-MCQUIRE, Rosanna; CHANE-CHING, Jean-Yves; VIGNAUD, E.; LEBUGLE, A.; MANN, Stephen. Synthesis and characterization of amino acid-functionalized

hydroxyapatite nanorods. **Journal of Materials Chemistry**, [S. l.], v. 14, n. 14, p. 2277, 2004. b. DOI: 10.1039/b400317a.

GOY, Rejane C.; BRITTO, Douglas De; ASSIS, Odilio B. G. A review of the antimicrobial activity of chitosan. **Polímeros**, [S. l.], v. 19, n. 3, p. 241–247, 2009. DOI: 10.1590/S0104-14282009000300013.

GREGORITZA, Manuel; BRANDL, Ferdinand P. The Diels–Alder reaction: A powerful tool for the design of drug delivery systems and biomaterials. **European Journal of Pharmaceutics and Biopharmaceutics**, [S. l.], v. 97, p. 438–453, 2015. DOI: 10.1016/j.ejpb.2015.06.007.

GREMA, Hafsat Ali. Methicillin Resistant Staphylococcus aureus (MRSA): A Review. **Advances in Animal and Veterinary Sciences**, [S. l.], v. 3, n. 2, p. 79–98, 2015. DOI: 10.14737/journal.aavs/2015/3.2.79.98.

GROSSNER, Tobias; HABERKORN, Uwe; GOTTERBARM, Tobias. Evaluation of the Impact of Different Pain Medication and Proton Pump Inhibitors on the Osteogenic Differentiation Potential of hMSCs Using 99mTc-HDP Labelling. **Life**, [S. l.], v. 11, n. 4, p. 339, 2021. DOI: 10.3390/life11040339.

Growth and Characterization of L-Alanine Crystals using FT-IR, UV Visible Spectra. [S. l.], [s.d.].

GUPTA, Deepak et al. Chemical and enzymatic stability of amino acid prodrugs containing methoxy, ethoxy and propylene glycol linkers. **Molecular pharmaceutics**, v. 6, n. 5, p. 1604–1611, 2009.

HEIN, Christopher D.; LIU, Xin-Ming; WANG, Dong. Click Chemistry, A Powerful Tool for Pharmaceutical Sciences. **Pharmaceutical Research**, [S. l.], v. 25, n. 10, p. 2216–2230, 2008. DOI: 10.1007/s11095-008-9616-1.

HOSSEINNEJAD, Mahmoud; JAFARI, Seid Mahdi. Evaluation of different factors affecting antimicrobial properties of chitosan. **International Journal of Biological Macromolecules**, [S. l.], v. 85, p. 467–475, 2016. DOI: 10.1016/j.ijbiomac.2016.01.022.

HOVEIZI, Elham; NABIUNI, Mohammad; PARIVAR, Kazem; RAJABI-ZELETI, Sareh; TAVAKOL, Shima. Functionalisation and surface modification of electrospun polylactic acid scaffold for tissue engineering. **Cell Biology International**, [S. l.], v. 38, n. 1, p. 41–49, 2014. DOI: 10.1002/cbin.10178.

HUANG, Ying; MÜLLER, Michael Thomas; BOLDT, Regine; ZSCHECH, Carsten; GOHS, Uwe; WIESSNER, Sven. A new strategy to improve viscoelasticity, crystallization and mechanical properties of polylactide. **Polymer Testing**, [S. l.], v. 97, p. 107160, 2021. DOI: 10.1016/j.polymertesting.2021.107160.

IGNJATOVIĆ, Nenad L. et al. Rare-earth (Gd³⁺, Yb³⁺/Tm³⁺, Eu³⁺) co-doped hydroxyapatite as magnetic, up-conversion and down-conversion materials for multimodal imaging. **Scientific Reports**, [S. l.], v. 9, n. 1, p. 16305, 2019. DOI: 10.1038/s41598-019-52885-0.

IGNJATOVIĆ, Nenad; VRANJEŠ DJURIĆ, Sanja; MITIĆ, Žarko; JANKOVIĆ, Drina; USKOKOVIĆ, Dragan. Investigating an organ-targeting platform based on hydroxyapatite nanoparticles using a novel in situ method of radioactive ¹²⁵Iodine labeling. **Materials Science and Engineering: C**, [S. l.], v. 43, p. 439–446, 2014. DOI: 10.1016/j.msec.2014.07.046.

ILYAS, R. A. et al. Polylactic Acid (PLA) Biocomposite: Processing, Additive Manufacturing and Advanced Applications. **Polymers**, [S. l.], v. 13, n. 8, p. 1326, 2021. DOI: 10.3390/polym13081326.

IREDALE, Robert J.; WARD, Carwyn; HAMERTON, Ian. Modern advances in bismaleimide resin technology: A 21st century perspective on the chemistry of addition polyimides. **Progress in Polymer Science**, [S. l.], v. 69, p. 1–21, 2017. DOI: 10.1016/j.progpolymsci.2016.12.002.

IZUNOBI, Josephat U.; HIGGINBOTHAM, Clement L. Polymer Molecular Weight Analysis by ¹H NMR Spectroscopy. **Journal of Chemical Education**, [S. l.], v. 88, n. 8, p. 1098–1104, 2011. DOI: 10.1021/ed100461v.

JAIN, Anjali; DUVVURI, L. Sailaja; FARAH, Shady; BEYTH, Nurit; DOMB, Abraham J.; KHAN, Wahid. Antimicrobial Polymers. **Advanced Healthcare Materials**, [S. l.], v. 3, n. 12, p. 1969–1985, 2014. DOI: 10.1002/adhm.201400418.

JANG, Hyunho; KWON, Sangwoo; KIM, Sun Jong; PARK, Su-il. Maleic Anhydride-Grafted PLA Preparation and Characteristics of Compatibilized PLA/PBSeT Blend Films. **International Journal of Molecular Sciences**, [S. l.], v. 23, n. 13, p. 7166, 2022. DOI: 10.3390/ijms23137166.

JAVADINEJAD, Hamid Reza; EBRAHIMI-KAHRIZSANGI, Reza. Thermal and kinetic study of hydroxyapatite formation by solid-state reaction. **International Journal of Chemical Kinetics**, [S. l.], v. 53, n. 5, p. 583–595, 2021. DOI: 10.1002/kin.21467.

JIAO, Yang; NIU, Li-na; MA, Sai; LI, Jing; TAY, Franklin R.; CHEN, Ji-hua. Quaternary ammonium-based biomedical materials: State-of-the-art, toxicological aspects and antimicrobial resistance. **Progress in Polymer Science**, [S. l.], v. 71, p. 53–90, 2017. DOI: 10.1016/j.progpolymsci.2017.03.001.

JIMÉNEZ, Alfonso; PELTZER, Mercedes; RUSECKAITE, Roxana (ORG.). **Poly(lactic acid) Science and Technology**. Cambridge: Royal Society of Chemistry, 2014. DOI: 10.1039/9781782624806.

JIN, Ling; PRUDEN, Amy; BOEHM, Alexandria B.; ALVAREZ, Pedro J. J.; RASKIN, Lutgarde; KOHN, Tamar; LI, Xiangdong. Integrating Environmental Dimensions of “One Health” to Combat Antimicrobial Resistance: Essential Research Needs. **Environmental Science & Technology**, [S. l.], v. 56, n. 21, p. 14871–14874, 2022. DOI: 10.1021/acs.est.2c01651.

JING, Shiyao; WANG, Xin; TAN, Yebang. Preparation of lysine-decorated polymer-brush-grafted magnetic nanocomposite for the efficient and selective adsorption of organic dye.

Applied Surface Science, [*S. l.*], v. 441, p. 654–662, 2018. DOI: 10.1016/j.apsusc.2018.01.259.

JOGIYA, Bhoomika; BHOJANI, Amit; SOLANKI, Pushpakant; JETHVA, H. O.; JOSHI, Mihir. Synthesis and Characterization of L-Alanine Functionalized Nano Hydroxyapatite. **Mechanics, Materials Science and Engineering**, [*S. l.*], 2017.

KADE, Matthew J.; BURKE, Daniel J.; HAWKER, Craig J. The power of thiol-ene chemistry. **Journal of Polymer Science Part A: Polymer Chemistry**, [*S. l.*], v. 48, n. 4, p. 743–750, 2010. DOI: 10.1002/pola.23824.

KAECH, C.; ELZI, L.; SENDI, P.; FREI, R.; LAIFER, G.; BASSETTI, S.; FLUCKIGER, U. Course and outcome of Staphylococcus aureus bacteraemia: a retrospective analysis of 308 episodes in a Swiss tertiary-care centre. **Clinical Microbiology and Infection**, [*S. l.*], v. 12, n. 4, p. 345–352, 2006. DOI: 10.1111/j.1469-0691.2005.01359.x.

KAITH, Balbir Singh; SINGH, Anjali; SHARMA, Amit Kumar; SUD, Dhiraj. Hydrogels: Synthesis, Classification, Properties and Potential Applications—A Brief Review. **Journal of Polymers and the Environment**, [*S. l.*], v. 29, n. 12, p. 3827–3841, 2021. DOI: 10.1007/s10924-021-02184-5.

KALAYCIOĞLU, Zeynep; TORLAK, Emrah; AKIN-EVINGÜR, Gülşen; ÖZEN, İlhan; ERİM, F. Bedia. Antimicrobial and physical properties of chitosan films incorporated with turmeric extract. **International Journal of Biological Macromolecules**, [*S. l.*], v. 101, p. 882–888, 2017. DOI: 10.1016/j.ijbiomac.2017.03.174.

KAMINSKAS, Lisa M.; BOYD, Ben J.; KARELLAS, Peter; KRIPPNER, Guy Y.; LESSENE, Romina; KELLY, Brian; PORTER, Christopher J. H. The Impact of Molecular Weight and PEG Chain Length on the Systemic Pharmacokinetics of PEGylated Poly-*l*-Lysine Dendrimers. **Molecular Pharmaceutics**, [*S. l.*], v. 5, n. 3, p. 449–463, 2008. DOI: 10.1021/mp7001208.

KIM, Ji-Heung; SON, Chang Mo; JEON, Young Sil; CHOE, Woo-Seok. Synthesis and characterization of poly(aspartic acid) derivatives conjugated with various amino acids. **Journal of Polymer Research**, [*S. l.*], v. 18, n. 5, p. 881–890, 2011. DOI: 10.1007/s10965-010-9485-2.

KIRCHHOF, Susanne; STRASSER, Andrea; WITTMANN, Hans-Joachim; MESSMANN, Viktoria; HAMMER, Nadine; GOEPFERICH, Achim M.; BRANDL, Ferdinand P. New insights into the cross-linking and degradation mechanism of Diels–Alder hydrogels. **Journal of Materials Chemistry B**, [*S. l.*], v. 3, n. 3, p. 449–457, 2015. DOI: 10.1039/C4TB01680G.

KONG, Ming; CHEN, Xi Guang; XING, Ke; PARK, Hyun Jin. Antimicrobial properties of chitosan and mode of action: A state of the art review. **International Journal of Food Microbiology**, [*S. l.*], v. 144, n. 1, p. 51–63, 2010. DOI: 10.1016/j.ijfoodmicro.2010.09.012.

KOZUMA, Wataru; KON, Kazuhiro; KAWAKAMI, Sawako; BOBOTHIKE, Aung; IJIMA, Hajime; SHIOTA, Makoto; KASUGAI, Shohei. Osteoconductive potential of a hydroxyapatite fiber material with magnesium: *In vitro* and *in vivo*

vivo</i> studies. **Dental Materials Journal**, [*S. l.*], v. 38, n. 5, p. 771–778, 2019. DOI: 10.4012/dmj.2018-333.

KRAMER, Ricardo Klaus; BELGACEM, Mohamed Naceur; CARVALHO, Antonio José Felix; GANDINI, Alessandro. Thermally reversible nanocellulose hydrogels synthesized via the furan/maleimide Diels-Alder click reaction in water. **International Journal of Biological Macromolecules**, [*S. l.*], v. 141, p. 493–498, 2019. a. DOI: 10.1016/j.ijbiomac.2019.09.027.

KRAMER, Ricardo Klaus; BELGACEM, Mohamed Naceur; CARVALHO, Antonio José Felix; GANDINI, Alessandro. Thermally reversible nanocellulose hydrogels synthesized via the furan/maleimide Diels-Alder click reaction in water. **International Journal of Biological Macromolecules**, [*S. l.*], v. 141, p. 493–498, 2019. b. DOI: 10.1016/j.ijbiomac.2019.09.027.

KRAULAND, Alexander H.; GUGGI, Davide; BERNKOP-SCHNÜRCH, Andreas. Oral insulin delivery: the potential of thiolated chitosan-insulin tablets on non-diabetic rats. **Journal of Controlled Release**, [*S. l.*], v. 95, n. 3, p. 547–555, 2004. DOI: 10.1016/j.jconrel.2003.12.017.

LAVANYA, P.; VIJAYAKUMARI, N. Fabrication of Poly (d, l - Alanine)/minerals substituted hydroxyapatite bio-composite for bone tissue applications. **Materials Discovery**, [*S. l.*], v. 11, p. 14–18, 2018. DOI: 10.1016/j.md.2018.07.001.

LEE, Andie S.; DE LENCASTRE, Hermínia; GARAU, Javier; KLUYTMANS, Jan; MALHOTRA-KUMAR, Surbhi; PESCHEL, Andreas; HARBARTH, Stephan. Methicillin-resistant *Staphylococcus aureus*. **Nature Reviews Disease Primers**, [*S. l.*], v. 4, n. 1, p. 18033, 2018. DOI: 10.1038/nrdp.2018.33.

LEE, Jung-Hee; KIM, Young-Jin. Hydroxyapatite nanofibers fabricated through electrospinning and sol–gel process. **Ceramics International**, [*S. l.*], v. 40, n. 2, p. 3361–3369, 2014. DOI: 10.1016/j.ceramint.2013.09.096.

LEE, Wing-Hin; LOO, Ching-Yee; CHRZANOWSKI, Wojciech; ROHANIZADEH, Ramin. Osteoblast response to the surface of amino acid-functionalized hydroxyapatite. **Journal of Biomedical Materials Research Part A**, [*S. l.*], v. 103, n. 6, p. 2150–2160, 2015. DOI: 10.1002/jbm.a.35353.

LEE, Wing-Hin; LOO, Ching-Yee; VAN, Kim Linh; ZAVGORODNIY, Alexander V.; ROHANIZADEH, Ramin. Modulating protein adsorption onto hydroxyapatite particles using different amino acid treatments. **Journal of The Royal Society Interface**, [*S. l.*], v. 9, n. 70, p. 918–927, 2012. a. DOI: 10.1098/rsif.2011.0586.

LEE, Wing-Hin; LOO, Ching-Yee; VAN, Kim Linh; ZAVGORODNIY, Alexander V.; ROHANIZADEH, Ramin. Modulating protein adsorption onto hydroxyapatite particles using different amino acid treatments. **Journal of The Royal Society Interface**, [*S. l.*], v. 9, n. 70, p. 918–927, 2012. b. DOI: 10.1098/rsif.2011.0586.

LI, Chenyang; GONG, Weiguang; DENG, Zhaopeng; YAO, Zhongyang; MENG, Xin; XIN, Zhong. Fully Biodegradable Long-Chain Branched Polylactic Acid with High Crystallization Performance and Heat Resistance. **Industrial & Engineering Chemistry Research**, [*S. l.*], v. 61, n. 30, p. 10945–10954, 2022. a. DOI: 10.1021/acs.iecr.2c01276.

LI, Xiyu; CHEN, Haifeng. Yb³⁺/Ho³⁺ Co-Doped Apatite Upconversion Nanoparticles to Distinguish Implanted Material from Bone Tissue. **ACS Applied Materials & Interfaces**, [*S. l.*], v. 8, n. 41, p. 27458–27464, 2016. DOI: 10.1021/acsami.6b05514.

LI, Ying-Qiu; HAN, Qing; FENG, Jian-Ling; TIAN, Wen-Li; MO, Hai-Zhen. Antibacterial characteristics and mechanisms of ε-poly-lysine against Escherichia coli and Staphylococcus aureus. **Food Control**, [*S. l.*], v. 43, p. 22–27, 2014. DOI: 10.1016/j.foodcont.2014.02.023.

LI, Yuchun et al. A new strategy to prepare fully bio-based poly(lactic acid) composite with high flame retardancy, UV resistance, and rapid degradation in soil. **Chemical Engineering Journal**, [*S. l.*], v. 428, p. 131979, 2022. b. DOI: 10.1016/j.cej.2021.131979.

LILING, Guo; DI, Zheng; JIACHAO, Xu; XIN, Gao; XIAOTING, Fu; QING, Zhang. Effects of ionic crosslinking on physical and mechanical properties of alginate mulching films. **Carbohydrate Polymers**, [*S. l.*], v. 136, p. 259–265, 2016. DOI: 10.1016/j.carbpol.2015.09.034.

LIU, Jun-Xian; YUE, Qin-Yan; GAO, Bao-Yu; WANG, Yan; LI, Qian; ZHANG, Pei-Dong. Research on microbial lipid production from potato starch wastewater as culture medium by *Lipomyces starkeyi*. **Water Science and Technology**, [*S. l.*], v. 67, n. 8, p. 1802–1808, 2013. DOI: 10.2166/wst.2013.059.

MA, Guoqing. Three common preparation methods of hydroxyapatite. **IOP Conference Series: Materials Science and Engineering**, [*S. l.*], v. 688, n. 3, p. 033057, 2019. DOI: 10.1088/1757-899X/688/3/033057.

MA, Minglu; CHENG, Yiyun; XU, Zhenhua; XU, Peng; QU, Haiou; FANG, Yujie; XU, Tongwen; WEN, Longping. Evaluation of polyamidoamine (PAMAM) dendrimers as drug carriers of anti-bacterial drugs using sulfamethoxazole (SMZ) as a model drug. **European Journal of Medicinal Chemistry**, [*S. l.*], v. 42, n. 1, p. 93–98, 2007. DOI: 10.1016/j.ejmech.2006.07.015.

MAJUMDER, Md Anwarul Azim; RAHMAN, Sayeeda; COHALL, Damian; BHARATHA, Ambadasu; SINGH, Keerti; HAQUE, Mainul; GITTENS-ST HILAIRE, Marquita. Antimicrobial Stewardship: Fighting Antimicrobial Resistance and Protecting Global Public Health. **Infection and Drug Resistance**, [*S. l.*], v. Volume 13, p. 4713–4738, 2020. DOI: 10.2147/IDR.S290835.

MARON, Dorothy M.; AMES, Bruce N. Revised methods for the Salmonella mutagenicity test. **Mutation Research/Environmental Mutagenesis and Related Subjects**, [*S. l.*], v. 113, n. 3–4, p. 173–215, 1983. DOI: 10.1016/0165-1161(83)90010-9.

MATSUBARA, Koshi; NAKATO, Takeshi; TOMIDA, Masayuki. H and ¹³C NMR Characterization of Poly(succinimide) Prepared by Thermal Polycondensation of <sc>l</sc>-Aspartic Acid¹. **Macromolecules**, [*S. l.*], v. 30, n. 8, p. 2305–2312, 1997. DOI: 10.1021/ma961579h.

MATSUMOTO, Takuya; OKAZAKI, Masayuki; INOUE, Masahiro; SASAKI, Jun-Ichi; HAMADA, Yoshinosuke; TAKAHASHI, Junzo. Role of Acidic Amino Acid for Regulating

Hydroxyapatite Crystal Growth. **Dental Materials Journal**, [S. l.], v. 25, n. 2, p. 360–364, 2006. DOI: 10.4012/dmj.25.360.

MATTHEWS, Dwight E. Review of Lysine Metabolism with a Focus on Humans. **The Journal of Nutrition**, [S. l.], v. 150, p. 2548S–2555S, 2020. DOI: 10.1093/jn/nxaa224.

MICHELOT, Audric; SARDA, Stéphanie; AUDIN, Catherine; DEYDIER, Eric; MANOURY, Eric; POLI, Rinaldo; REY, Christian. Spectroscopic characterisation of hydroxyapatite and nanocrystalline apatite with grafted aminopropyltriethoxysilane: nature of silane–surface interaction. **Journal of Materials Science**, [S. l.], v. 50, n. 17, p. 5746–5757, 2015. DOI: 10.1007/s10853-015-9122-x.

MIN, Tiantian; ZHU, Zhu; SUN, Xiaoli; YUAN, Zhipeng; ZHA, Junwei; WEN, Yongqiang. Highly efficient antifogging and antibacterial food packaging film fabricated by novel quaternary ammonium chitosan composite. **Food Chemistry**, [S. l.], v. 308, p. 125682, 2020. DOI: 10.1016/j.foodchem.2019.125682.

MOHD PU'AD, N. A. S.; ABDUL HAQ, R. H.; MOHD NOH, H.; ABDULLAH, H. Z.; IDRIS, M. I.; LEE, T. C. Synthesis method of hydroxyapatite: A review. **Materials Today: Proceedings**, [S. l.], v. 29, p. 233–239, 2020. DOI: 10.1016/j.matpr.2020.05.536.

MOROZOVA, Sofia M. Recent Advances in Hydrogels via Diels–Alder Crosslinking: Design and Applications. **Gels**, [S. l.], v. 9, n. 2, p. 102, 2023. DOI: 10.3390/gels9020102.

MORRISON, Lindsay; ZEMBOWER, Teresa R. Antimicrobial Resistance. **Gastrointestinal Endoscopy Clinics of North America**, [S. l.], v. 30, n. 4, p. 619–635, 2020. DOI: 10.1016/j.giec.2020.06.004.

MORTELMANS, Kristien; ZEIGER, Errol. The Ames Salmonella/microsome mutagenicity assay. **Mutation Research/Fundamental and Molecular Mechanisms of Mutagenesis**, [S. l.], v. 455, n. 1–2, p. 29–60, 2000. DOI: 10.1016/S0027-5107(00)00064-6.

MURRAY, Christopher J. L. et al. Global burden of bacterial antimicrobial resistance in 2019: a systematic analysis. **The Lancet**, [S. l.], v. 399, n. 10325, p. 629–655, 2022. DOI: 10.1016/S0140-6736(21)02724-0.

MURUGAIYAN, Jayaseelan et al. Progress in Alternative Strategies to Combat Antimicrobial Resistance: Focus on Antibiotics. **Antibiotics**, [S. l.], v. 11, n. 2, p. 200, 2022. DOI: 10.3390/antibiotics11020200.

NAIR, Devatha P.; PODGÓRSKI, Maciej; CHATANI, Shunsuke; GONG, Tao; XI, Weixian; FENOLI, Christopher R.; BOWMAN, Christopher N. The Thiol-Michael Addition Click Reaction: A Powerful and Widely Used Tool in Materials Chemistry. **Chemistry of Materials**, [S. l.], v. 26, n. 1, p. 724–744, 2014. DOI: 10.1021/cm402180t.

NAKATO, Takeshi; KUSUNO, Atsushi; KAKUCHI, Toyoji. Synthesis of poly(succinimide) by bulk polycondensation of L-aspartic acid with an acid catalyst. **Journal of Polymer Science Part A: Polymer Chemistry**, [S. l.], v. 38, n. 1, p. 117–122, 2000. DOI: 10.1002/(SICI)1099-0518(20000101)38:1<117::AID-POLA15>3.0.CO;2-F.

NEFFE, Axel T. et al. Multivalent grafting of hyperbranched oligo- and polyglycerols shielding rough membranes to mediate hemocompatibility. **J. Mater. Chem. B**, [S. l.], v. 2, n. 23, p. 3626–3635, 2014. DOI: 10.1039/C4TB00184B.

NO, H. Antibacterial activity of chitosans and chitosan oligomers with different molecular weights. **International Journal of Food Microbiology**, [S. l.], v. 74, n. 1–2, p. 65–72, 2002. DOI: 10.1016/S0168-1605(01)00717-6.

NOÈ, Camilla; TONDA-TURO, Chiara; CHIAPPONE, Annalisa; SANGERMANO, Marco; HAKKARAINEN, Minna. Light Processable Starch Hydrogels. **Polymers**, [S. l.], v. 12, n. 6, p. 1359, 2020. DOI: 10.3390/polym12061359.

OCANDO, Connie; DINESCU, Sorina; SAMOILA, Iuliana; DANIELA GHITULICA, Cristina; CUCURUZ, Andra; COSTACHE, Marieta; AVEROUS, Luc. Fabrication and properties of alginate-hydroxyapatite biocomposites as efficient biomaterials for bone regeneration. **European Polymer Journal**, [S. l.], v. 151, p. 110444, 2021. DOI: 10.1016/j.eurpolymj.2021.110444.

OLAFSSON, Patrick G.; BRYAN, Ashley M. Evaluation of thermal decomposition temperatures of amino acids by differential enthalpic analysis. **Mikrochimica Acta**, [S. l.], v. 58, n. 5, p. 871–878, 1970. DOI: 10.1007/BF01225712.

OLIVER-ORTEGA, Helena; REIXACH, Rafel; ESPINACH, Francesc Xavier; MÉNDEZ, José Alberto. Maleic Anhydride Poly(lactic Acid) Coupling Agent Prepared from Solvent Reaction: Synthesis, Characterization and Composite Performance. **Materials**, [S. l.], v. 15, n. 3, p. 1161, 2022. DOI: 10.3390/ma15031161.

OZTURK, Turan; AMNA, Bibi. Click chemistry: a fascinating method of connecting organic groups. **Organic Communications**, [S. l.], n. 2, p. 97–120, 2021. DOI: 10.25135/acg.oc.100.21.03.2006.

PAGE, B.; PAGE, M.; NOEL, C. A new fluorometric assay for cytotoxicity measurements in vitro. **International journal of oncology**, [S. l.], v. 3, n. 3, p. 473–6, 1993.

PARK, Ji-Won; HWANG, Jin-Uk; BACK, Jong-Ho; JANG, Seong-Wook; KIM, Hyun-Joong; KIM, Pan-Seok; SHIN, Seunghan; KIM, Taejin. High strength PLGA/Hydroxyapatite composites with tunable surface structure using PLGA direct grafting method for orthopedic implants. **Composites Part B: Engineering**, [S. l.], v. 178, p. 107449, 2019. DOI: 10.1016/j.compositesb.2019.107449.

PENG, Erwin; DING, Jun; XUE, Jun Min. Succinic anhydride functionalized alkenoic ligands: a facile route to synthesize water dispersible nanocrystals. **Journal of Materials Chemistry**, [S. l.], v. 22, n. 27, p. 13832, 2012. DOI: 10.1039/c2jm30942d.

Peptides and Proteins as Biomaterials for Tissue Regeneration and Repair. [s.l.] : Elsevier, 2018. DOI: 10.1016/C2015-0-01811-1.

PEREIRA, Gabriela G.; FIGUEIREDO, Sara; FERNANDES, Ana Isabel; PINTO, João F. Polymer Selection for Hot-Melt Extrusion Coupled to Fused Deposition Modelling in

Pharmaceutics. **Pharmaceutics**, [*S. l.*], v. 12, n. 9, p. 795, 2020. DOI: 10.3390/pharmaceutics12090795.

PERVAIZ, Muhammad; RIAZ, Aqsa; MUNIR, Anfal; SAEED, Zohaib; HUSSAIN, Shah; RASHID, Ayoub; YOUNAS, Umar; ADNAN, Ahmad. Synthesis and characterization of sulfonamide metal complexes as antimicrobial agents. **Journal of Molecular Structure**, [*S. l.*], v. 1202, p. 127284, 2020. DOI: 10.1016/j.molstruc.2019.127284.

PIATKOWSKI, Marek; RADWAN-PRAGŁOWSKA, Julia; RACLAVSKÝ, Konstantin. Application of Poly (aspartic acid) and its Derivatives in Medicine and Pharmacy. **Asian Journal of Applied Sciences**, v. 3, n. 5, 2015.

PIGORSCH, Enrico. Spectroscopic Characterisation of Cationic Quaternary Ammonium Starches. **Starch - Stärke**, [*S. l.*], v. 61, n. 3–4, p. 129–138, 2009. DOI: 10.1002/star.200800090.

PIRES, Ana Luiza R.; BIERHALZ, Andréa C. K.; MORAES, Ângela M. BIOMATERIALS: TYPES, APPLICATIONS, AND MARKET. **Química Nova**, [*S. l.*], 2015. DOI: 10.5935/0100-4042.20150094.

PULINGAM, Thiruchelvi; PARUMASIVAM, Thaigarajan; GAZZALI, Amirah Mohd; SULAIMAN, Azlinah Mohd; CHEE, Jiun Yee; LAKSHMANAN, Manoj; CHIN, Chai Fung; SUDESH, Kumar. Antimicrobial resistance: Prevalence, economic burden, mechanisms of resistance and strategies to overcome. **European Journal of Pharmaceutical Sciences**, [*S. l.*], v. 170, p. 106103, 2022. DOI: 10.1016/j.ejps.2021.106103.

RAJESHKUMAR, G. et al. Environment friendly, renewable and sustainable poly lactic acid (PLA) based natural fiber reinforced composites – A comprehensive review. **Journal of Cleaner Production**, [*S. l.*], v. 310, p. 127483, 2021. DOI: 10.1016/j.jclepro.2021.127483.

REVELAS, Angela. Healthcare - associated infections: A public health problem. **Nigerian Medical Journal**, [*S. l.*], v. 53, n. 2, p. 59, 2012. DOI: 10.4103/0300-1652.103543.

RIGOLIN, Talita R.; COSTA, Lidiane C.; VENÂNCIO, Tiago; PERLATTI, Bruno; BETTINI, Sílvia H. P. The effect of different peroxides on physical and chemical properties of poly(lactic acid) modified with maleic anhydride. **Polymer**, [*S. l.*], v. 179, p. 121669, 2019. DOI: 10.1016/j.polymer.2019.121669.

RODANTE, F.; MARROSU, G.; CATALANI, G. Thermal analysis of some α -amino acids with similar structures. **Thermochimica Acta**, [*S. l.*], v. 194, p. 197–213, 1992. DOI: 10.1016/0040-6031(92)80018-R.

RODRÍGUEZ-FÉLIX, D. E.; PÉREZ-CABALLERO, D.; DEL CASTILLO-CASTRO, T.; CASTILLO-ORTEGA, M. M.; GARMENDÍA-DIAGO, Y.; ALVARADO-IBARRA, J.; PLASCENCIA-JATOMEA, M.; LEDEZMA-PÉREZ, A. S.; BURRUEL-IBARRA, S. E. Chitosan hydrogels chemically crosslinked with L-glutamic acid and their potential use in drug delivery. **Polymer Bulletin**, [*S. l.*], v. 80, n. 3, p. 2617–2636, 2023. DOI: 10.1007/s00289-022-04152-y.

RODRÍGUEZ-NÚÑEZ, Jesús R.; LÓPEZ-CERVANTES, Jaime; SÁNCHEZ-MACHADO, Dalia I.; RAMÍREZ-WONG, Benjamin; TORRES-CHAVEZ, Patricia; CORTEZ-ROCHA, Mario O. Antimicrobial activity of chitosan-based films against *Salmonella typhimurium* and *Staphylococcus aureus*. **International Journal of Food Science & Technology**, [S. l.], v. 47, n. 10, p. 2127–2133, 2012. DOI: 10.1111/j.1365-2621.2012.03079.x.

ROSSI, Ezequiel; RAMÍREZ, Jhon Alejandro Ávila; ERREA, María Inés. Preparation of an environmentally friendly lead adsorbent. A contribution to the rational design of heavy metal adsorbents. **Journal of Environmental Chemical Engineering**, [S. l.], v. 8, n. 5, p. 104210, 2020. DOI: 10.1016/j.jece.2020.104210.

ROTMAN, Stijn G.; MORIARTY, Thomas F.; NOTTELET, Benjamin; GRIJPMMA, Dirk W.; EGLIN, David; GUILLAUME, Olivier. Poly(Aspartic Acid) Functionalized Poly(ϵ -Caprolactone) Microspheres with Enhanced Hydroxyapatite Affinity as Bone Targeting Antibiotic Carriers. **Pharmaceutics**, [S. l.], v. 12, n. 9, p. 885, 2020. DOI: 10.3390/pharmaceutics12090885.

RUDY, Bruce C.; SENKOWSKI, Bernard Z. Sulfamethoxazole. In: **Analytical profiles of drug substances**. Academic Press, 1973. p. 467-486.

RYU, Yeon Sung; OH, Kyung Wha; KIM, Seong Hun. Synthesis and characterization of a furan-based self-healing polymer. **Macromolecular Research**, [S. l.], v. 24, n. 10, p. 874–880, 2016. DOI: 10.1007/s13233-016-4122-5.

RZAYEV, Zakir M. O.; ŞİMŞEK, Murat; BUNYATOVA, Ulviya; SALAMOV, Bahtiyar. Novel colloidal nanofiber semiconductor electrolytes from solution blends of PVA/ODA–MMT, poly (itaconic anhydride- alt -2-vinyl-1,3-dioxalan) and its Ag-carrying polymer complex by reactive electrospinning. **Colloids and Surfaces A: Physicochemical and Engineering Aspects**, [S. l.], v. 492, p. 26–37, 2016. DOI: 10.1016/j.colsurfa.2015.12.011.

SAHARIAH, Priyanka; MÁSSON, Már. Antimicrobial Chitosan and Chitosan Derivatives: A Review of the Structure–Activity Relationship. **Biomacromolecules**, [S. l.], v. 18, n. 11, p. 3846–3868, 2017. DOI: 10.1021/acs.biomac.7b01058.

SCHACHSCHAL, Susann; PICH, Andrij; ADLER, Hans-Juergen. Growth of hydroxyapatite nanocrystals on polymer particle surface. **Colloid and Polymer Science**, [S. l.], v. 285, n. 10, p. 1175–1180, 2007. DOI: 10.1007/s00396-007-1685-x.

SCHIAVONE, Nicola; VERNEY, Vincent; ASKANIAN, Haroutioun. Effect of 3D Printing Temperature Profile on Polymer Materials Behavior. **3D Printing and Additive Manufacturing**, [S. l.], v. 7, n. 6, p. 311–325, 2020. DOI: 10.1089/3dp.2020.0175.

SHAH, Kamal; CHAUHAN, Durgesh Nandini; CHAUHAN, Nagendra Singh; MISHRA, Pradeep. **Recent Advancement in Prodrugs**. [s.l.] : CRC Press, 2020. DOI: 10.1201/9780429328275.

SHAN, Yukai; QIN, Yuyue; CHUAN, Yongming; LI, Hongli; YUAN, Minglong. The Synthesis and Characterization of Hydroxyapatite- β -Alanine Modified by Grafting Polymerization of γ -Benzyl-L-glutamate-N-carboxyanhydride. **Molecules**, [S. l.], v. 18, n. 11, p. 13979–13991, 2013. DOI: 10.3390/molecules181113979.

SHARMIN, Nusrat; ROSNES, Jan Thomas; PRABHU, Leena; BÖCKER, Ulrike; SIVERTSVIK, Morten. Effect of Citric Acid Cross Linking on the Mechanical, Rheological and Barrier Properties of Chitosan. **Molecules**, [*S. l.*], v. 27, n. 16, p. 5118, 2022. DOI: 10.3390/molecules27165118.

SHIBUYA, Naohiro; JUPITER, Daniel C. Bone Graft Substitute. **Clinics in Podiatric Medicine and Surgery**, [*S. l.*], v. 32, n. 1, p. 21–34, 2015. DOI: 10.1016/j.cpm.2014.09.011.

SINITSYNA, O. V.; VERESOV, A. G.; KOVALEVA, E. S.; KOLEN'KO, Yu. V.; PUTLYAEV, V. I.; TRETYAKOV, Yu. D. Synthesis of hydroxyapatite by hydrolysis of α -Ca₃(PO₄)₂. **Russian Chemical Bulletin**, [*S. l.*], v. 54, n. 1, p. 79–86, 2005. DOI: 10.1007/s11172-005-0220-9.

SIQUEIRA, L.; PASSADOR, F. R.; COSTA, M. M.; LOBO, A. O.; SOUSA, E. Influence of the addition of β -TCP on the morphology, thermal properties and cell viability of poly (lactic acid) fibers obtained by electrospinning. **Materials Science and Engineering: C**, [*S. l.*], v. 52, p. 135–143, 2015. DOI: 10.1016/j.msec.2015.03.055.

SMITH, Laura J.; TAIMOORY, S. Maryamdokht; TAM, Roger Y.; BAKER, Alexander E. G.; BINTH MOHAMMAD, Niema; TRANT, John F.; SHOICHET, Molly S. Diels–Alder Click-Cross-Linked Hydrogels with Increased Reactivity Enable 3D Cell Encapsulation. **Biomacromolecules**, [*S. l.*], v. 19, n. 3, p. 926–935, 2018. DOI: 10.1021/acs.biomac.7b01715.

SOWMYA, Appunni; MEENAKSHI, Sankaran. An efficient and regenerable quaternary amine modified chitosan beads for the removal of nitrate and phosphate anions. **Journal of Environmental Chemical Engineering**, [*S. l.*], v. 1, n. 4, p. 906–915, 2013. DOI: 10.1016/j.jece.2013.07.031.

Standard, I. “Biological evaluation of medical devices—Part 5: Tests for in vitro cytotoxicity.” Geneve, Switzerland: International Organization for Standardization (2009). , [s.d.].

SZYC, Łukasz; PILORZ, Sylwia; CZARNIK-MATUSEWICZ, Bogusława. FTIR-ATR investigations of an α -helix to β -sheet conformational transition in poly(l-lysine). **Journal of Molecular Liquids**, [*S. l.*], v. 141, n. 3, p. 155–159, 2008. DOI: 10.1016/j.molliq.2008.04.016.

TANAKA, Hideji; MIYAJIMA, Koichiro; NAKAGAKI, Masayuki; SHIMABAYASHI, Saburo. Interactions of aspartic acid, alanine and lysine with hydroxyapatite. **Chemical and Pharmaceutical Bulletin**, [*S. l.*], v. 37, n. 11, p. 2897–2901, 1989. DOI: 10.1248/cpb.37.2897.

TAVAFOGHI, M.; CERRUTI, M. The role of amino acids in hydroxyapatite mineralization. **Journal of The Royal Society Interface**, [*S. l.*], v. 13, n. 123, p. 20160462, 2016. DOI: 10.1098/rsif.2016.0462.

Test No. 492: Reconstructed human Cornea-like Epithelium (RhCE) test method for identifying chemicals not requiring classification and labelling for eye irritation or serious eye damage. [s.l.] : OECD, 2019. DOI: 10.1787/9789264242548-en.

THOMPSON, Marisa; SCHOLZ, Carmen. Highly Branched Polymers Based on Poly(amino acid)s for Biomedical Application. **Nanomaterials**, [S. l.], v. 11, n. 5, p. 1119, 2021. DOI: 10.3390/nano11051119.

TILLET, Guillaume; BOUTEVIN, Bernard; AMEDURI, Bruno. Chemical reactions of polymer crosslinking and post-crosslinking at room and medium temperature. **Progress in Polymer Science**, [S. l.], v. 36, n. 2, p. 191–217, 2011. DOI: 10.1016/j.progpolymsci.2010.08.003.

TIWARY, Praphulla; KONTOPOULOU, Marianna. Tuning the Rheological, Thermal, and Solid-State Properties of Branched PLA by Free-Radical-Mediated Reactive Extrusion. **ACS Sustainable Chemistry & Engineering**, [S. l.], v. 6, n. 2, p. 2197–2206, 2018. DOI: 10.1021/acssuschemeng.7b03617.

TORLAK, Emrah; NIZAMLIOĞLU, Mustafa. Antimicrobial effectiveness of chitosan-essential oil coated plastic films against foodborne pathogens. **Journal of Plastic Film & Sheeting**, [S. l.], v. 27, n. 3, p. 235–248, 2011. DOI: 10.1177/8756087911407391.

TORRES, Fernando G.; COMMEAUX, Solene; TRONCOSO, Omar P. Starch-based biomaterials for wound-dressing applications. **Starch - Stärke**, [S. l.], v. 65, n. 7–8, p. 543–551, 2013. DOI: 10.1002/star.201200259.

TROVATTI, Eliane; LACERDA, Talita M.; CARVALHO, Antonio J. F.; GANDINI, Alessandro. Recycling Tires? Reversible Crosslinking of Poly(butadiene). **Advanced Materials**, [S. l.], v. 27, n. 13, p. 2242–2245, 2015. a. DOI: 10.1002/adma.201405801.

TROVATTI, Eliane; LACERDA, Talita M.; CARVALHO, Antonio J. F.; GANDINI, Alessandro. Recycling Tires? Reversible Crosslinking of Poly(butadiene). **Advanced Materials**, [S. l.], v. 27, n. 13, p. 2242–2245, 2015. b. DOI: 10.1002/adma.201405801.

ULLAH, Faheem; OTHMAN, Muhammad Bisyrul Hafi; JAVED, Fatima; AHMAD, Zulkifli; AKIL, Hazizan Md. Classification, processing and application of hydrogels: A review. **Materials Science and Engineering: C**, [S. l.], v. 57, p. 414–433, 2015. DOI: 10.1016/j.msec.2015.07.053.

USCATEGUI, Yomaira; DÍAZ, Luis; VALERO, Manuel. BIOMEDICAL APPLICATIONS OF POLYURETHANES. **Química Nova**, [S. l.], 2018. DOI: 10.21577/0100-4042.20170191.

VAUTHIER, Madeline; JIERRY, Loïc; MARTINEZ MENDEZ, Miguel L.; DURST, Yann-Matthieu; KELBER, Julien; ROUCOULES, Vincent; BALLY-LE GALL, Florence. Interfacial Diels–Alder Reaction between Furan-Functionalized Polymer Coatings and Maleimide-Terminated Poly(ethylene glycol). **The Journal of Physical Chemistry C**, [S. l.], v. 123, n. 7, p. 4125–4132, 2019. DOI: 10.1021/acs.jpcc.8b10533.

VEIGA, Anabela; CASTRO, Filipa; ROCHA, Fernando; OLIVEIRA, Ana L. Protein-Based Hydroxyapatite Materials: Tuning Composition toward Biomedical Applications. **ACS**

Applied Bio Materials, [*S. l.*], v. 3, n. 6, p. 3441–3455, 2020. DOI: 10.1021/acsabm.0c00140.

VISWANATHAN, Tito; JETHMALANI, Jagdish. The Aqueous Ring-Opening Metathesis Polymerization of Furan-Maleic Anhydride Adduct: Increased Catalytic Activity Using a Recyclable Transition Metal Catalyst. **Journal of Chemical Education**, [*S. l.*], v. 70, n. 2, p. 165, 1993. DOI: 10.1021/ed070p165.

WANG, Peipei; LI, Caihong; GONG, Haiyan; JIANG, Xuerong; WANG, Hongqiang; LI, Kaixing. Effects of synthesis conditions on the morphology of hydroxyapatite nanoparticles produced by wet chemical process. **Powder Technology**, [*S. l.*], v. 203, n. 2, p. 315–321, 2010. DOI: 10.1016/j.powtec.2010.05.023.

WANG, Yayue; ZHANG, Chang; WU, Haoxing; FENG, Ping. Activation and Delivery of Tetrazine-Responsive Bioorthogonal Prodrugs. **Molecules**, [*S. l.*], v. 25, n. 23, p. 5640, 2020. DOI: 10.3390/molecules25235640.

WANG, Zhongyi et al. Potential Osteoinductive Effects of Hydroxyapatite Nanoparticles on Mesenchymal Stem Cells by Endothelial Cell Interaction. **Nanoscale Research Letters**, [*S. l.*], v. 16, n. 1, p. 67, 2021. DOI: 10.1186/s11671-021-03522-1.

WEI, Hongliang; LI, Weikun; CHEN, Hongli; WEN, Xuejun; HE, Juan; LI, Jingjing. Simultaneous Diels-Alder click reaction and starch hydrogel microsphere production via spray drying. **Carbohydrate Polymers**, [*S. l.*], v. 241, p. 116351, 2020. DOI: 10.1016/j.carbpol.2020.116351.

WEI, Zhengkai; WANG, Yi; FU, Xiaowei; JIANG, Liang; WANG, Yuechuan; YUAN, Anqian; XU, Hualiang; LEI, Jingxin. Recyclable and Reprocessable Thermosetting Polyurea with High Performance Based on Diels-Alder Dynamic Covalent Crosslinking. **Macromolecular Research**, [*S. l.*], v. 29, n. 8, p. 562–568, 2021. DOI: 10.1007/s13233-021-9064-x.

WEINER-LASTINGER, Lindsey M. et al. Antimicrobial-resistant pathogens associated with adult healthcare-associated infections: Summary of data reported to the National Healthcare Safety Network, 2015–2017. **Infection Control & Hospital Epidemiology**, [*S. l.*], v. 41, n. 1, p. 1–18, 2020. DOI: 10.1017/ice.2019.296.

WIGLUSZ, Rafal J.; POZNIAK, Blazej; ZAWISZA, Katarzyna; PAZIK, Robert. An up-converting HAP@ β -TCP nanocomposite activated with Er³⁺/Yb³⁺ ion pairs for bio-related applications. **RSC Advances**, [*S. l.*], v. 5, n. 35, p. 27610–27622, 2015. DOI: 10.1039/C5RA00675A.

XIAO, Bo; WAN, Ying; ZHAO, Maoqi; LIU, Yiqun; ZHANG, Shengmin. Preparation and characterization of antimicrobial chitosan-N-arginine with different degrees of substitution. **Carbohydrate Polymers**, [*S. l.*], v. 83, n. 1, p. 144–150, 2011. DOI: 10.1016/j.carbpol.2010.07.032.

XIONG, Xuhai; AI, Jianxin; REN, Rong; WANG, Jing; LI, Guiyang. Curing behavior and properties of ultra-high temperature resistant RTM bismaleimide resin. **High Performance Polymers**, [*S. l.*], p. 095400832211469, 2022. DOI: 10.1177/09540083221146926.

YABLOKOV, V. Ya.; SMEL'TSOVA, I. L.; ZELYAEV, I. A.; MITROFANOVA, S. V. Studies of the rates of thermal decomposition of glycine, alanine, and serine. **Russian Journal of General Chemistry**, [S. l.], v. 79, n. 8, p. 1704–1706, 2009. DOI: 10.1134/S1070363209080209.

YANG, Lijun et al. Triclosan-based supramolecular hydrogels as nanoantibiotics for enhanced antibacterial activity. **Journal of Controlled Release**, [S. l.], v. 324, p. 354–365, 2020. DOI: 10.1016/j.jconrel.2020.05.034.

YAO, Xiyu; HU, Huixia; QIN, Yan; LIU, Jun. Development of antioxidant, antimicrobial and ammonia-sensitive films based on quaternary ammonium chitosan, polyvinyl alcohol and betalains-rich cactus pears (*Opuntia ficus-indica*) extract. **Food Hydrocolloids**, [S. l.], v. 106, p. 105896, 2020. DOI: 10.1016/j.foodhyd.2020.105896.

YELTEN-YILMAZ, Azade; YILMAZ, Suat. Wet chemical precipitation synthesis of hydroxyapatite (HA) powders. **Ceramics International**, [S. l.], v. 44, n. 8, p. 9703–9710, 2018. DOI: 10.1016/j.ceramint.2018.02.201.

YONG, Khai Jie; WU, Ta Yeong; LEE, Cornelius Basil Tien Loong; LEE, Zhi Jin; LIU, Qinpu; JAHIM, Jamaliah Md; ZHOU, Qiaoqiao; ZHANG, Lian. Furfural production from biomass residues: Current technologies, challenges and future prospects. **Biomass and Bioenergy**, [S. l.], v. 161, p. 106458, 2022. DOI: 10.1016/j.biombioe.2022.106458.

YOSHIKAWA, Yuki et al. Amidation of carboxy groups in TEMPO-oxidized cellulose for improving surface hydrophobization and thermal stability of TEMPO-CNCs. **Carbohydrate Polymers**, p. 122654, 2024.

YOUNES, Islem; RINAUDO, Marguerite. Chitin and Chitosan Preparation from Marine Sources. Structure, Properties and Applications. **Marine Drugs**, [S. l.], v. 13, n. 3, p. 1133–1174, 2015. DOI: 10.3390/md13031133.

ZANDER, Zachary K.; BECKER, Matthew L. Antimicrobial and Antifouling Strategies for Polymeric Medical Devices. **ACS Macro Letters**, [S. l.], v. 7, n. 1, p. 16–25, 2018. DOI: 10.1021/acsmacrolett.7b00879.

ZHANG, Borui; JAYALATH, Isuru M.; KE, Jun; SPARKS, Jessica L.; HARTLEY, C. Scott; KONKOLEWICZ, Dominik. Chemically fueled covalent crosslinking of polymer materials. **Chemical Communications**, [S. l.], v. 55, n. 14, p. 2086–2089, 2019. DOI: 10.1039/C8CC09823A.

ZHANG, Chang; CUI, Fang; ZENG, Guang-ming; JIANG, Min; YANG, Zhong-zhu; YU, Zhi-gang; ZHU, Meng-ying; SHEN, Liu-qing. Quaternary ammonium compounds (QACs): A review on occurrence, fate and toxicity in the environment. **Science of The Total Environment**, [S. l.], v. 518–519, p. 352–362, 2015. DOI: 10.1016/j.scitotenv.2015.03.007.

ZHANG, Hai-bin; ZHOU, Ke-chao; LI, Zhi-you; HUANG, Su-ping. Plate-like hydroxyapatite nanoparticles synthesized by the hydrothermal method. **Journal of Physics and Chemistry of Solids**, [S. l.], v. 70, n. 1, p. 243–248, 2009. DOI: 10.1016/j.jpcs.2008.10.011.

ZHI, Xuelian; LI, Pengfei; GAN, Xucheng; ZHANG, Weiwei; SHEN, Tianjiao; YUAN, Jiang; SHEN, Jian. Hemocompatibility and anti-biofouling property improvement of poly(ethylene terephthalate) via self-polymerization of dopamine and covalent graft of lysine. **Journal of Biomaterials Science, Polymer Edition**, [S. l.], v. 25, n. 14–15, p. 1619–1628, 2014. DOI: 10.1080/09205063.2014.943537.

ZHOU, Tianyi et al. Toward stable zinc aqueous rechargeable batteries by anode morphology modulation via polyaspartic acid additive. **Energy Storage Materials**, [S. l.], v. 45, p. 777–785, 2022. DOI: 10.1016/j.ensm.2021.12.028.